(NASA CR 52133

OTS PRICE

XEROX $ 3.00 ff

MICROFILM $ .50 ff

JET PROPULSION LABORATORY
CALIFORNIA INSTITUTE OF TECHNOLOGY
PASADENA, CALIFORNIA

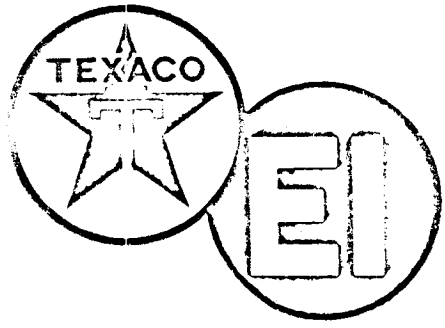

SURVEYOR GEOPHYSICAL INSTRUMENT

Interim Report

TP-192

Volume I

Surface Geophysical Instrument

Prototype No. I

TEXACO

EXPERIMENT INCORPORATED

RICHMOND 2, VIRGINIA

EXP 387 1 May 1962

SURVEYOR GEOPHYSICAL INSTRUMENT

Interim Report

TP-192

Volume I

Surface Geophysical Instrument

Prototype No. I

R. E. Canup, R. H. Clinard, Jr., V. M. Barnes, Jr.,
J. R. Bond, R. P. Doelling, and N. E. Flournoy

TEXACO EXPERIMENT INCORPORATED
Richmond 2, Virginia

Submitted to
California Institute of Technology
Jet Propulsion Laboratory
under Contract 950155

CONTENTS

CONTENTS (cont'd)

CONTENTS (cont'd)

FIGURES

FIGURES (cont'd)

FIGURES (cont'd)

FIGURES (cont'd)

FIGURES (cont'd)

TABLES

Surface Temperature Instrument

Surface Thermal Diffusivity Instrument

TABLES (cont'd)

1. ABSTRACT

This report covers the work completed prior to the delivery of the first prototypes of the Surface Geophysical Instrument for the Surveyor Spacecraft. The instruments included are designed to measure temperature, thermal diffusivity, magnetic susceptibility, density, penetrability, and acoustic velocity of the lunar surface. For each instrument a system and equipment description, report of testing and calibration, components outline, description of packaging philosophy, theoretical studies, and environmental test results, and a recommendations section is included. A summary of quality assurance practices employed is included which covers all six of the surface geophysical instruments.

2. INTRODUCTION

Under contract 950155 with the California Institute of Technology, Jet Propulsion Laboratory, Texaco Experiment Incorporated has designed, developed, conducted acceptance tests on, and delivered one set of prototype instruments (P-1) for the Surveyor, the NASA soft-landing, unmanned moon vehicle. This set of prototype instruments is defined as the Surveyor Geophysical Instrument and consists of the Surface Geophysical Instrument and the Subsurface Geophysical Instrument.

The Surface Geophysical Instrument is a group of separate instruments designed to conduct certain experiments on the lunar surface. These instruments include the Surface Temperature Instrument, the Surface Thermal Diffusivity Instrument, the Surface Magnetic Susceptibility Instrument, the Surface Density Instrument, which also contains an Acoustic Sensor for the sonic-velocity experiment, a Surface Penetrability Instrument, which consists of three Penetrometers, and a Surface Acoustic Velocity Instrument, which consists of an Acoustic Source and an Acoustic Sensor.

The Subsurface Geophysical Instrument or Subsurface Sonde contains a group of instruments packaged in an elongated cylinder and designed to conduct certain experiments in a hole previously drilled into the lunar surface. The Subsurface Geophysical Instrument contains a Subsurface Density Instrument, a Subsurface Acoustic Velocity Instrument, a Subsurface Magnetic Susceptibility Instrument, a Subsurface Temperature Instrument, a Subsurface Thermal Diffusivity Instrument, and a Subsurface Caliper Instrument.

This report describes the design, development, and testing of the first prototype (P-1), Surveyor Surface Geophysical Instrument. Prior to the work herein reported the Bellaire Research Laboratories of Texaco Inc. conducted a study under contract N-33552 with the California Institute of Technology, Jet Propulsion Laboratory, on the feasibility of making certain geophysical measurements on and in the lunar surface. Breadboard models of the instruments designed to make the desired geophysical measurements were designed, fabricated, and tested. The prototype instruments developed at Texaco Experiment Incorporated and described in this report were based on the instruments conceived at the Bellaire Research Laboratories, Texaco Inc.

3. SURFACE TEMPERATURE INSTRUMENT

URD 27

Control Item X239278

3.1 System Description

The interferometer spectrometer is a modified Michelson interferometer which utilizes an electromechanical mirror-drive mechanism and a bolometer detector to convert incident infrared radiation into audio frequencies whose amplitude varies proportionally as the fourth power of the differential temperature between the object being viewed and the bolometer detector. The frequency of the resultant audio signal is a direct function of the wavelength of the incident radiation.

The detected signal is amplified approximately 50 db between the bolometer detector output and the instrument output by a three-stage preamplifier physically located in the sensor head and a three-stage postamplifier located in a remote electronic package.

The mirror-drive power is generated by a linear sawtooth generator and amplified sufficiently to drive the mirror by appropriate electronic circuitry in the electronic package.

Bias voltages for the bolometer, resistance thermometer, and transistor circuitry are generated by a dc-to-dc converter and electronically regulated within the electronics package. This electronic package is designed to operate within the temperature-controlled electronic compartment of the spacecraft. Power for this package is taken from the spacecraft regulated 29-volt supply.

The optical section, or sensor head, contains an infrared window, beamsplitter, stationary mirror, focusing lens, movable mirror, bolometer detector, and thermostatically controlled heater.

3.1.1 Theory of Operation. The incident radiation enters the window of the sensor head, strikes the beamsplitter, and is split at right angles into two equal parts (A and B). The amplitude of the two parts plus the losses in the beamsplitter and window equals the total amplitude of the incoming wave.

Part A of the radiation for discussion purposes is reflected 90° by the beamsplitter towards the stationary mirror; part B is passed through the beamsplitter to the movable mirror. Part B strikes the movable mirror and is reflected back to the beamsplitter, where it is reflected 90° to the bolometer. When monochromatic radiation is being viewed

and the constants of the system have been correctly chosen, the optical path of part A of the incident radiation from the beamsplitter to the bolometer is the same as the length of the optical path of part B from the beamsplitter to the bolometer. When the path lengths are exactly the same, the phase of the two parts of the radiation are the same, and they add, or in optical terms, constructively interfere with each other. When the optical distance traveled by part A differs from the optical distance traveled by part B by one half of one wavelength, the two beams are out of phase with each other and therefore cancel, or in optical terms, destructively interfere with each other. When the path lengths are such that the two parts of the incident radiation are additive, maximum energy is transferred by radiation from the object being viewed to the bolometer detector. This transfer of energy causes the bolometer, which has a low thermal mass, to increase in temperature.

The bolometer detector is a carefully selected thermistor which has a large change in resistance with temperature; therefore, the increase in temperature of the bolometer causes a decrease in its resistance. The bolometer, in operation, is fed by a constant current source, so that changes in bolometer resistance appear as voltage changes across the bolometer.

When the path length of the two parts of the incident radiation are such that destructive interference occurs, no energy is transferred to the bolometer, and its temperature returns to that of its surroundings. Hence, no voltage change is apparent across the bolometer.

Assume that the movable mirror is moving towards the beamsplitter starting from a point at which the path lengths of part A and part B of the incident radiation are the same. At this time there is constructive interference, and maximum energy is transferred to the bolometer. As the mirror moves, the path length of part B becomes shorter, and the phase of part B to part A shifts until it is 180° phase-shifted when the optical path length is one-half wavelength shorter than when constructive interference occurred. At this time part A is cancelled by part B, and no energy reaches the bolometer. As the mirror continues to move, the phase of part B continues to shift until it is again in phase with the radiation of part A. At that time constructive interference again occurs. When the mirror is moving continuously parts A and B of the radiation are continually going through constructive and destructive interference patterns at a rate which is proportional

to the velocity of the movable mirror and the wavelength of the incident radiation. Therefore, the bolometer, which is alternately heating and cooling, causes a voltage which is related to the velocity of the mirror and the wavelength of the incident radiation. The frequency of this voltage change is proportional to the velocity of the mirror and the radiation wavelength, while its amplitude is proportional to the amount of radiant energy entering the window.

Assume a wavelength of incident radiation, X_1, in microns, and a mirror velocity, V. Also, assume a second wavelength, X_2, such that X_1 is a shorter wavelength than X_2. Inductively, the constructive and destructive interference patterns will occur at a faster rate for X_1 than they will for X_2; that is, the mirror moves shorter distances (one wavelength) between constructive peaks of X_1 than for X_2. Therefore, the frequency at which interference peaks occur is inversely proportional to the wavelength of the radiation.

The audio-frequency output, F_a, from the bolometer is a function of wavelength, λ, and mirror velocity, V_m, or

$$F_a = NV_m \qquad (1)$$

where N is the wave number $(1/\lambda)$.

The moving mirror is coupled to the armature of an electromechanical transducer. The armature is driven by a ramp-function electrical signal which is generated in the electronics package. The shape of this ramp function is given in Figure 1. During the time interval t_1 the mirror progresses from one end of its excursion to the other. The total mirror travel, B, is a function of the ramp-function voltage, V_1. Its velocity, V_m, then is the total distance traveled, B, divided by t_1, the travel time, or $V_m = B/t_1$. Substituting this in Equation 1 gives

$$F_a = NB/t_1 \qquad (2)$$

Therefore, the audio-frequency signal generated by the bolometer is determined by the wavelength of the incident radiation, the mirror sweep time, t_1, and the amplitude of the sweep voltage, V_1, since B, the mirror travel, is a function of V_1.

When monochromatic radiation is being detected, there will be a single discrete audio frequency present in the bolometer output. When the

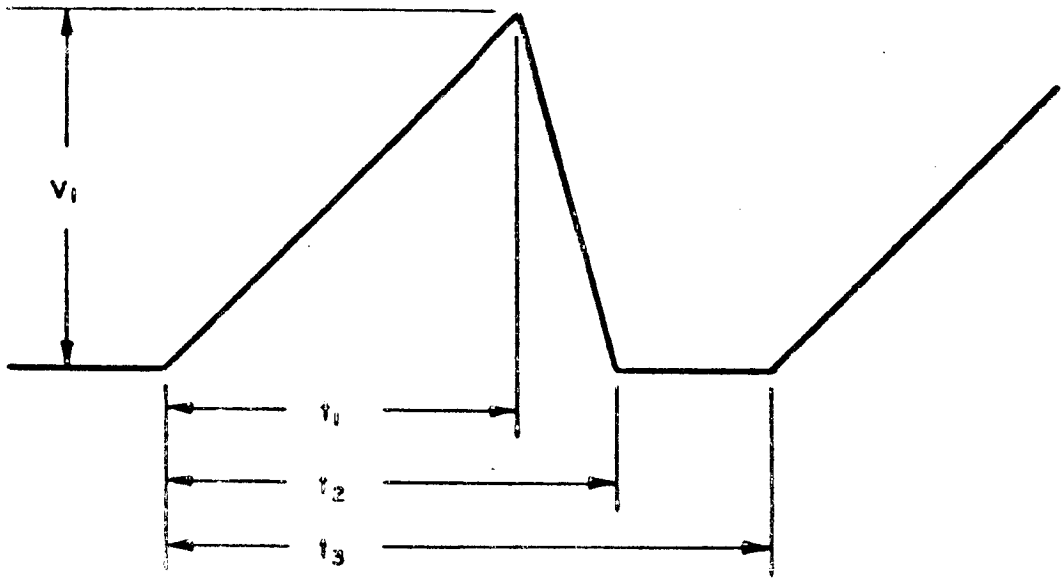

FIGURE 1. SWEEP-DRIVE VOLTAGE WAVEFORM

t_1 LINEAR INCREASING-VOLTAGE TIME

$t_2 - t_1$ FLYBACK TIME

$t_3 - t_2$ DEAD TIME

V_1 VOLTAGE OF RAMP FUNCTION

incident radiation is composed of a band of frequencies, the audio-frequency output from the bolometer will be an interferogram which contains the audio frequencies corresponding to the entire band of radiation.

If the entire band of radiation is not present because of the selective absorption of some particular wavelength, there will be a similar gap in the audio-frequency spectrum. Therefore the output from the spectrometer can be used to identify materials which have selective infrared absorption characteristics.

3.1.2 Interpretation of Data. The output from the bolometer consists of a spectrum of audio frequencies, the band width of which is determined by the incident radiation upon the spectrometer, the cut-off characteristics of the optical material used for the lens, the mirror travel, B, and the travel time, t_1.

The amplitude of each of the audio frequencies is dependent upon the energy contained in the wavelength of the incident radiation.

Planck's Radiation Formula states that the emissive power of a blackbody at wavelength, λ, is

$$E\lambda = C_1 \lambda^{-5}/(\exp C_2/\lambda T - 1)$$

where C_1 and C_2 are constants and T is the absolute temperature in degrees Kelvin, and the exp term represents a power of e.

The Stefan-Boltzmann Law states that the energy transfer between two blackbodies is

$$E = \sigma (T_1^4 - T_2^4)$$

where σ = Boltzmann constant

T_1 = absolute temperature of first body

T_2 = absolute temperature of second body

Since the average bolometer temperature is accurately monitored by a resistance thermometer, an analysis of the spectral distribution of the radiation interchange between the bolometer and the object being viewed allows the absolute temperature of the object to be computed accurately by application of these two radiation laws (1) (see Appendix A).

3.1.3 Precision of Measurements. It is obvious from the discussion of section 3.1.1 that the identification of a particular wavelength of radiation is dependent upon, among other things, the sensitivity of the bolometer, the accuracy of the total mirror travel, B, and the mirror velocity, V_1.

Other factors influencing the detection of a single wavelength of radiation are the noise output of the detector and amplifier, the relative absorption characteristics of the optics for the wavelengths in question compared to other wavelengths, and the resolving power of the spectrometer.

3.1.3.1 Effect of changes in mirror travel time.

Consideration will be given below to the effect on audio-frequency output signals with changes in t_1. In the event t_1 increases or decreases by some quantity Δt because of temperature effects on the electronics, it will affect the audio-frequency of the output signal as shown below:

$$F_a = N \frac{B}{t_1 \pm \Delta t} \qquad (3)$$

where

F_a = audio frequency

N = wave number

B = mirror travel

t_1 = travel time

Δt = small change in t

When the travel time increases a small amount Equation 3 becomes

$$F_a - \Delta F_a = N \frac{B}{t_1 + \Delta t}$$

where $F_a - \Delta F_a$ is the audio frequency when t is increased by Δt. When the travel time decreases by a small amount, Δt, Equation 3 becomes

$$F_a + \Delta F_a = N \frac{B}{t_1 - \Delta t}$$

where $F_a + \Delta F_a$ is the audio frequency when t is decreased by a small amount Δt. Solving for F_a in both equations and equating we have,

$$\frac{NB}{t_1 + \Delta t} + \Delta F_a = \frac{NB}{t_1 - \Delta t} - \Delta F_a$$

$$\frac{NB\,\Delta t}{t_1^2 - \Delta t^2} = \Delta F_a$$

and neglecting Δt^2,

$$\Delta F_a \cong \frac{NB\Delta t}{t_1^2}$$

The ratio of ΔF_a to F_a is then

$$\Delta F_a / F_a = \frac{NB\Delta t / t_1^2}{NB/t_1}$$

$$\Delta F_a = F_a \Delta t / t_1$$

Therefore the change in audio frequency due to a change in travel time is the audio frequency which would be present if there were no error times the ratio of the change in travel time to the total travel time.

3.1.3.2 Effects of changes in sweep amplitude.

The total mirror travel, B, is directly proportional to the sweep amplitude voltage, V_1. This voltage may change when the temperature of the electronic package is varied.

Using the same line of reasoning as in section 3.1.3.1 it can be shown that the ratio of the change in audio frequency, ΔF_a, to the true frequency, F_a, is:

$$\Delta F_a = F_a \Delta V / V_1$$

where ΔV is the change in voltage.

3.1.3.3 Analysis of variation in output due to changes in sweep amplitudes and sweep lengths.

The present interferometer measures the infrared radiation from 5 to 25 μ, which corresponds to wave numbers from 2000 to 400. With the ideal sweep constants of the device, the audio frequencies corresponding to these wave numbers range from 150 to 30 cps.

The spectral resolution of the device is about 80 wave numbers, which corresponds to an audio resolution of 6 cycles. As an example of the error in audio frequency caused by changes in t_1, the mirror travel length, consider the following example. Assume the $\Delta t/t_1$ ratio is 0.01; then the variation of audio frequency due to this error is 0.01 F_a. At 30 cycles this is an error of ±0.3 cycles and at 150 cycles, an error of ±1.5 cycles, which in each case is below the resolution of the device.

It is evident then that the ratio of the $\Delta t/t_1$ must be greater than 0.04 before there will be a significant error in output audio frequencies from a change of t_1. Likewise, the ratio of the voltage change of sweep, ΔV_1, to the normal voltage, V_1, must be held to less than 0.04 to keep the error to a minimum.

3.1.3.4 Notes on checkout of Iota-001 interferometer.

Procedures for operational checkout of the interferometer for the most part follow logically those indicated by Block Associates (2). Points covered here are largely an expansion of those directions.

It is of critical importance to delineate the instrument behavior with respect to stability of operation and calibration. Stability tests should demonstrate both electrical and mechanical behavior of the wavelength scan system and the electrical and optical aspects of the instrument gain. Optical and mechanical behavior will generally have to be deduced by comparison of over-all and electrical characteristics. Calibration consists of the generation of a normalization of instrument wavelength response curve and also investigation of the results to be expected as a function of difference between object and instrument temperature. Both stability and calibration tests should spell out instrument behavior as a function of:

(a) Instrument operating temperature. Although hopefully instrument temperature will be thermostated at 40°F, it is necessary to investigate behavior over at least a 40° ± 30°F range.

(b) Temperature cycling of instrument. During blastoff and during the flight to the moon, the device will probably be temperature-cycled several times, and the effects of this on its operation should be determined. Most probable detrimental effects will be on optical and mechanical characteristics.

(c) Instrument operating time. It is possible that the thermal and mechanical equilibrium may not be attained in the instrument until some time after turn-on.

Two other points (at least) should be noted; namely, (a) many of these tests can be run simultaneously if the data collection is organized efficiently, and (b) testing should be programmed so that potentially destructive tests (such as high-temperature operation) are run late in the series.

3.1.4 General Test Discussion. After setup and interconnection of the instrument and electronics the following should be checked both initially and at suitable intervals to detect drift.

1. Actuator coil wave forms.
   a. Ramp voltage timing
   b. Ramp voltage amplitude
   c. Flyback and dead time
   d. dc bias applied to minor actuator coil
2. Bolometer bias voltage
3. Noise level in amplifier output
4. Power-supply voltages

A qualitative check for proper operation of instrument can be obtained with a hot soldering iron as a source mounted about 5 inches away from the interferometer. A typical interferogram waveform will be seen in postamplifier output.

3.1.4.1 Audio frequency versus optical wavelength.

A filter is used to isolate from a hot blackbody source a band of radiation narrow compared to the instrument resolution limit. For these instruments resolution is an approximately constant 80 wave numbers for the whole spectral region, and the wavelength resolution can be calculated from $\Delta N/N = \Delta\lambda/\lambda$, where N is the wave number and λ is the corresponding wavelength. Thus for a wavelength of 5 μ corresponding to a wave number of 2000 the wavelength resolution, $\Delta\lambda/\lambda$, is about 80/2000 or 0.04. When the instrument aperture is filled with the radiation from this filter, the instrument output will be principally a pure sinusoid.

Measurement of the instrument constant relating wave number (or wavelength) to frequency is best done with a wave analyzer. Wave analyzer bandwidth should be consistent with spectral resolution of the interferometer. As an example of the factors involved consider the following. The wave-number region covered by these instruments is from 2000 (5μ) to 400 (25 μ) or a total of 1600 cm^{-1}. The resolution is 80 cm^{-1}, so qualitatively the spectral region is divided roughly into 1600/80 = 20 independently measured intervals. Ideally, this wavelength region should be modulated to the audio-frequency range of 30 to 150 cps, and if this frequency range is divided by the wave-analyzer bandwidth into 20 uniform intervals, then the analyzer bandwidth will be consistent with the spectral resolution. This gives 6 cps as a reasonable wave-analyzer bandwidth. The bandwidth should not be narrowed much more than this because there is also a "fine structure modulation" due to scan-mirror repetition rate (about 3 cps), which is superimposed on the instrument output, and it is desirable to "smear" or average this out in the wave-analyzer output.

Since the fundamental interpretation of the interferogram depends on the wavelength to audio frequency calibration, it is evident that drift and temperature sensitivity in this parameter should be measured very carefully.

3.1.4.2 Linearity of scan-mirror motion.

The instrumental setup for measuring this is the same as for wavelength-to-frequency calibration; that is, the interferometer aperture should be filled with essentially monochromatic

radiation from an interference filter. If the scan-mirror motion is nonlinear, the resulting output audio frequency will vary accordingly during the sweep. For instance, if a 5-μ filter is used, the output frequency should be 150 cps; if by the end of the sweep the scan mirror velocity has dropped off by 10%, then the output frequency would have dropped to 135 cps. Therefore, the instrument output mixed with a sine wave of the same frequency from a stable oscillator will show beats if the interferometer output frequency changes. It is instructive to calculate the magnitude of effects which may be observed. For a 5-μ radiation line generating a 150-cps audio signal, there will be 44 cycles in a single 0.294-sec scan. Nonlinearity of 1 part in 50 (which is the maximum permitted) would yield about a 1-cycle beat in this scan time; this probably would be plainly visible if the oscilloscope scan were adjusted to permit observation of the whole mirror scan. If, on the other hand, a tenth of the mirror scan were observed on the scope, it would be easy to misinterpret the oscilloscope display.

For this test it is important that the filter fill the aperture of the instrument and be at approximately the same temperature as the instrument. Otherwise, radiation of the other than the test wavelength will be observed by the interferometer and will produce corresponding audio frequencies which will tend to beat with the oscillator and obscure the interpretation of the observed scope pattern.

3.1.4.3 Linearity of scan mirror driving voltage.
The ramp voltages which drive the mirror must be linear so that the resultant mirror motion will not be distorted by nonlinearities in the ramp voltage. The linearity can be checked by applying the drive voltage output to the external sweep of an oscilloscope and intensity modulating the sweep with a calibrated time marker. If the ramp voltage is linear, the intensity modulation pulses will occur evenly spaced over the full sweep.

3.1.4.4 Calibration of interferometer response.
When a wavelength-resolving ideal instrument such as a spectrometer or scanning interferometer at temperature T_1 looks at a blackbody at temperature T_2, it sees the difference in spectral distribution for the two temperatures, called the differential

radiance. The output curve for a nonideal instrument will not have the same proportionality constant for all the wavelengths of the differential radiance, and so an instrument calibration as a function of wavelength must be developed. The calibration consists of producing an instrument curve for a blackbody at some reasonable temperature and comparing the instrument curve with the theoretical calculable differential radiance.

3.1.4.5 Factors influencing interferometer calibration.

(a) The temperature differential between the instrument and the source must be large enough to give a high signal-to-noise ratio in the instrument output.

(b) The source must be truly a blackbody (or have a calibrated emissivity) and should fill the interferometer aperture without heating the instrument case. To this end the instrument case should be in good thermal contact with a fixed temperature heat sink and the instrument temperature should be measured with an accuracy of 0.1°C. Measurements should be made to determine whether there is any excessive time lag or actual differential between the instrument case temperature and the temperature indicated by the internal resistance thermometer.

(c) Absorbing gases such as water vapor or carbon dioxide must be excluded from the optical path between the source and interferometer. One means of doing this is to flush the space surrounding the setup with dry nitrogen gas.

(d) The wave-number scale should be expanded on the output strip chart to permit easy interpolation. Reasonable interpolation based on resolution considerations requires 20 to 30 individual points; therefore, 8 to 10 inches would appear reasonable for the wavelength scale expansion.

(e) The maximum amplitude on the output strip chart should be consistent with the signal-to-noise ratio.

(f) The temperature of both source and instrument must be kept constant to the desired accuracy for the duration of

the calibration test run. Since, as is discussed below, the analysis time required for one run is about 60 times the measuring time, it may be convenient for very accurate calibrations to put the measured data on magnetic tape and analyze the tape. In this case the time duration of the temperature-stability requirement is reduced by the factor of 60.

(g) An averaging filter should be inserted between the wave-analyzer output and the strip-chart recorded to smooth the strip-chart record. This will also have the benefit of defining the number of individual interferometer scans which are being averaged. If, for instance, it is desired to average 10 interferometer scans, the time constant of the averaging filter should be roughly 3 sec since each scan requires 0.3 sec. The use of such a filter in turn limits the rate at which the wave-analyzer frequency can be swept. Since as indicated previously the interferometer output frequency range of 30 to 150 cps is in essence divided into roughly 20 independent intervals, the use of a second averaging filter necessitates looking at each interval for at least 3 sec, so the total frequency sweep must take at least 60 sec. Allowing a time factor of three for overlap, this implies a maximum frequency sweep rate of 2/3 cps per sec for the wave analyzer. We can visualize use of even longer time-constant averaging filters, up to possibly 100 or more scans. For such tests instrument and source stability is required for much longer periods, and the use of a tape system becomes almost necessary. Note that it is necessary to use a tape loop long enough to contain at least 100 scans to obtain the full benefit from averaging 100 scans.

Obviously one can average several strip chart records instead of using one long-average record or one can even average several calibration curves. The relative merits of such procedures have to do with considerations of system drift, statistical errors, and efficiency in use of time.

(h) A calibration should be made of interferometer noise output as a function of audio frequency. This is necessary for the purpose of subtraction from low-level signals derived during

measurements where the source-to-instrument temperature differential is small. This measurement is of significance only if the analyzer band width and averaging filter time constant are recorded. For general information it would also be desirable to check the noise with a dummy load substituted for the actuator. This would show how much of the low-frequency noise is due to thermal fluctuation, actuator crosstalk, or microphonics.

3.1.4.6 Determination of gain stability of interferometer. It is very possible that to obtain the temperature resolution required at a low-temperature differential, the interferometer will have to be used as a total radiation detector. (This is likely because of the limitations of the Hughes analog-to-digital converter.) In view of this it is desirable to calibrate the over-all gain of the interferometer amplifier as a function of temperature. This is probably best done by accurately measuring the instrument output while calibrating the wavelength-to-frequency factor. Note that even at constant source temperature the instrument response as a function of instrument temperature should vary as T^4, since the instrument detector is heated by radiative transfer from the source.

3.2 Equipment Description

An outline and mounting drawing of the Surface Temperature Instrument is shown in Figure 2.

3.2.1 Sensor Head. Length, 5.082 inches; diameter, 1.25 inches; and weight, 0.56 lb.

3.2.2 Platter (Electronics Package). Length, 8.70 inches; width, 4.00 inches; depth, 0.917 inch; and weight, 1.291 lb.

3.2.3 Power Requirements. Current, 120 ma; and voltage, 29 v dc.

3.3 Testing and Calibration

3.3.1 Results of Functional Tests.

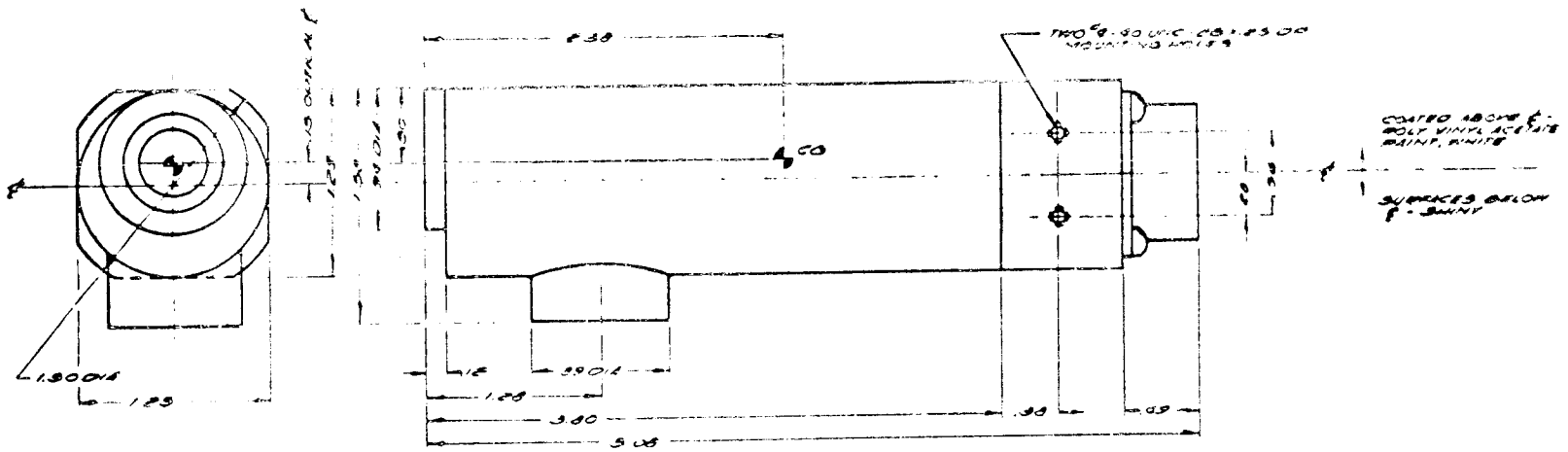

FIGURE 2. OUTLINE AND MOUNTING DRAWING OF THE SURFACE TEMPERATURE INSTRUMENT

3.3.1.1 Platter functional tests.

The platter functions were tested at temperature extremes to determine variations of total travel time, t, sweep length, B, and bolometer bias voltage ripple with temperature. Table 1 shows the test temperatures and results.

TABLE 1

TEMPERATURE EFFECTS ON ELECTRONICS

Temperature, °F	Sweep-drive Output		Bolometer Bias, vdc	Bolometer Bias Ripple, mv
	Amplitude, v	Time Duration, msec		
0	1.3	270	260	16.5
77	1.3	255	260	21.0
100	1.3	260	261	23.5

Sweep-drive output characteristics were obtained from the photographs in Figure 3 for the different temperatures. Time duration in Table 1 is the total period, or t_3. Sweep-drive amplifier output linearity was measured at 0 and 100°F. The interferometer sweep was used to drive the external sweep of an intensity modulated oscilloscope. Intensity modulation was accomplised by applying the 25-volt output of a time marker generator to the cathode of the cathode-ray tube. Table 2 shows the results of test.

TABLE 2

SWEEP LINEARITY AT TEMPERATURE EXTREMES

Temperature, °F	Distance between 5-msec Marks, mm		
	Start of Sweep	Middle	End of Sweep
0	1.6	1.8	1.7
100	1.5	1.8	1.6

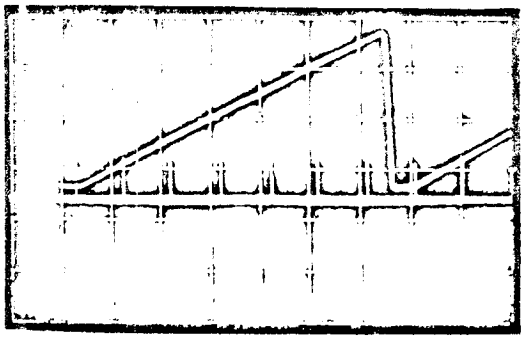

0°F

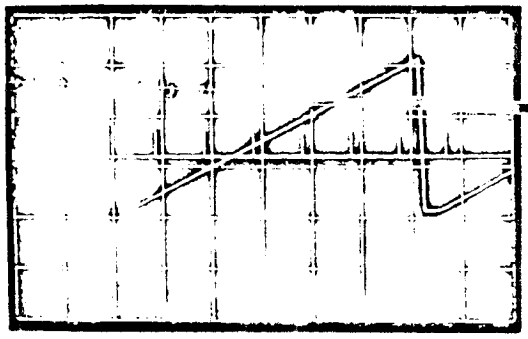

77°F

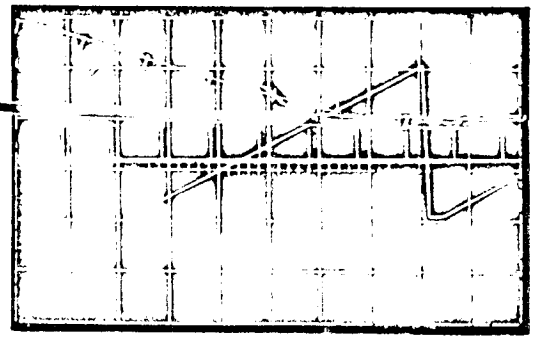

100°F

FIGURE 3. SWEEP DRIVE OUTPUT WAVEFORM AT VARIOUS TEMPERATURES

SWEEP DRIVE AMPLIFIER OUTPUT
MARKERS OCCUR AT 50-msec INTERVALS
AMPLITUDE, 0.5 volt/cm
OSCILLOSCOPE TIME SCALE, 50 msec/cm

The information shown in Table 2 was obtained by measuring distances under 10x magnification between 5-msec pulses on the photographs in Figures 4a and 5a for the two temperatures. Figures 4b and 5b show results of amplifying the output an unmeasured amount before applying it to the external sweep of oscilloscope. Note increased distance between markers. The accuracy obtained in measuring linearity by this method cannot be defined at this time.

3.3.1.2 System functional test.
With the sensor viewing a blackbody which was at a temperature of 399°K a spectrogram was obtained (Figure 6). From this spectrogram the total absolute response (TAR) for the instrument was calculated in Table 3. Figures 7, 8, 9, and 10 were obtained for the sensor viewing the same blackbody as that for Figure 6 at temperatures of 324°, 278.5°, 250°, and 282°K, respectively. The blackbody temperatures were then calculated as in Tables 4, 5, 6, and 7, respectively. The calculated values were compared with the measured values and the results listed in Table 8. The detailed test procedures are given in TEI Acceptance Test Procedure 387-212-89 (1).

3.3.1.3 Summary of objective and results of experiments.
The objective of the functional tests listed in this report was to prove that the instrument is capable of determining the surface temperature of the moon using its infrared spectrographic characteristics. The test results are not conclusive. System errors induced by test procedures far exceed the minimum error allowed for the system. These errors are explained in detail in the TEI letter dated April 11, 1962 to J. J. Thomas/E. L. Brown (Appendix B).

3.3.2 Results of Developmental Tests. The developmental tests performed at Block Associates are included in their final report (3).

3.4 Components Outline

The components listed in Table 9 are deviations from JPL preferred parts list. An explanation for the deviations are included.

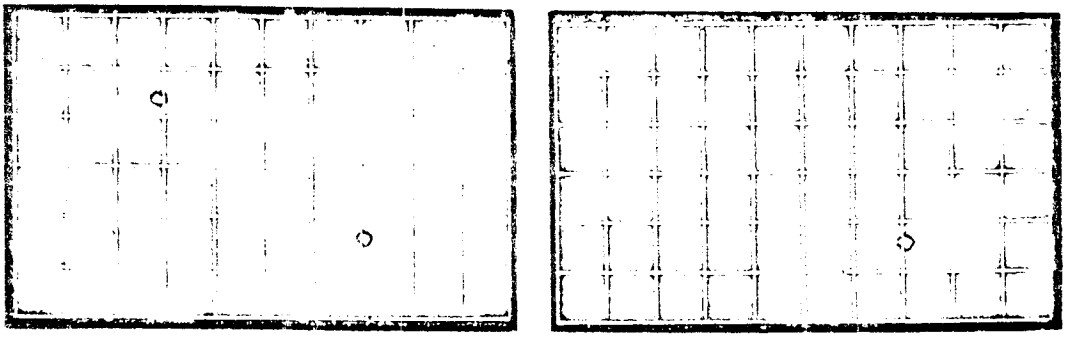

a. BEFORE AMPLIFICATION b. AFTER AMPLIFICATION

FIGURE 4. SWEEP LINEARITY CHECK AT 0°F

INTENSITY MODULATION, 5-msec PULSES
TOP TRACE (LEFT TO RIGHT), MIDDLE TO END OF SWEEP
BOTTOM TRACE (LEFT TO RIGHT), BEGINNING TO MIDDLE OF SWEEP
TEMPERATURE OF ELECTRONICS, 0°F

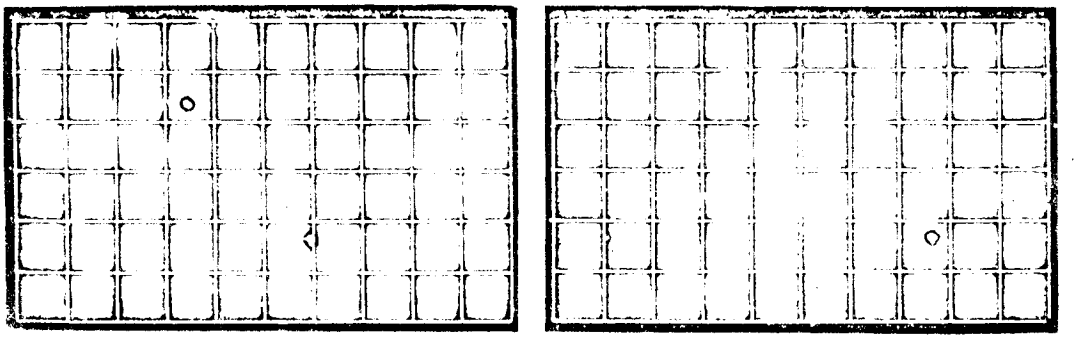

a. BEFORE AMPLIFICATION b. AFTER AMPLIFICATION

FIGURE 5. SWEEP LINEARITY CHECK AT 100°F

INTENSITY MODULATION, 5-msec PULSES
TOP TRACE (LEFT TO RIGHT), MIDDLE TO END OF SWEEP
BOTTOM TRACE (LEFT TO RIGHT), BEGINNING TO MIDDLE OF SWEEP
TEMPERATURE OF ELECTRONICS, 100°F

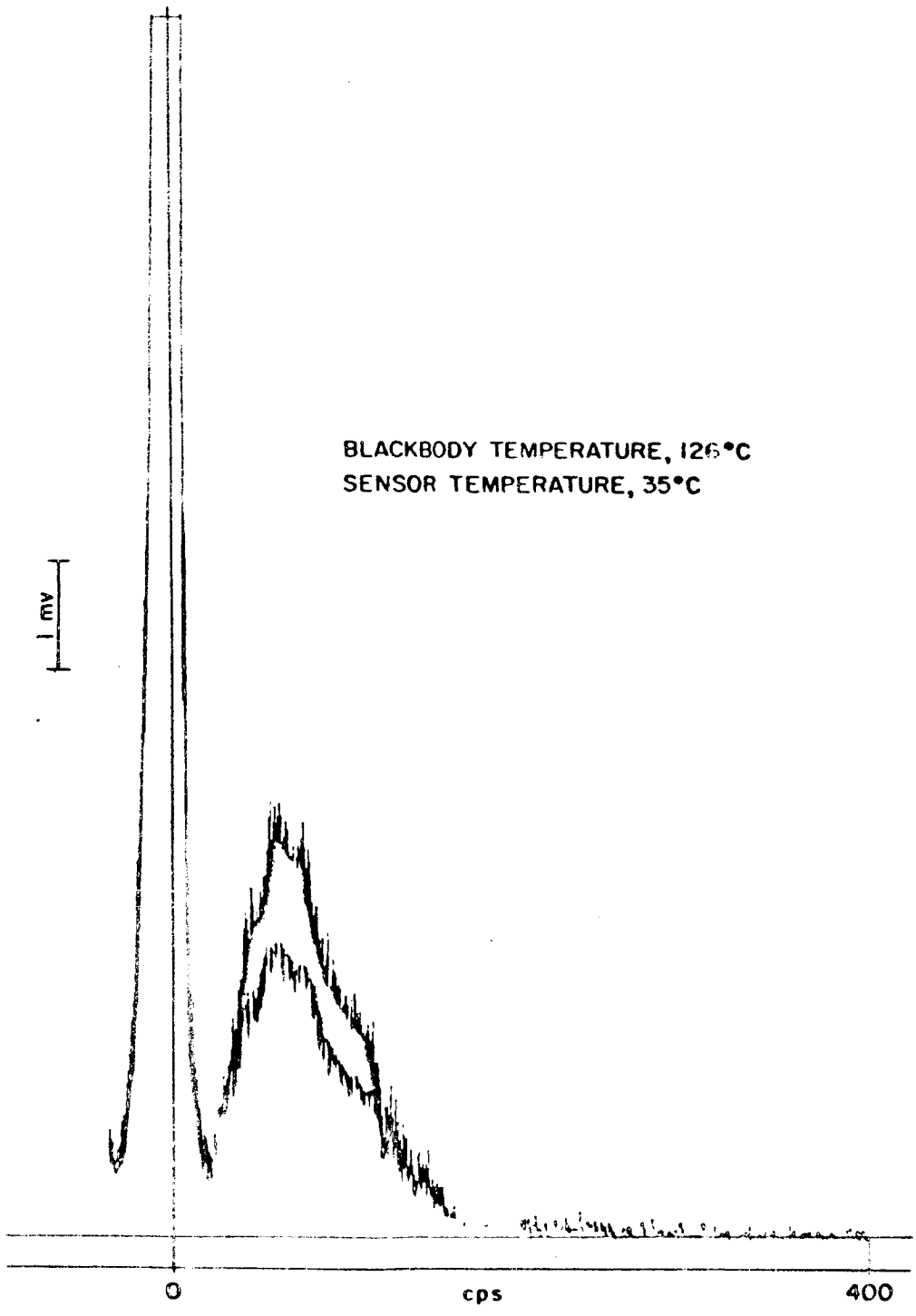

FIGURE 6. SPECTROGRAM I

TABLE 3

TOTAL ABSOLUTE RESPONSE CALCULATION

Blackbody Temperature, 399°K Sensor Temperature, 308°K

Wave No., n	Spectrogram Voltage, mv	Wavelength, λ, 10^{-4} cm	N_1 at 308°K,[a] w/cm-sr	N_2 at 399°K,[a] w/cm-sr	ΔN	λ^2, 10^{-8} cm^2	ΔN_σ,[b] 10^{-3} w/cm-sr	TAR,[c] mv/w/cm-sr
300	0.9990	33.3	0.9494	1.490	0.5406	1108.	5990	.1667
350		28.6				817.9		
400	1.609	25.0	2.228	3.778	1.550	625.0	9688	.1661
450		22.2				492.8		
500	2.742	20.0	3.992	7.352	3.360	400.0	13,440	.2040
550		18.2				331.2		
600	3.870	16.7	5.963	11.98	6.017	278.9	16,781	.1829
650		15.4				237.2		
700	3.008	14.3	7.910	17.42	9.510	204.5	19,448	.1547
750		13.3				175.9		
800	2.660	12.5	9.549	23.15	13.59	156.3	21,241	.1294
850		11.8				129.2		
900	2.309	11.1	10.69	28.60	17.91	123.2	22,065	.1044
950		10.5				110.5		
1000	1.943	10.0	11.28	33.52	22.04	100.0	22,040	.0882
1050		9.50				90.25		
1100	1.637	9.10	11.55	37.07	25.72	82.81	21,299	.0769
1150		8.70				75.69		
1200	1.303	8.50	11.32	39.20	27.98	72.25	20,906	.0699
1250		8.00				64.00		
1300	1.054	7.70	10.26	41.18	30.92	59.29	18,532	.0575
1350		7.40				54.76		
1400	0.7770	7.15	9.315	41.50	32.19	51.12	16,456	.0472
1450		6.90				47.61		
1500	0.5550	6.66	8.060	40.60	32.54	44.36	14,435	.0384

[a] Absolute spectral radiance in terms of wavelength.

[b] Absolute spectral radiance in terms of wave number.

[c] Total absolute response.

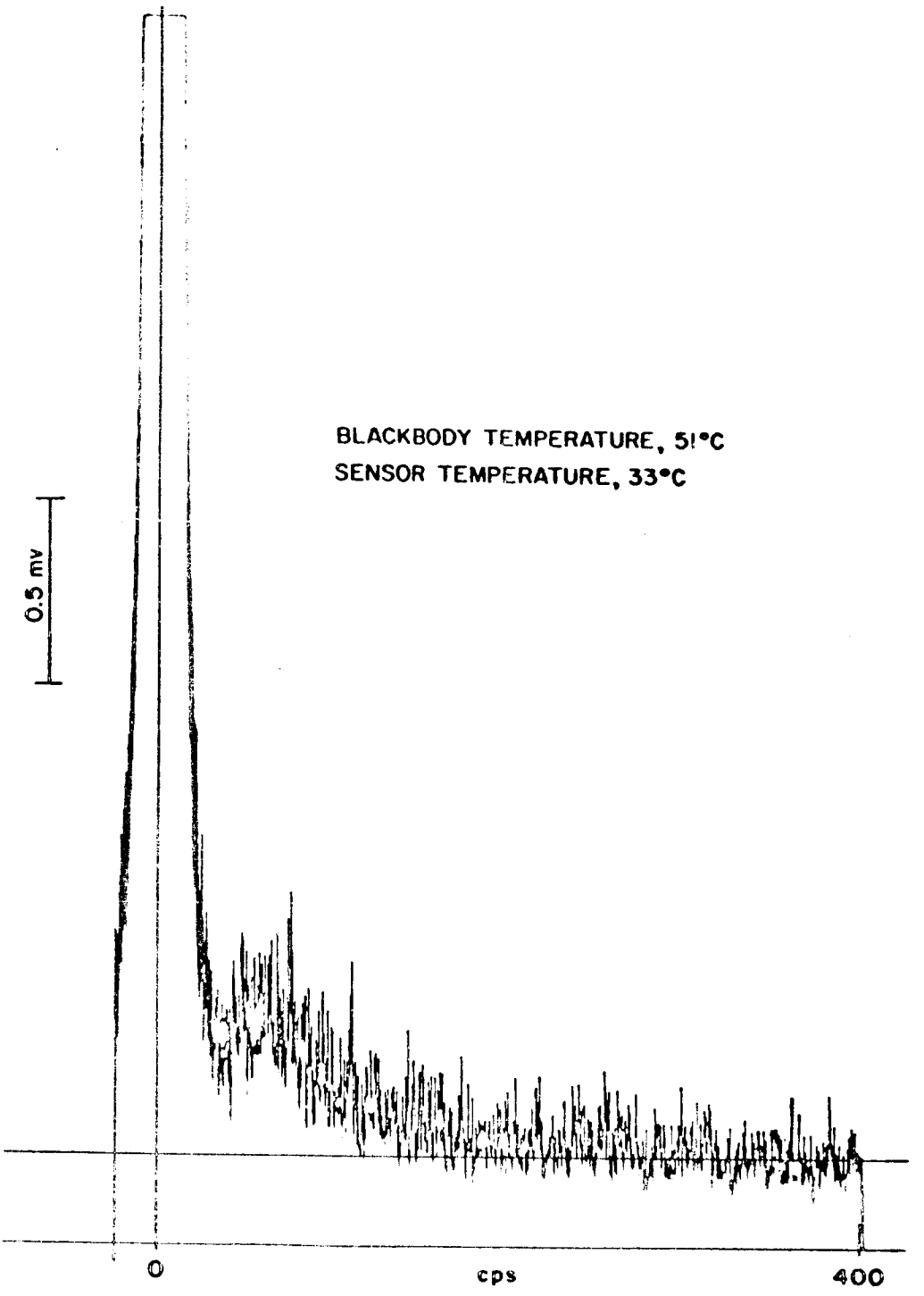

FIGURE 7. SPECTROGRAM II

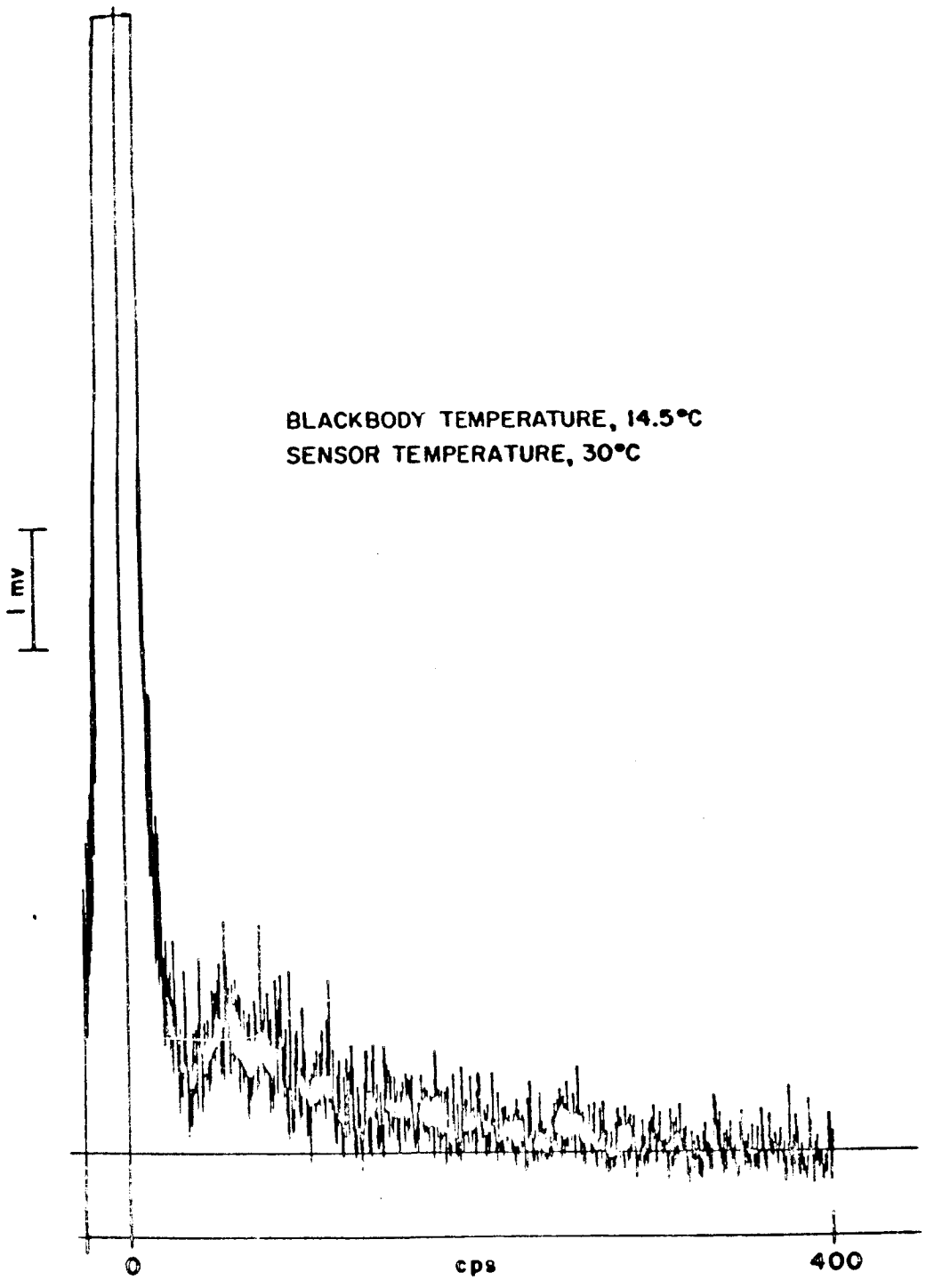

FIGURE 8. SPECTROGRAM III

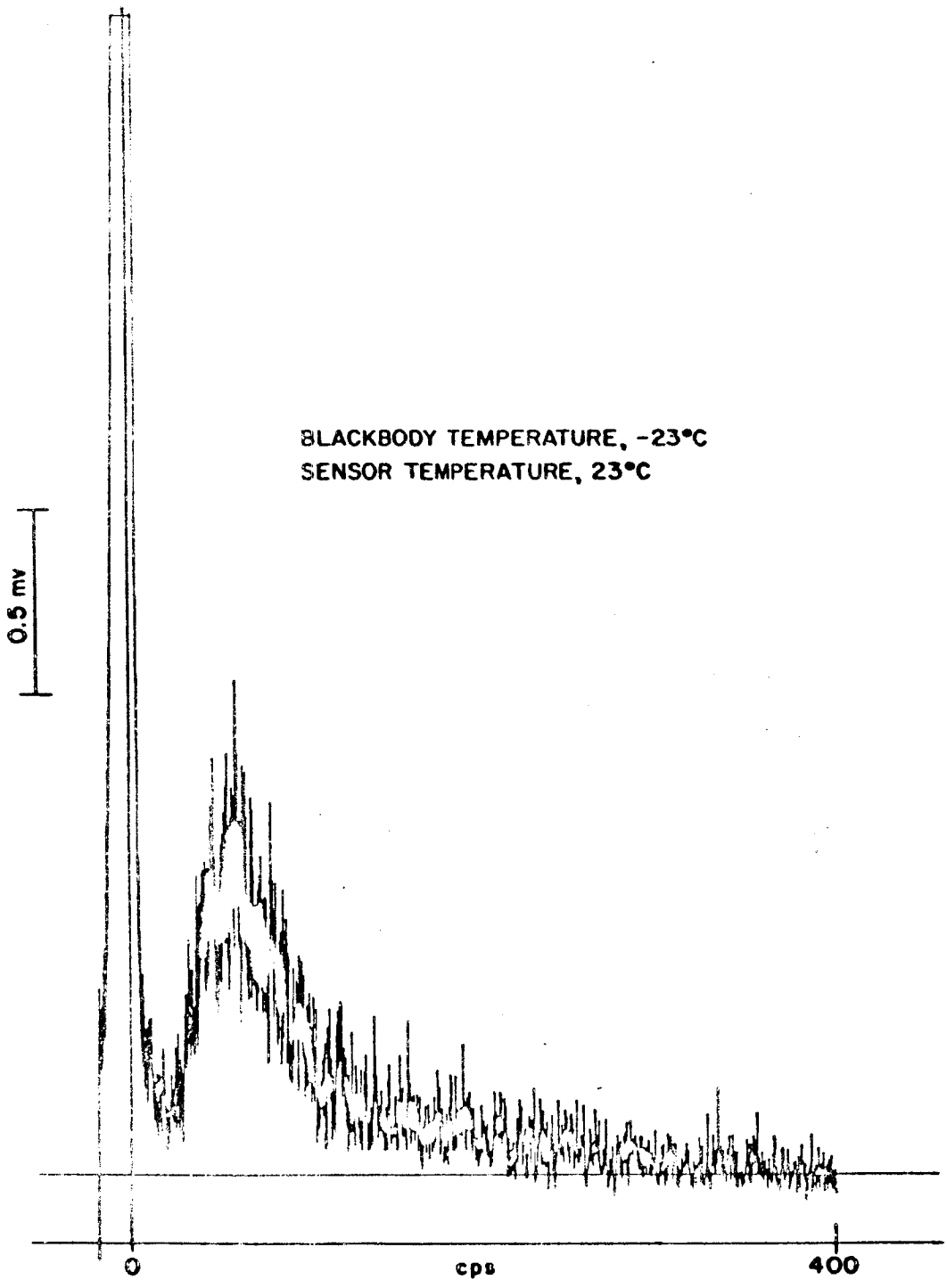

FIGURE 9. SPECTROGRAM IV

TABLE 5

BLACKBODY TEMPERATURE CALCULATION AT 278.5°K

Sensor Temperature, 303°K

Wave No., n	Spectrogram Voltage, mv	Wavelength, λ, 10^{-4} cm	W_1 at 278.5 °K[a] w/cm-sr	W_0 at 303°K[a] w/cm-sr	ΔN	λ^2, 10^{-8} cm^2	ΔN_w[b] 10^{-3} µw/cm-sr	TAR,[c] mv/w/cm-sr	Blackbody Temp. (calc.), °K
300	0.8000	33.3	0.4877	0.9208	0.4331	1108.	4799	.1467	223
350		28.6				817.9			
400	0.6000	25.0	1.841	2.149	0.5779	625.0	3612	.1461	284
450		22.2				492.8			
500	0.8800	20.0	2.746	3.825	1.079	400.0	4316	.2040	268
550		18.2				331.2			
600	1.100	16.7	3.522	5.678	2.156	278.9	6014	.1829	261
650		15.4				237.2			
700	1.050	14.3	4.161	7.480	3.319	204.5	6787	.1547	259
750		13.3				175.9			
800	0.9500	12.5	4.113	8.960	4.847	156.3	7576	.1254	252
850		11.8				129.2			
900	0.8200	11.1	9.590	9.965	6.375	123.2	7854	.1044	245
950		10.5				110.3			
1000	0.7500	10.0	1.957	10.44	8.503	100.0	8503	.0882	224
1050		9.50				90.25			
1100	0.6170	9.10	3.7420	10.45	9.688	82.81	8029	.0769	207
1150		8.70				75.69			
1200	0.5100	8.34	5.7800	10.16	10.94	72.95	7981	.0539	208
1250		8.00				64.00			
1300	0.5050	7.70	5.529	9.281	14.81	59.29	8789	.0575	279
1350		7.40				54.76			
1400	0.6800	7.15	11.55	8.361	19.89	51.12	10,169	.0472	318
1450		6.90				47.61			
1500	0.6300	6.66	18.07	7.171	25.24	44.36	11,198	.0386	349
								Average	281
								Error	± 2.5°

[a] Absolute spectral radiance in terms of wavelength.

[b] Absolute spectral radiance in terms of wave number.

[c] Total absolute response.

TABLE 6

BLACKBODY TEMPERATURE CALCULATION AT 250°K

Sensor Temperature, 296°K

Wave No., ν	Spectrogram Voltage, mv	Wavelength, λ, 10^{-4} cm.	N_1 at 250°K[a], w/cm-sr	N_2 at 296°K[a], w/cm-sr	ΔN	λ^2, 10^{-8} cm^2	ΔN_ν[b] 10^{-3} μw/cm-sr	TAR,[c] mv/μw/cm-sr	Blackbody Temp. (calc.), °K
300	.5163	33.3	0.7098	0.8810	0.1712	1108.	1897	.1667	265
350		28.6				817.9			
400	.5394	25.0	1.519	2.038	0.5195	625.0	3247	.1661	261
450		22.2				492.8			
500	.8025	20.0	2.613	3.596	0.9835	400.0	3934	.2040	264
550		18.2				331.2			
600	.8158	16.7	3.688	5.287	1.599	278.9	4460	.1829	264
650		15.4				237.2			
700	.7492	14.3	4.527	6.895	2.368	204.5	4863	.1547	264
750		13.3				175.9			
800	.6160	12.5	5.031	8.174	3.143	156.3	4912	.1254	264
850		11.8				129.2			
900	.5161	11.1	4.983	8.995	4.012	123.2	4963	.1044	261
950		10.5				110.3			
1000	.4329	10.0	4.412	9.320	4.908	100.0	4908	.0882	257
1050		9.50				90.25			
1100	.3665	9.10	3.458	9.230	5.752	82.81	4763	.0769	250
1150		8.70				75.69			
1200	.2997	8.34	2.472	8.902	6.431	72.93	4690	.0639	242
1250		8.00				64.00			
1300	.2364	7.70	1.906	8.020	6.934	59.29	4113	.0575	225
1350		7.40				54.76			
1400	.1998	7.15	1.716	7.145	8.281	51.12	4233	.0472	233
1450		6.90				47.61			
1500	.1665	6.66	1.726	6.049	9.775	44.36	4336	.0384	278
								Average	277
								Error =	27°

[a] Absolute spectral radiance in terms of wavelength.

[b] Absolute spectral radiance in terms of wave number.

[c] Total absolute response.

TABLE 7

BLACKBODY TEMPERATURE CALCULATION AT 282°K

Sensor Temperature, 298°K

Wave No., n	Spectrogram Voltage, mv	Wavelength, λ, 10^{-4} cm	N_1 at 282°K[a], w/cm-sr	N_2 at 298°K[a], w/cm-sr	ΔN	ν, 10^{-4} cm^{-1}	ΔN_n[b], 10^{-3} w/cm-sr	TAR[c], mv/w/cm-sr	Blackbody Temp. (calc.), °K
300	.1415	33.3	0.8146	0.8923	0.0777	3108.	861	.1667	284
350		28.6				817.9			
400	.1925	25.0	1.885	2.070	0.1854	625.0	1159	.1661	286
450		22.2				492.8			
500	.2777	20.0	3.321	3.661	0.3403	400.0	1361	.2040	287
550		18.2				331.2			
600	.3107	16.7	4.789	5.398	0.6092	278.9	1699	.1829	287
650		15.4				237.2			
700	.3025	14.3	6.100	7.060	0.9560	204.5	1955	.1547	286
750		13.3				175.9			
800	.2822	12.5	6.955	8.395	1,440	156.5	2250	.1254	285
850		11.8				129.2			
900	.2612	11.1	7.237	9.266	2.029	123.2	2502	.1044	282
950		10.5				110.5			
1000	.2392	10.0	6.919	9.631	2.712	100.0	2712	.0882	279
1050		9.50				90.25			
1100	.2145	9.10	6.179	9.547	3.368	82.81	2789	.0769	276
1150		8.70				75.69			
1200	.1875	8.34	5.227	9.250	4.023	72.93	2934	.0639	273
1250		8.00				64.00			
1300	.1677	7.70	3.447	8.367	4.920	59.79	2917	.0579	261
1350		7.40				54.76			
1400	.1485	7.15	1.325	7.479	6.154	51.12	3146	.0472	257
1450		6.90				47.61			
1500	.1320	6.66	1.394	8.356	7.750	44.36	3438	.0384	247
									Average 274
									Error ±4°

[a] Absolute spectral radiance in terms of wavelength.

[b] Absolute spectral radiance in terms of wave number.

[c] Total absolute response.

TABLE 8

BLACKBODY TEMPERATURE CALCULATION

ACCURACIES

Sensor Temperature, °K	Blackbody Temperature (Measured), °K	Blackbody Temperature (Calc.), °K	Error, °K
306	324	324	0.0
303	278.5	281	+2.5
296	250	277	+27.0
298	282	274	-8.0

TABLE 9

COMPONENT DEVIATIONS FROM JPL PREFERRED PARTS LIST

Component	Reason for Deviation
Microdot Cable No. SO-3819MC - 30	Availability
Sealectro Ft-M2 WP20 Teflon Feed Through	Availability
Cambion Type 1785-A Chessman	Availability
Cambion Type 1488-4 Solderlug	Availability
Fairchild 2N2049 Transistors in TO - 18 Case	This item not on JPL list but were listed as preferred by HAC
Stevens MX-9 Thermostat	The MX-9 was used over the MX-1 because MX-9 has ground terminal
Corning Glass WL-5-510 Capacitor	Physical size consideration
Vitramon CK Series Capacitors	Parts delivery precluded the use of preferred UK series
Triad EC 1500 1.5 h Inductor	Physical size limitations
Fairchild 2N 2049 Transistor Standard Case	Not on JPL list but were listed as preferred by HAC
Transformers, Block T-700, T-701	Block designed for specific use
Minco Model S-31 Platinum Resistance Thermometer	This was used to provide a reduction of components over circuit required

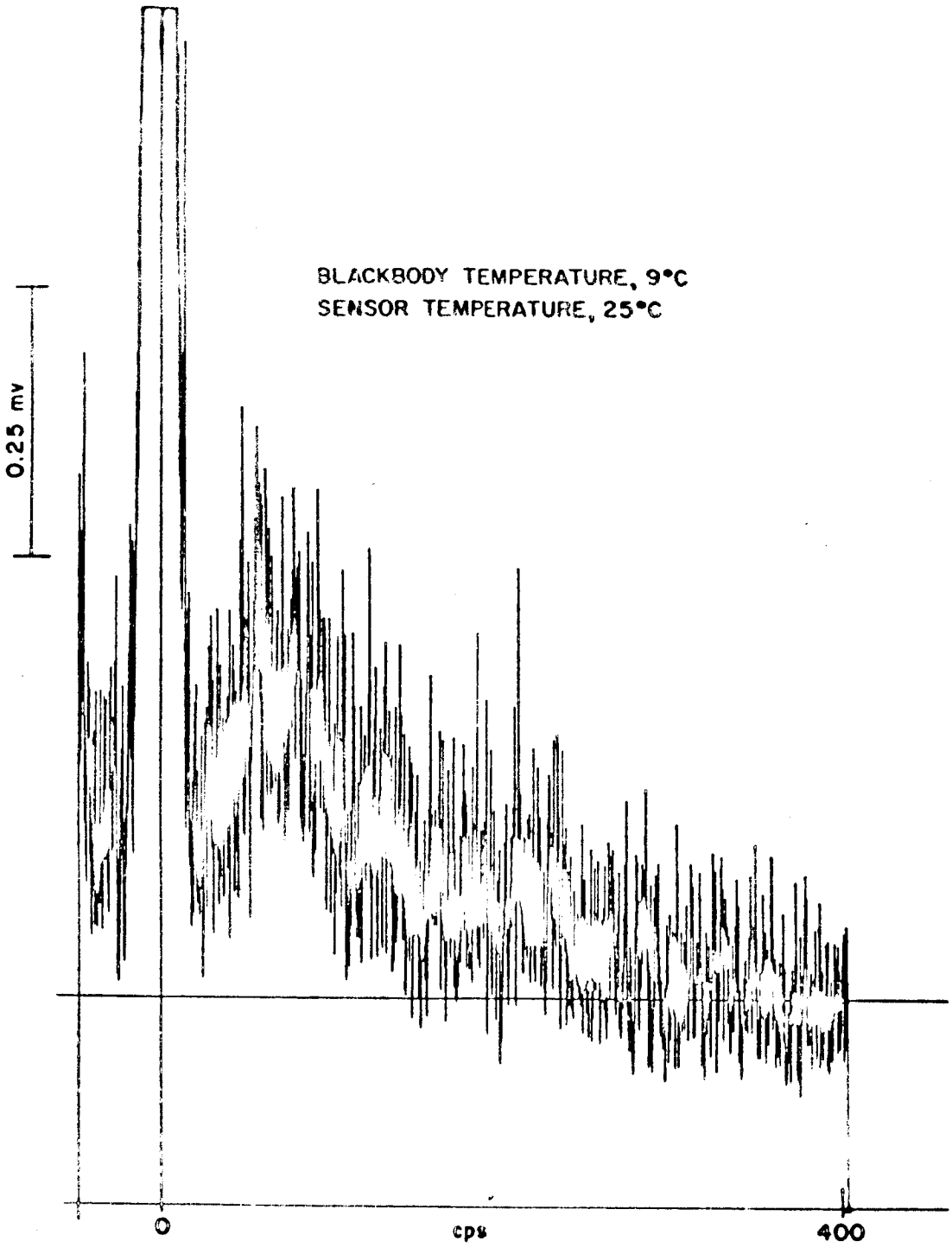

FIGURE 10. SPECTROGRAM V

TABLE 4

BLACKBODY TEMPERATURE CALCULATION AT 324°K

Sensor Temperature, 306°K

Wave No., a	Spectrogram Voltage, mv	Wavelength λ, 10^{-4} cm	N_1 at 306°K,[b] w/cm-sr	N_2 at 324°K,[b] w/cm-sr	ΔN	λ^2, 10^{-8} cm^2	ΔN_n,[b] 10^{-1} μw/cm-sr	TAR,[c] mv/μw/cm-sr	Blackbody Temp. (calc.), a °K
300	.3330	33.3	3.9379	4.418	0.4801	1108.	1998	.1667	337
350		28.6				817.9			
400	.2990	25.0	2.797	4.485	0.2880	625.0	1800	.1661	324
450		22.2				492.8			
500	.3890	20.0	3.925	4.402	0.4768	400.0	1907	.2040	320
550		18.2				331.2			
600	.4290	16.7	5.869	6.690	0.8412	278.9	2346	.1829	321
650		15.4				237.2			
700	.3830	14.3	7.735	8.947	1.212	204.5	2476	.1547	319
750		13.3				175.9			
800	.3330	12.5	9.508	11.01	1.699	156.3	2656	.1254	320
850		11.8				139.2			
900	.2890	11.1	10.40	12.65	2.247	123.2	2768	.1044	320
950		10.5				110.3			
1000	.2060	10.0	10.91	13.26	2.346	100.0	2336	.0882	319
1050		9.50				90.25			
1100	.1998	9.10	10.98	14.01	3.031	82.81	2510	.0769	321
1150		8.70				75.69			
1200	.1665	8.34	10.75	14.30	3.575	72.93	2606	.0639	323
1250		8.00				64.00			
1300	.1398	7.70	9.860	13.96	4.100	59.29	2431	.0575	324
1350		7.40				54.76			
1400	.1165	7.15	8.924	13.75	4.828	51.12	2468	.0472	327
1450		6.90				47.61			
1500	.0999	6.66	7.695	13.56	5.866	44.36	2602	.0384	332
								Average	324
								Error	± 8

[a] Absolute spectral radiance in terms of wavelength.

[b] Absolute spectral radiance in terms of wave number.

[c] Total absolute response.

3.5 Packaging Philosophy

The packaging philosophy used by Block Associates is included in their final report (3).

3.6 Theoretical Studies

The theoretical studies were performed at Block Associates and are included in their final report (3).

3.7 Environmental Test Results

Environmental tests were limited to those performed on the electronics platter as reported in the functional test section of this report (3.3.1.1).

3.8 Recommendations

Thought should be given to the practicability of increasing the diameter of surface units to allow repackaging of the preamplifier in sensor heads for increased reliability. Present space limitations necessitate deviations from accepted practices.

4. SURFACE THERMAL DIFFUSIVITY INSTRUMENT

URD 9

Control Item X239229

The detected signal is amplified approximately 50 db between the bolometer detector output and the instrument output by a three-stage transistor preamplifier located in the transducer and a three-stage postamplifier. The power for the mirror drive is generated by a sawtooth generator and amplified by a single-stage amplifier, push-pull phase inverter, and a push-pull amplifier. Bias voltages for the transistor circuits are generated by a dc-to-dc converter having outputs of +12 volts, -12 volts, +150 volts, and -150 volts. All voltages are regulated within the electronics package, which is to be located in a temperature-controlled electronic compartment in the spacecraft.

4.2 Equipment Description

The description of the device capable of performing both day and night thermal diffusivity experiments is given below. Figure 11 shows the assembly drawing, Figure 12 is a mounting diagram, and Figure 13 is a photograph of the completed shield.

The top member of the solar radiation shield is a truncated cone with a surface area of 92 $in.^2$ This cone is spun from 0.032 inch 6061T6 aluminum plate. A white polyvinyl acetate paint is used to coat the outer or convex surface, which is exposed to solar radiation. The inner or concave surface is brightly polished and coated with a thin film of silicone monoxide to prevent oxidation. The low thermal emissivity of polished aluminum is desired for the concave surface to reduce heat flow from the cone to the other components. A triangular epoxy glass-fiber mounting bracket connects the cone to the rest of the shield. Glass fiber is used both for strength and thermal isolation. The dimensions of the cone are (a) diameter, 10 inches; (b) height, 2.70 inches; and (c) slope of cone, 31°. The weight of the cone is 0.262 lb.

A radiation shield is placed between the top cone and the bottom heater plate. This reflecting inner shield is constructed from 0.020-inch 5052 aluminum sheet. Both surfaces of the shield are brightly polished and coated with silicone monoxide film. This radiation shield prevents heat flow from the top cone to the heater plate during the day and from the heated plate to the cone during the night. A rolled edge of the shield provides a mounting surface for the reflecting skirt. The shield is 10 inches in diameter and 0.345 inch in height and weighs 0.136 lb.

The heater plate is fabricated from a single section of copper-clad epoxy glass-fiber laminate. Insulating voids are produced in the copper by a

4.1 System Description

The thermal diffusivity measurement of a substance is accomplished by abruptly altering the radiation to or from a region of known geometry. A study of the surface temperature of this region immediately following abrupt change in radiation provides information necessary in calculating thermal conductivity and diffusivity (4). Two methods of producing an abrupt change in radiation are described below.

First, a shadow-free area of the lunar surface will be exposed to solar radiation for a period of not less than 1 hour prior to this experiment. A shield will then be placed over a portion of this surface to prevent the solar radiation from reaching an area of known geometry. This shield will be lowered from the Surveyor spacecraft to a position approximately 2 inches above the surface of the moon. A reflecting skirt extending downward from the shield will obstruct both incoming and outgoing scatter radiation. The coating of the surface of the shield exposed to solar radiation is selected to provide a low equilibrium temperature; i.e., the coating has a relatively low absorptivity in the region of the spectrum occupied by solar radiation and a high emissivity in the infrared region. Appendix C demonstrates the calculations necessary in the selection of this coating.

In the second method a thermal-diffusivity measurement is made during the night by first allowing the surface in question to cool to the normal night-time temperature. A heated plate thermostatically controlled to a temperature of 400°K with a known surface emissivity will then be placed over the area in question and the time rate of change of the surface monitored. It is necessary that the plate reach operating temperature within 0.5 hour and maintain this temperature for a period of not less than 1 hour for this experiment. The heat radiated from the plate to the lunar surface is determined by the parameters illustrated in the calculations found in Appendix D.

Temperature measurements of the lunar surface in the above-mentioned experiments will be made with an interferometer spectrometer mounted in the center of the combination solar shield and heated plate. The interferometer is a modified Michelson interferometer which utilizes an electro-mechanical mirror-drive mechanism and a bolometer detector to convert incident infrared radiation into audio frequencies whose amplitudes vary with variations in radiation differences between the object being viewed and the interferometer bolometer.

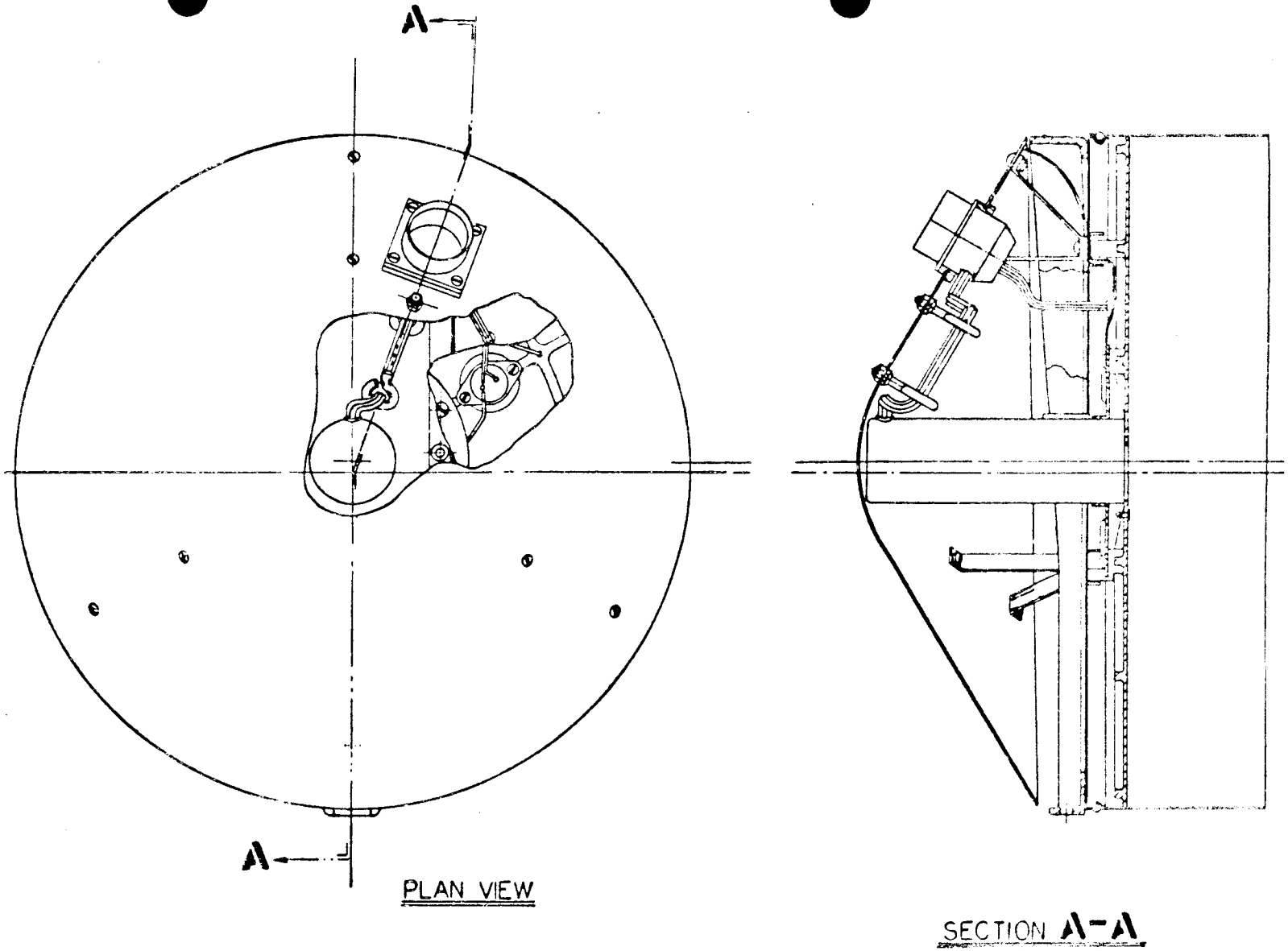

FIGURE 11. ASSEMBLY DRAWING OF THE SURFACE THERMAL DIFFUSIVITY INSTRUMENT

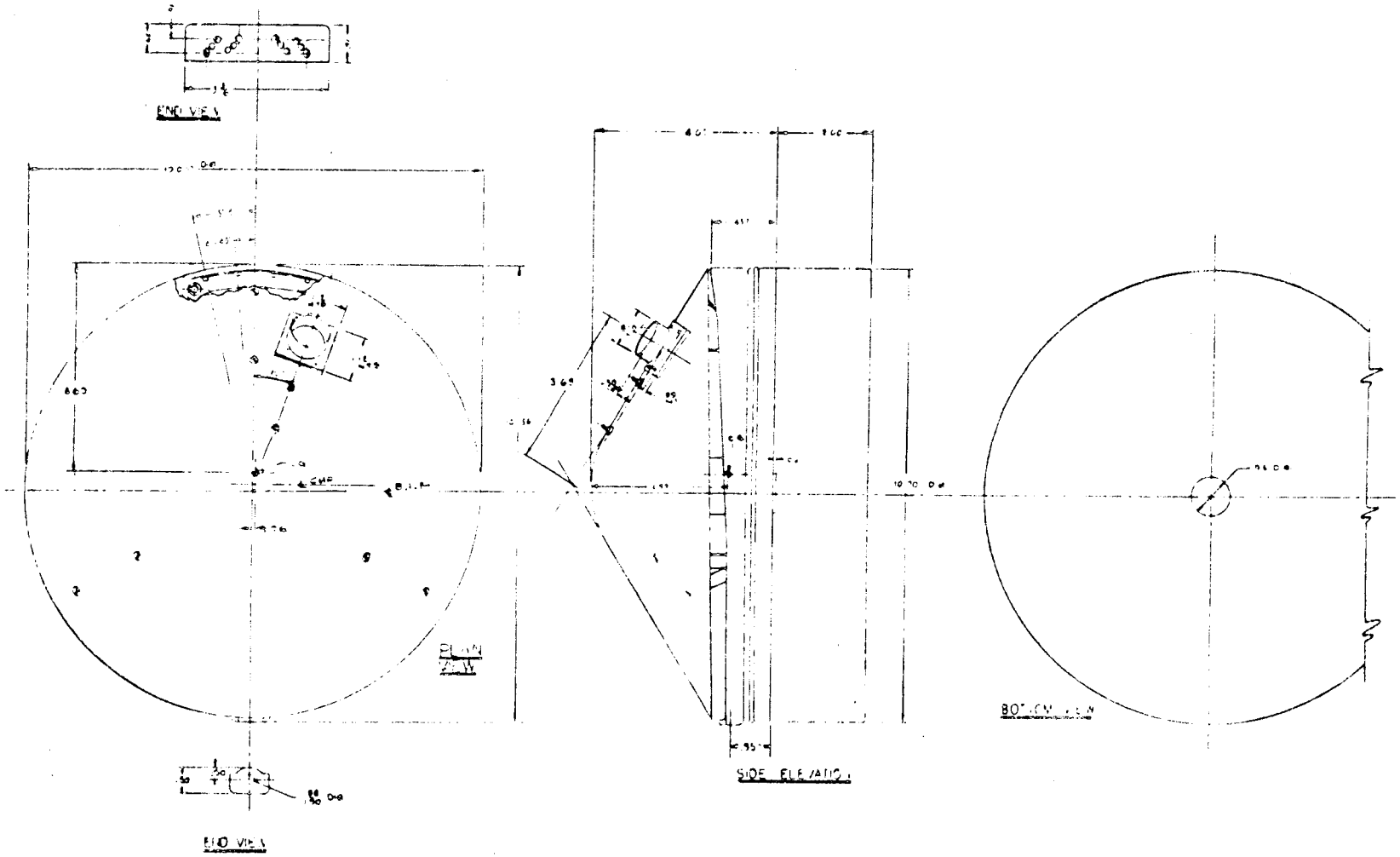

FIGURE 12. OUTLINE & MOUNTING DIAGRAM OF THE SURFACE THERMAL DIFFUSIVITY INSTRUMENT

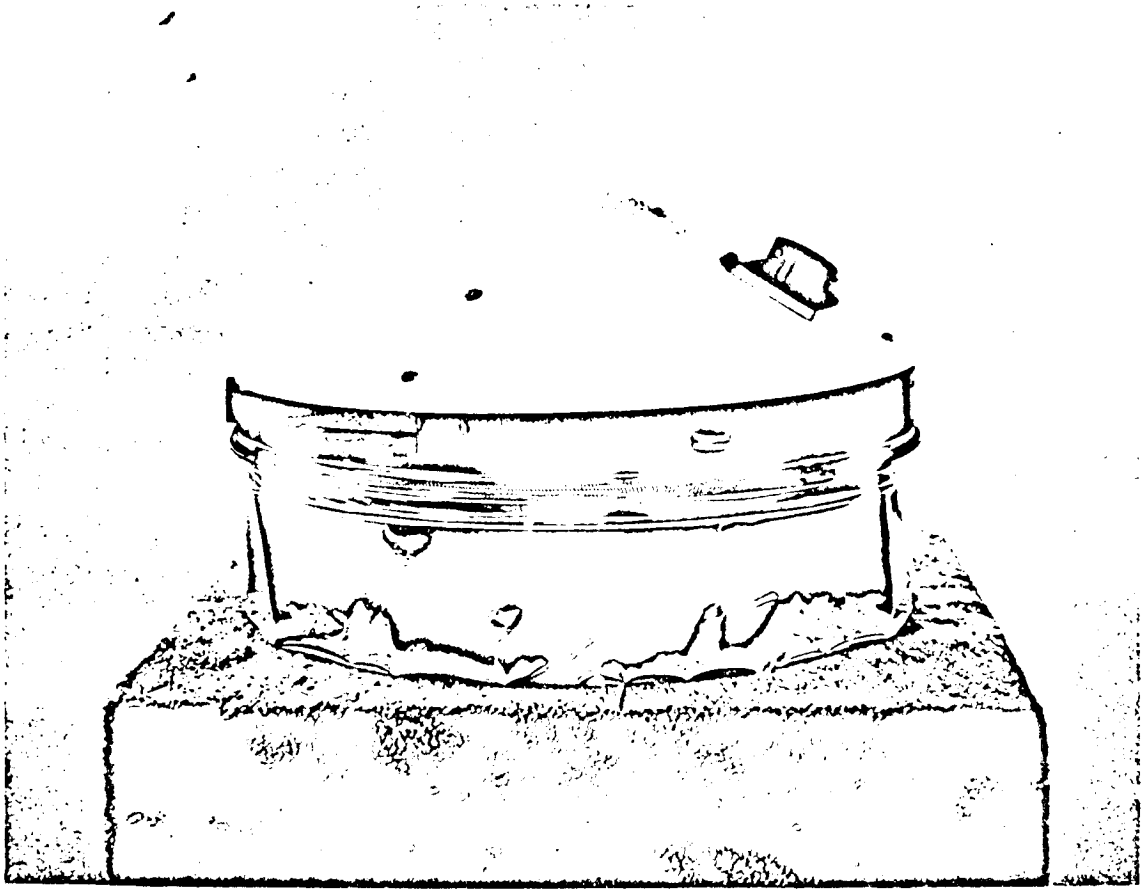

FIGURE 13. PHOTOGRAPH OF THE COMPLETED SURFACE THERMAL DIFFUSIVITY INSTRUMENT

photo-etching process, leaving an electrical conductor in the form of an Archimedes' spiral. This configuration was chosen to obtain an even power distribution over the radiating surface of the plate. The calculations necessary in designing the heating element are given in Appendix E. The radiating surface of the plate is coated with a flat black paint having an emissivity of 0.93-0.95. The temperature of the plate is controlled by a bimetallic disk thermostat which regulates the electrical power supplied to the heater element. A thermocouple is embedded in the laminate to sense the heater-plate temperature.

The heater plate is attached to a epoxy glass-fiber laminate mounting bracket by three posts which are an integral part of the laminate. The spacecraft mounting bracket is riveted to the top side of the inner shield. Stiffeners between the inner shield and the heater plate are riveted to the mounting bracket and extend outward to the heater-plate mounting posts. To assemble the shield a single screw is passed through the bottom of each of the triangular glass-fiber mounting brackets through a hole in the inner radiation shield, then through a hole in the stiffener, and finally it is threaded into the heater-plate mounting post. The heater plate is 10 inches in diameter and 0.6 inch high, and its weight is 0.550 lb. Its nominal power requirements are 18 to 28 volts dc, and the heater resistance is 3.8 ohms at 300°K. The power requirements of the heater plate over a temperature range of 70 to 400°K at input voltages of 18 and 28 volts are given in Figure 14.

A spider mounting bracket attaches the interferometer spectrometer to the heater plate. The interferometer spectrometer is positioned above a centrally located hole in the heater through which the lens housing extends. A half-angle field of view of 12° is provided by the lens, which is located approximately 2 inches above the lunar surface. The interferometer spectrometer sensor head is 3.8125 inches in length, and its diameter is 1.25 inches without the spider and 3.50 inches with it. Its total weight is 0.499 lb. The dimensions of the electronics package (platter) are as follows: (a) length, 8.70 inches; (b) width, 4.00 inches; (c) depth, 0.917 inch; and (d) weight 1.291 lb. Its total power requirements are 120 ma and 29 volts dc. Aluminized Mylar film is used as the reflecting skirt, which is cemented to the inner shield. A stainless-steel coiled spring is used for added attachment strength. The aluminized side of the skirt is placed toward the center of the instrument, because this side is more reflective. The dimensions of the skirt are as follows: (a) diameter, 10 inches; (b) height, 2.68 inches; and (c) thickness,

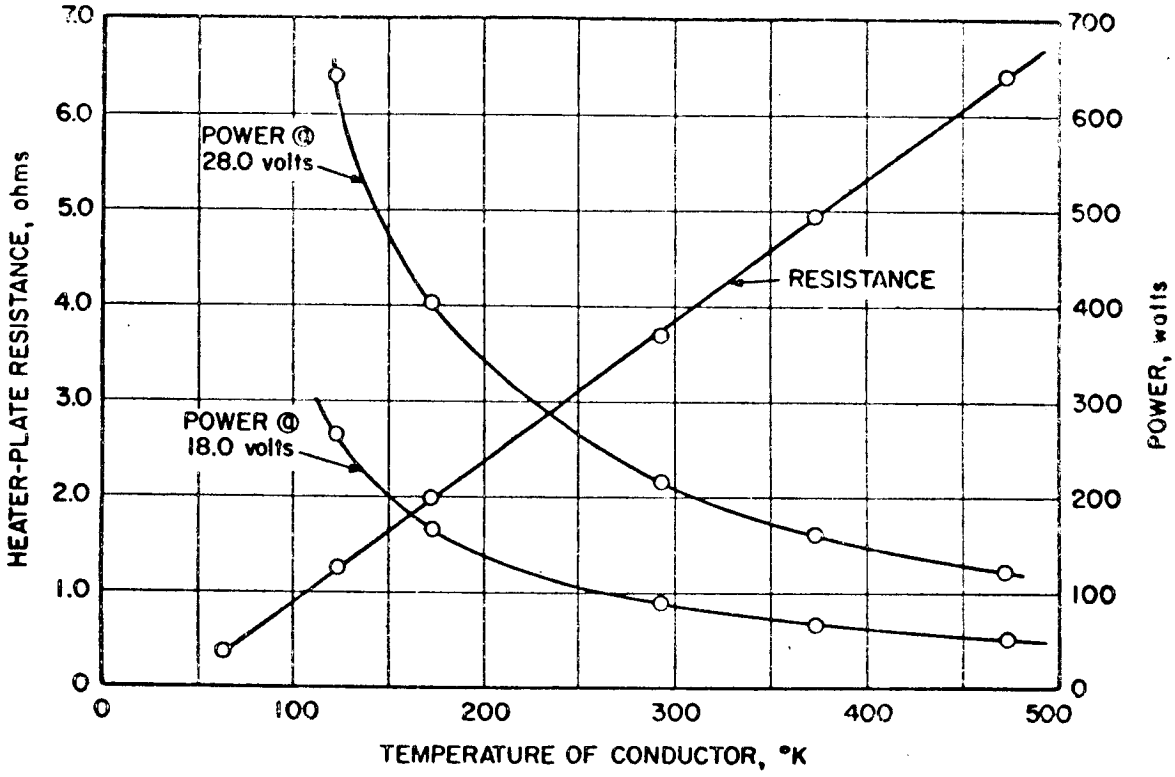

FIGURE 14. POWER REQUIREMENTS OF THE HEATER PLATE

0.0005 inch. Its weight is 0.002 lb. The dimensions of the completely assembled instrument are: (a) diameter, 10 inches; (b) height with skirt extended, 6.0 inches: and (c) height with skirt folded, 4.0 inches. Its weight is 1.73 lb including miscellaneous structural pieces.

4.3 Testing and Calibration

Only minimum testing of the device was made because of the lack of sufficient time between fabrication and the required delivery of the instrument. A vacuum system of sufficient capacity to reduce the pressure to 10^{-5} mm Hg with diffusivity samples in place was not available; therefore, no tests were conducted to determine accuracies in measuring thermal diffusivity. However, certain functional tests were made on the individual components.

4.3.1 Results of Functional Tests.

4.3.1.1 Interferometer spectrometer functional tests.
The platter functions were tested at temperatures from 273 to 373°K to determine variations with temperature. Results are given in Table 10. (These temperature variations are those expected in the thermal-controlled spacecraft electronics compartments.)

TABLE 10

TEMPERATURE EFFECTS ON ELECTRONICS

Ambient Temperature, °F	Mirror-sweep Drive Output		Bolometer Bias Voltage, v dc	Bolometer Bias Voltage Ripple, mv
	Amplitude, v	Time Duration, msec		
0	1.2	265	190	7.5
77	1.6	255	194	12.9
100	1.6	320	194	14.8

Sweep-drive output characteristics were obtained from the photographs in Figure 15 for three temperatures. Time duration in

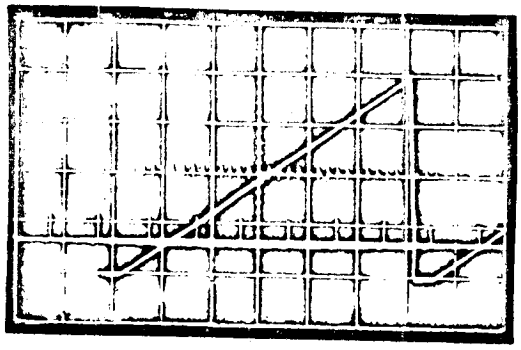

0°F

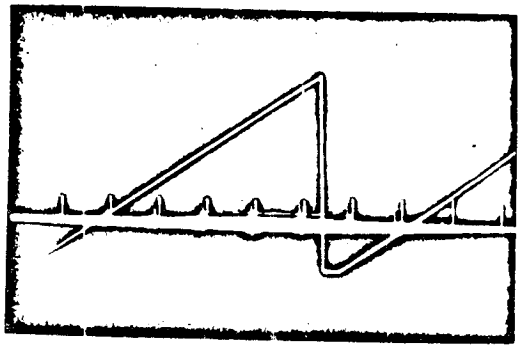

77°F

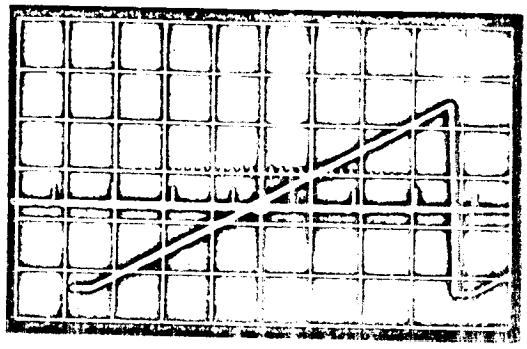

100°F

FIGURE 15. SWEEP DRIVE OUTPUT WAVEFORM AT VARIOUS TEMPERATURES

SWEEP-DRIVE AMPLIFIER OUTPUT
MARKERS OCCUR AT 50-msec INTERVALS
AMPLITUDE, 0.5 volt/cm
OSCILLOSCOPE TIME SCALE, 50 msec/cm

Table 10 is the total period and includes flyback time.

Linearity of the sweep drive amplifier output was measured at 0, 77, and 100°F. The sweep output was used to drive the external sweep of an intensity modulated oscilloscope. Intensity modulation was accomplished by applying the 25-volt output of a time marker generator to the cathode of the cathode-ray tube. Table 11 shows the results of these tests.

TABLE 11

SWEEP LINEARITY

Temperature, °F	Distance between 5-msec Marks, mm		
	Start of Sweep	Middle	End of Sweep
0	2.1	2.1	2.0
77	2.1	2.1	1.9
100	2.2	2.0	2.1

The information shown in Table 11 was obtained by measuring distance between 5-msec pulses under 10x magnification on Figures 16a, 17a, and 18a for the three temperatures. Figures 16b, 17b, and 18b show results of amplifying the output an unmeasured amount before applying it to the external sweep of the oscilloscope. Note the increased distance between markers. The accuracy obtained in measuring linearity by this method cannot be defined at this time.

With the sensor viewing a blackbody which was at a temperature of 403°K a spectrogram was obtained (Figure 19). From this spectrogram the total absolute response (TAR) for the instrument was calculated in Table 12. Figures 20, 21, and 22 were obtained for the sensor viewing the same blackbody as that for Figure 19 but at temperatures of 318, 276, and 248°K, respectively. The blackbody temperatures were then calculated as in Tables 13, 14, and 15, respectively. The calculated values were compared with the measured values and the results listed in Table 16.

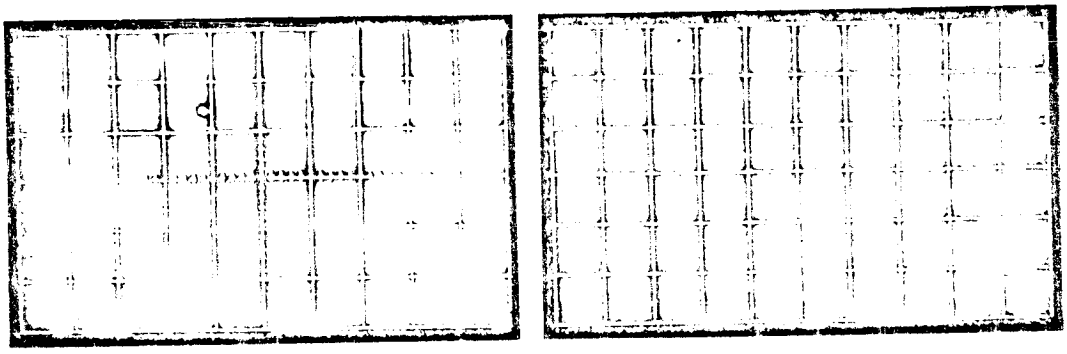

a. BEFORE AMPLIFICATION

b. AFTER AMPLIFICATION

FIGURE 16. SWEEP LINEARITY CHECK AT 0°F

INTENSITY MODULATION, 5-msec PULSES
TOP TRACE (LEFT TO RIGHT), MIDDLE TO END OF SWEEP
BOTTOM TRACE (LEFT TO RIGHT), BEGINNING TO MIDDLE OF SWEEP
TEMPERATURE OF ELECTRONICS, 0°F

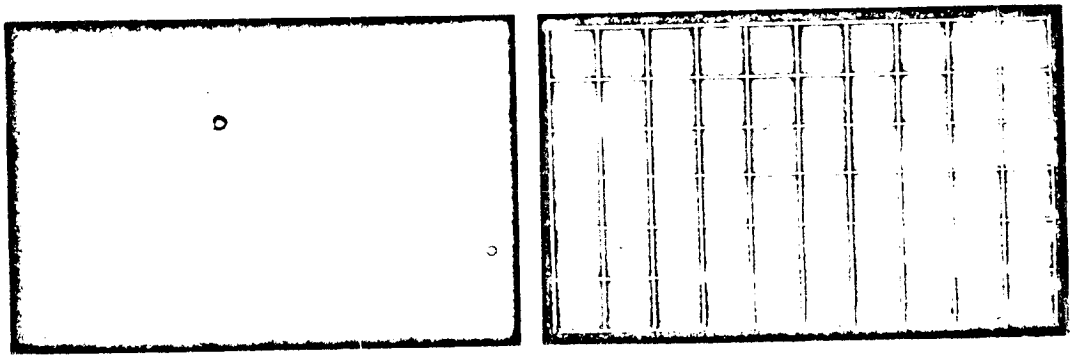

a. BEFORE AMPLIFICATION

b. AFTER AMPLIFICATION

FIGURE 17. SWEEP LINEARITY CHECK AT 77°F

INTENSITY MODULATION, 5-msec PULSES
TOP TRACE (LEFT TO RIGHT), MIDDLE TO END OF SWEEP
BOTTOM TRACE (LEFT TO RIGHT), BEGINNING TO MIDDLE OF SWEEP
TEMPERATURE OF ELECTRONICS, 77°F

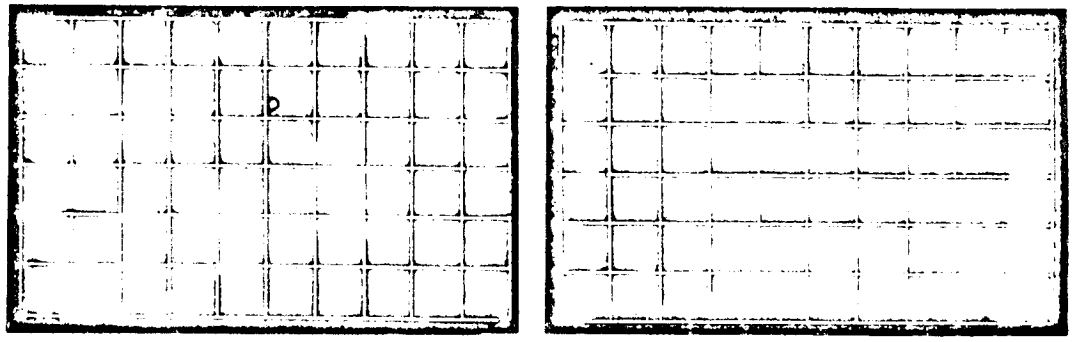

a. BEFORE AMPLIFICATION

b. AFTER AMPLIFICATION

FIGURE 18. SWEEP LINEARITY CHECK AT 100°F

INTENSITY MODULATION, 5-msec PULSES
TOP TRACE (LEFT TO RIGHT), MIDDLE TO END OF SWEEP
BOTTOM TRACE (LEFT TO RIGHT), BEGINNING TO MIDDLE OF SWEEP
TEMPERATURE OF ELECTRONICS, 100°F

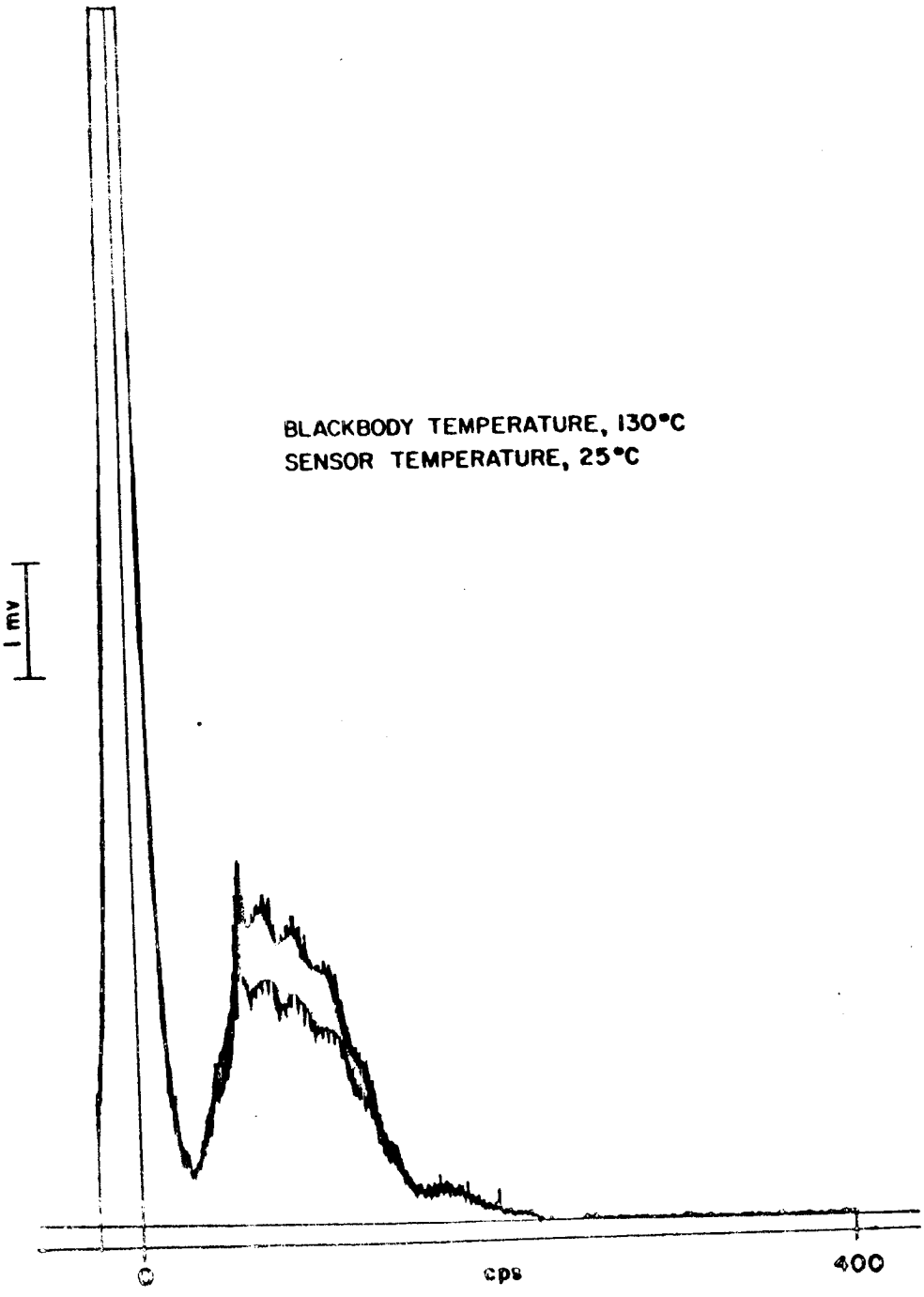

FIGURE 19. SPECTROGRAM I

TABLE 12

TOTAL ABSOLUTE RESPONSE CALCULATION

Blackbody Temperature, 401°K
Sensor Temperature, 298°K

URD 9

Wave No., n	Spectrogram Voltage, mv	Wavelength, λ, 10^{-4} cm	N_1 at 298°K,[a] w/cm-sr	N_2 at 401°K,[a] w/cm-sr	ΔN	λ^2, 10^{-8} cm^2	ΔN_n,[b] 10^{-3} µw/cm-sr	TAR,[c] mv/µw/cm-sr
300	0.4440	33.3	0.8923	1.515	0.6227	1108.	6900	.0644
350		28.6				817.9		
400	0.8047	25.0	2.070	3.850	1.780	625.0	11,125	.0723
450		22.2				492.8		
500	1.665	20.0	3.663	7.512	3.851	400.0	15,404	.1081
550		18.2				331.2		
600	2.525	16.7	5.398	12.27	6.872	278.9	19,166	.1317
650		15.4				237.2		
700	2.503	14.3	7.060	17.90	10.84	204.5	22,168	.1329
750		13.3				175.9		
800	2.386	12.5	8.395	23.84	15.45	156.3	24,148	.0988
850		11.8				129.2		
900	2.220	11.1	9.266	29.56	20.33	123.2	25,072	.0887
950		10.5				110.3		
1000	2.025	10.0	9.633	34.56	24.93	100.0	24,930	.0812
1050		9.50				90.25		
1100	1.804	9.10	9.547	38.59	29.04	82.81	24,048	.0750
1150		8.70				75.69		
1200	1.526	8.34	9.256	40.80	31.55	72.93	23,009	.0663
1250		8.00				64.00		
1300	1.226	7.70	8.967	43.16	34.79	59.29	20,627	.0594
1350		7.40				54.76		
1400	0.9720	7.15	7.479	43.65	36.17	51.12	18,490	.0525
1450		6.90				47.61		
1500	0.7770	6.66	6.356	42.87	36.51	44.36	16,196	.0480

[a] Absolute spectral radiance in terms of wavelength.

[b] Absolute spectral radiance in terms of wave number.

[c] Total absolute response.

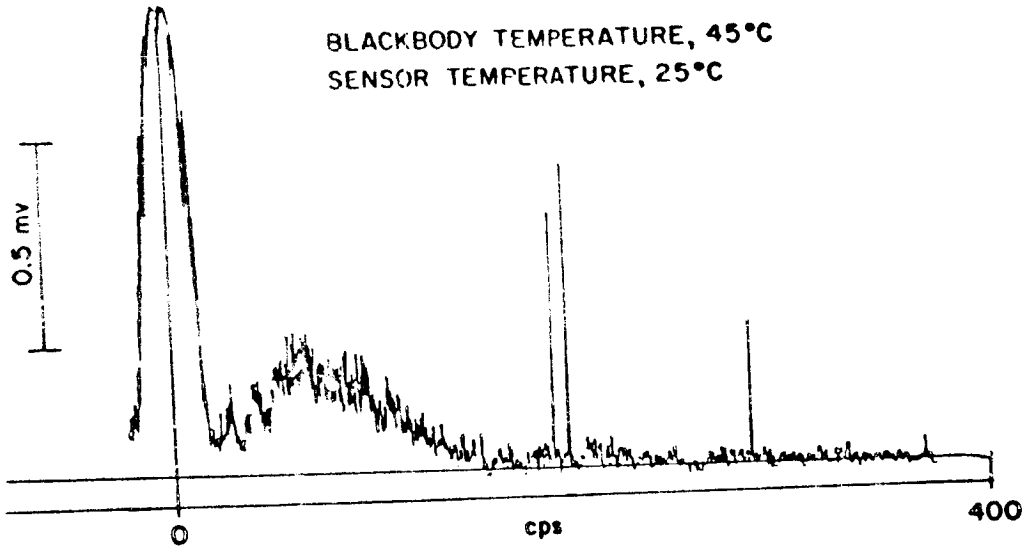

FIGURE 20. SPECTROGRAM II

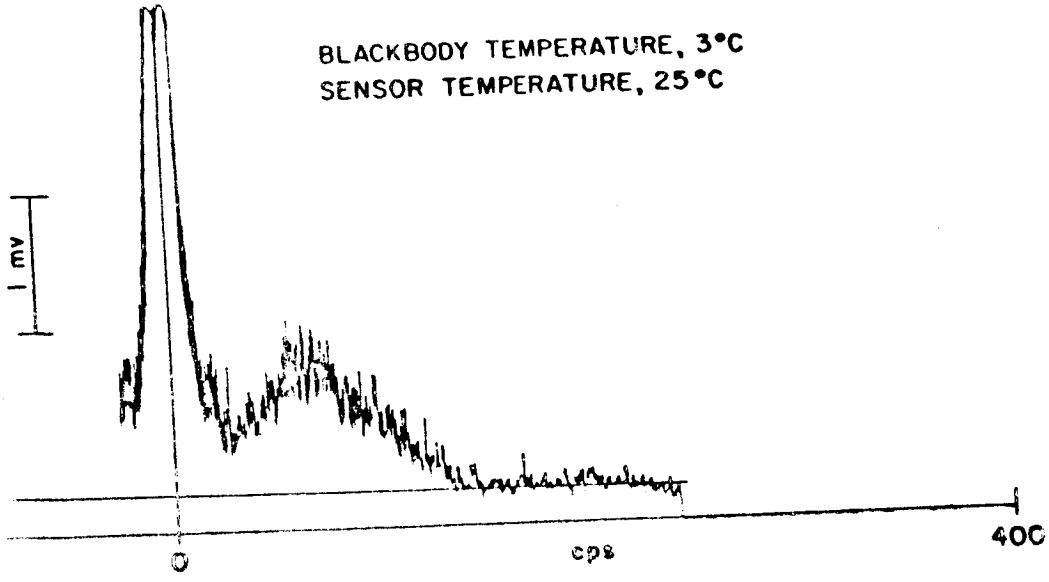

FIGURE 21. SPECTROGRAM III

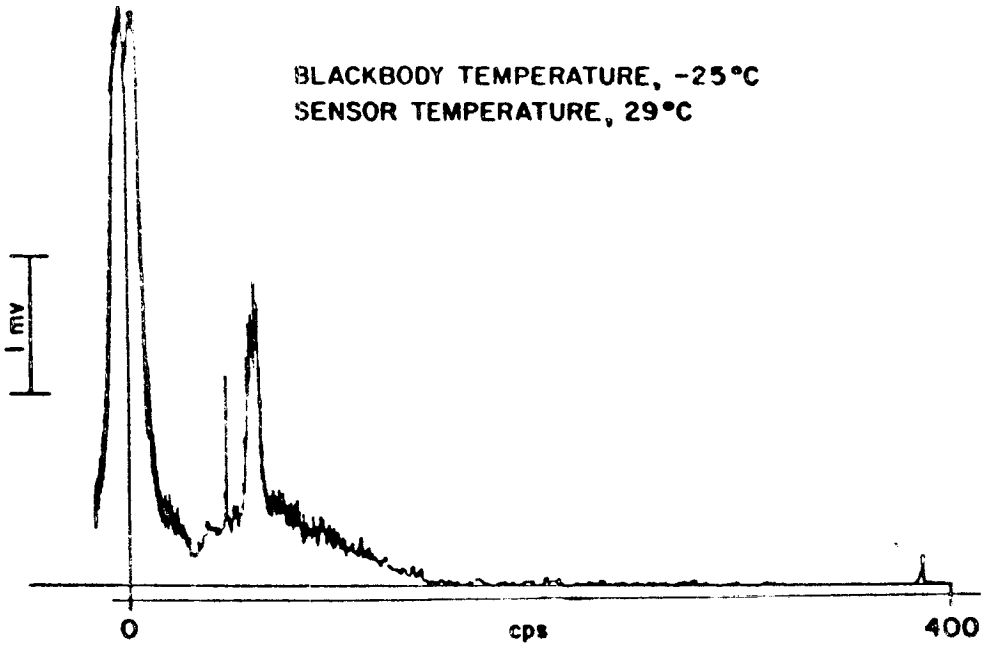

FIGURE 22. SPECTROGRAM IV

TABLE 13

BLACKBODY TEMPERATURE CALCULATION AT 310°K

Sensor Temperature, 298°K — URD 9

Wave No., n	Spectrogram Voltage, mv	Wavelength, λ, 10^{-4} cm	N_1 at 298°K[a], w/cm-sr	N_2 at 310°K[a], w/cm-sr	ΔN	λ^2, 10^{-8} cm^2	ΔN_n[b], 10^{-8} w/cm-sr	TAR[c], mv/w/cm-sr	Blackbody Temp. (calc.), °K
300		33.3	0.8929			3106.		.0666	
350		28.6				817.9			
400	.0999	25.0	2.070	2.291	0.2211	625.0	1382	.0729	512
450		22.2				497.8			
500	.1565	20.0	3.661	4.144	0.4830	400.0	1932	.1001	515
550		18.2				331.2			
600	.2264	16.7	5.596	6.014	0.6185	278.9	1719		509
650		15.4				237.2			
700	.2696	14.3	7.060	8.142	1.082	204.5	2213	.1129	510
750		13.3				175.9			
800	.2360	12.5	8.395	9.926	1.531	156.5	2393	.0988	512
850		11.8				129.2			
900	.2098	11.1	9.266	11.19	1.920	123.2	2365	.0887	511
950		10.5				110.3			
1000	.1796	10.0	9.651	11.85	2.214	100.0	2214	.0812	511
1050		9.50				90.25			
1100	.1552	9.10	9.547	12.01	2.467	82.81	2043	.0750	512
1150		8.70				75.69			
1200	.1265	8.34	9.250	11.87	2.616	72.93	1908	.0663	512
1250		8.00				64.00			
1300	.0966	7.70	8.367	11.11	2.742	59.29	1626	.0590	512
1350		7.40				54.76			
1400	.0833	7.15	7.479	9.856	2.359	51.12	1206	.0525	511
1450		6.90				47.61			
1500	.0533	6.66	6.356	7.920	1.564	44.36	694	.0480	507
								Average	511
								Error =	9°

[a] Absolute spectral radiance in terms of wavelength.

[b] Absolute spectral radiance in terms of wave number.

[c] Total absolute response.

TABLE IV

BLACKBODY TEMPERATURE CALCULATION AT 276°K

Sensor Temperature, 298°K

URD 9

Wave No., n	Spectrogram Voltage, mv	Wavelength, λ 10^{-4} cm	N_1 at 276°K,[a] w/cm-sr	N_2 at 298°K,[a] w/cm-sr	ΔN	ν, 10^{-3}/cm	ΔN_n,[b] 10^{-3} w/cm-sr	TAR,[c] mv/w/cm-sr	Blackbody Temp. (calc.), °K
500	.3700	31.2	0.5738	0.8925	0.5185	3108.	5765	.0640	299
550		28.6				817.9			
600	.5800	25.0	0.7860	2.070	1.284	625.0	8022	.0725	206
650		22.2				492.8			
700	.7500	20.2	3.926	5.667	3.735	400.0	6938	.1081	259
750		18.2				331.2			
800	.9100	16.7	2.920	5.398	2.478	278.9	6910	.1317	248
850		15.4				237.2			
900	.8500	14.3	5.378	7.060	5.682	204.5	7529	.1129	266
950		13.3				175.9			
1000	.7700	12.5	5.408	8.395	4.987	156.3	7794	.0988	242
1050		11.8				129.2			
1100	.7000	11.1	2.866	9.266	6.406	123.2	7892	.0887	235
1150		10.5				110.3			
1200	.6000	10.0	2.242	9.631	7.389	100.0	7389	.0812	229
1250		9.50				90.25			
1300	.4800	9.10	1.818	9.547	7.729	82.81	6400	.0750	227
1350		8.70				75.69			
1400	.3500	8.34	2.012	9.250	7.238	72.99	5279	.0663	235
1450		8.00				64.00			
1500	.2000	7.70	2.688	8.367	5.679	59.29	3367	.0599	252
1550		7.40				54.76			
1600	.1000	7.15	3.752	7.479	3.727	51.12	1905	.0525	270
1650		6.90				47.61			
1700	.0200	6.66	5.416	6.356	0.9400	44.36	417	.0480	292
								Average	240
								Error	36°

[a] Absolute spectral radiance in terms of wavelength.

[b] Absolute spectral radiance in terms of wave number.

[c] Total absolute response.

TABLE 15

BLACKBODY TEMPERATURE CALCULATION AT 248°K

Sensor Temperature, 302°K — URD 9

Wave No., n	Spectrograph Voltage, mv	Wavelength, λ, 10^{-4} cm	N_1 at 248°K[a], w/cm-sr	N_2 at 302°K[a], w/cm-sr	ΔN	λ^2, 10^{-8} cm^2	ΔN_n[b], 10^{-3} µw/cm-sr	TAR[c], mv/µw/cm-sr	Blackbody Temp. (calc.), °K
300	.3500	33.3	0.4246	0.9151	0.4905	1108.	5435	.0644	211
350		28.6				817.9			
400	.5000	25.0	1.469	2.135	0.6638	625.0	4149	.0723	250
450		22.2				492.8			
500	.4800	20.0	2.682	3.792	1.110	400.0	4440	.1001	26
550		18.2				331.2			
600	.6400	16.7	3.879	5.622	1.743	278.9	4869	.1317	269
650		15.4				237.2			
700	.6200	14.3	4.709	7.395	2.686	204.5	5492	.1129	267
750		13.3				175.9			
800	.5800	12.5	5.323	8.845	5.522	156.5	5870	.0988	241
850		11.8				139.2			
900	.4700	11.1	5.522	9.823	4.301	123.2	5299	.0887	267
950		10.5				110.3			
1000	.4000	10.0	5.344	10.27	4.926	100.0	4926	.0812	266
1050		9.50				90.25			
1100	.3500	9.10	4.614	10.25	5.636	82.81	4667	.0750	262
1150		8.70				75.69			
1200	.2700	8.34	4.389	9.972	5.583	72.93	4072	.0663	26
1250		8.00				64.00			
1300	.1800	7.70	3.983	9.093	5.110	59.29	3030	.0594	267
1350		7.40				54.76			
1400	.1200	7.15	3.707	8.179	4.472	51.12	2286	.0525	270
1450		6.90				47.61			
1500	.0800	6.66	3.244	7.002	3.758	44.36	1667	.0480	273
								Average	260
								Error	12°

[a] Absolute spectral radiance in terms of wavelength.

[b] Absolute spectral radiance in terms of wave number.

[c] Total absolute response.

TABLE 16

BLACKBODY TEMPERATURE CALCULATION ACCURACIES

Sensor Temperature, °K	Blackbody Temperature (Measured), °K	Blackbody Temperature (Calc.), °K	Error, °K
298	318	311	7
298	276	240	36
302	248	260	12

Detailed test procedures are given in TEI Acceptance Test Procedure 387-212-89 (2).

4.3.1.2 Summary of objective and results of experiments.
The objective of the functional tests was to prove that the instrument was capable of determining the surface temperature of the moon by using its infrared spectrographic characteristic. The test results are not conclusive. System errors induced by test procedure far exceed the minimum error allowed for the system. These errors are explained in detail in the TEI letter of 11 April 1962, to J. J. Thomas/ E. L. Brown found in Appendix B.

4.3.1.3 Heater-plate functional tests.

a. Accuracies obtained
An initial power dissipation of 160 watts was attained when the heater plate was connected to 28 volts dc at room temperature. After approximately 5 min the average power dissipated was 110 watts.

b. Departures from JPL functional requirements
The requirement was for 150 watts boost preheat for 0.5 hour with 96 watts average sustained for 1 hour. The heater plate will not meet this requirement as indicated in the paragraph above.

c. Departures from JPL design specifications
None.

d. General summary of scientific objectives obtained and experimental results
The prime function of the heater plate is to reach its maximum temperature as quickly as possible while radiating energy to the lunar surface. The above-mentioned test was performed in a vacuum chamber at a pressure of 10^{-3} mm Hg. A glass plate of 1-inch thickness was placed beneath the heater plate to simulate the lunar surface. The glass plate having an absorptivity higher than that expected of the lunar surface should remain at a lower temperature and thereby receive more radiant energy from the heater plate. During this test the heater plate reached the maximum operating temperature within 9 min. A decrease in the resistance of the copper conductor caused an appreciable increase in power input at lower

temperature. Also the power output was greatly reduced at lower temperatures since the radiant energy is proportional to the fourth power of the temperature. As a result of this time-temperature curve shown in Figure 23 has been extropolated into the lower temperature ranges to obtain an estimate of the total time required to bring the heater plate up to maximum temperature.

4.3.1.4 Heater-plate temperature sensor.

a. Accuracies obtained
The thermocouple embedded in the laminate and secured with an epoxy resin was found to be accurate to within ±2°C.

b. Departures from JPL function requirements
None.

c. Departures from JPL design specifications
None.

d. General summary of scientific objectives and experimental results
A standard thermocouple was attached to the laminate as near to the temperature sensor as possible. The heater assembly was placed in a temperature chamber and allowed to come to thermal equilibrium. The embedded thermocouple indicated a temperature to within 2°C of the temperature indicated by the standard thermocouple.

4.3.2 Results of Developmental Tests.

4.3.2.1 Outline of tests conducted.
In order to obtain an optimum material for each component of the instrument, methods of fabrication of various materials were investigated. Many tests were performed with epoxy resin and glass fiber in the molding of mounting brackets and the heater plate. Satisfactory results were obtained in the development of the mounting brackets. However, the development of a suitable method of fabricating a heater plate from glass fiber and epoxy resin was not accomplished. An attempt was made to perfect a custom laminate composed of glass-fiber strands, glass-fiber cloth, and epoxy resin. The strands were bunched together to

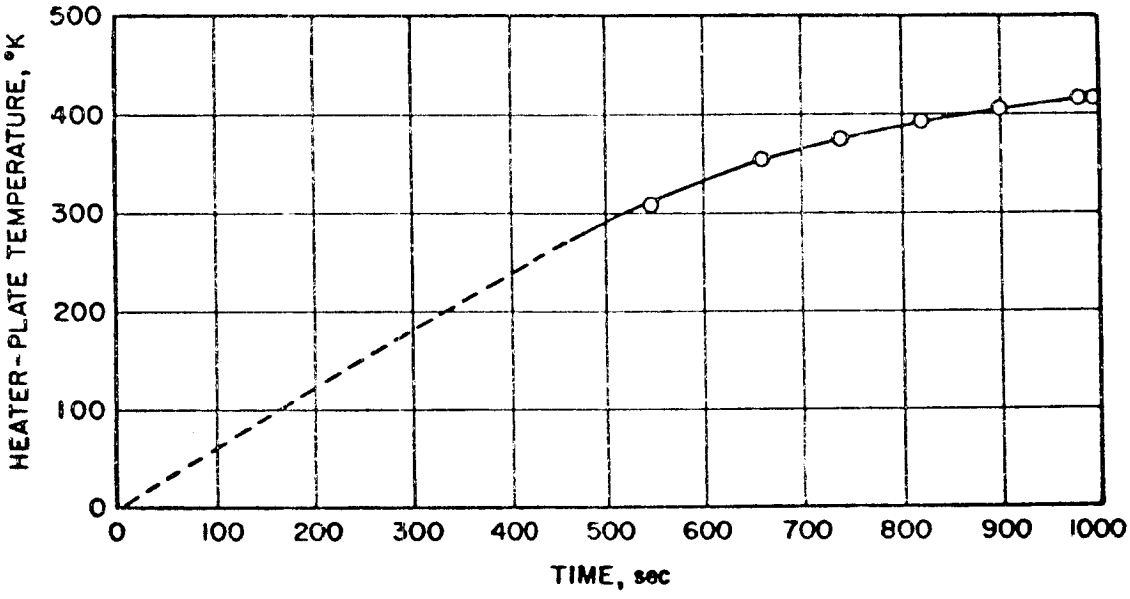

FIGURE 23. HEATER PLATE WARM-UP TIME

form mounting posts and stiffeners and also interwoven between layers of the glass-fiber cloth. Difficulty was experienced not only in attaching a copper conductor to the laminate but also in acquiring a quality molding free of air bubbles and other flaws.

4.3.2.2 Failure reports of developmental models.
Failure of a developmental plate occurred during temperature environmental tests. At 400°K warping became excessive.

4.3.2.3 Summary of corrective measures.
A different approach to the problem was provided by the acquisition of a thick copper-clad epoxy glass fiber laminate. The bulk of the laminate was machined away to leave mounting posts and stiffeners and a thin layer of glass fiber above the copper conductor.

4.3.2.4 Summary of experimental results.
Little or no warping occurred when the improved version was subjected to a temperature of 400°K.

4.4 Components Outline

Two commercial components in addition to those found in the spectrometer are used in the device:

1. Thermostat, Texas Instrument C4344-9779-1
2. Connector, Bendix PT 500P-16-23 P (005)

4.4.1 Notation and Explanation of Deviation from JPL and/or HAC Preferred Parts Lists. Deviations from the JPL and HAC preferred parts list are given in Table 17.

4.4.2 Results of Component Tests. No tests were conducted on the connector or the interferometer parts; however, the following tests were made on the thermostat.

1. The operating temperature was determined by emmersing the thermostat in an oil bath and noting the temperatures at which the contacts opened and closed.

TABLE 17

COMPONENT DEVIATIONS

FROM JPL PREFERRED PARTS LISTS

INCLUDING THOSE USED IN INTERFEROMETER SPECTROMETER

Component	Reason for Deviation
Microdot Cable No. SO-3819MC-30	Availability
Selectro FT-M2WP20 Teflon Feed Through	Availability
Cambion Type 1785-A Chessman	Availability
Cambion Type 1488-4 Solder Lug	Availability
Fairchild 2N2049 Transistors in TO-18 Case	This item not on JPL list but were listed as preferred by HAC
Stevens MX-9 Thermostat	The MX-9 was used over the MX-1 because MX-9 has ground terminal
Corning Glass WL-S-510 Capacitor	Physical size consideration
Vitramon CK Series Capacitors	Parts delivery precluded the use of preferred UK series
Triad EC 1500 1.5-h Inductor	Physical size limitations
Fairchild 2N2049 Transistor Standard Case	Not on JPL list but were listed as preferred by HAC
Transformers, Block T-700, T-701	Block designed for specific use
Minco Model S31 Platinum Resistance Thermometer	This was used to provide a reduction of components

2. The thermostat was subjected to temperature extremes of 78 to 400°K.

3. The thermostat was subjected to accelerations of 15 g's in both the horizontal and vertical axis at frequencies of 10 to 20,000 cps for 10 min. The frequency was varied in one sweep while the acceleration was held constant.

4. Test No. 1 was repeated following Tests 2 and 3. No malfunctions were noted.

4.5 Packaging Philosophy

During the development of the Surface Thermal Diffusivity Instrument, the packaging philosophy was governed by the scientific requirements, HAC outline and mounting drawing No. X239229 and JPL design specification No. 30848. There were no deviations from the specifications.

The functional requirements of the device dictate the relative position of the individual components. A conical shape of the solar radiation shield provides shielding of the spectrometer, which is centrally located, and at the same time prevents normal solar radiation over a large area at any angle of incidence. A convenient and necessary position of the heater plate is near the lunar surface and below the solar shield. The design of each component was influenced by weight considerations. All materials selected have a good strength-to-mass ratio.

4.6 Theoretical Studies

The theoretical studies necessary in the development of the device are illustrated in Appendices C, D, and E.

4.7 Environmental Test Results

The instrument was subjected to pressures ranging from atmospheric to 10^{-3} mm Hg without damage. The heater plate was subjected to temperatures ranging from 295 to 400°K. All other components were subjected to temperatures ranging from 295 to 328°K. No failures were reported.

The following acceleration tests were performed on the instrument with the interferometer spectrometer represented by a wooden replica. The accelerations were produced by a Ling Tempco Type 219-CP-3/4 vibration exciter. All vibration was applied along the thrust axis of the instrument as mounted to the surveyor spacecraft.

1st Test

5-14 cps 0.2-inch displacement
14 to 5,000 cps, constant 2 g acceleration
5-min sweep from 5 to 5,000 cps

2nd Test

5-14 cps, 0.5-inch displacement
14 to 5,000 cps, constant 5 g acceleration
10-min sweep from 5 to 5,000 to 5 cps
Stop for 30 sec at 130 cps

3rd Test

5-20 cps, 0.5-inch displacement
14 to 5,000 cps, constant 10 g acceleration
5-min sweep from 5 to 5,000 cps

4th Test

5-24 cps, 0.5-inch displacement
24 to 5,000 cps, constant 15 g acceleration
5-min sweep from 5 to 5,000 cps
Test was stopped at 400 cps (3 min 20 sec)

A maximum resonant condition was observed during each test at approximately 140 cps but was reduced at the higher frequency harmonics.

At resonance during the 15 g test two of the three screws attaching the solar shield mounting brackets to the inner shield and heater plate loosened. Although Type C Loctite had been used it had not been heat cured.

4.8 Recommendations

Poor regulation of the heater-plate temperature is caused by a thermostat differential of 20°C and poor thermal contact between thermostat and heater plate. A miniature thermostat having a current carrying capacity of 5 amp and a suitable workable temperature differential has not been located. It is suggested that the heater element be divided into two interwoven conductors, each being controlled by a separate thermostat. Each conductor would require a current of only 2 to 3 amp, which is readily controlled by a thermostat having a small temperature differential.

Thought should be given to the practicability of increasing the diameter of the interferometer spectrometer to allow repackaging of the preamplifier in the sensor head for increased reliability. Present space limitations necessitate deviation from the accepted practices.

5. SURFACE MAGNETIC SUSCEPTIBILITY INSTRUMENT

URD 10

Control Item X239211

5.1 System Description

The Surface Magnetic Susceptibility Instrument is designed to measure the ac magnetic susceptibility of the lunar material adjacent to the spacecraft. The experiment employs an induction balance system of an air-core transformer in which the material inductance between primary and secondary has been reduced nominally to zero for a surrounding medium of permeability approximately equal to one (air or vacuum).

The principle underlying the use of an induction balance for the measurement of magnetic susceptibility is that any material brought into the magnetic field of the balance will change the mutual inductance between two coils and thus change the induced voltage. This change in voltage represents the change in magnetic susceptibility in the field of the balance (5).

As shown in Figure 24, a 3800-cps sine wave is amplified and connected to the magnetic susceptibility device through an isolation transformer. Resistance R_1 is used to measure power consumption. With coils A and B phased 180° apart and the proper turns ratio and spacing employed, there will be no output voltage (neglecting leakage) in coil C, as detected by the tuned voltmeter with the system situated in air. With the introduction of a material sample that has evidence of magnetic susceptibility, an increase in the coupling will occur between coils B and C which is greater than the increase between A and C, and the resultant signal will appear at the output. By empirical means such signal voltage may be correlated to the magnetic susceptibility of the material.

Temperature information is obtained from a thermocouple embedded near the coils.

5.2 Equipment Description

The over-all assembly of the Surface Magnetic Susceptibility Instrument is as shown in TEI drawing No. 387-253-OA (Figure 25). The coils are wound with No. 29 B and S gauge high-temperature magnet wire into epoxy glass-fiber laminate forms. The coils are epoxy-cemented to a holding rod of the same material. An epoxy-glass section is molded to the upper end of the rod to house the nine-pin connector. Terminals are provided for interconnecting the coils and the lead wires. Three epoxy-glass feet are cemented to the bottom side of the large coil form to

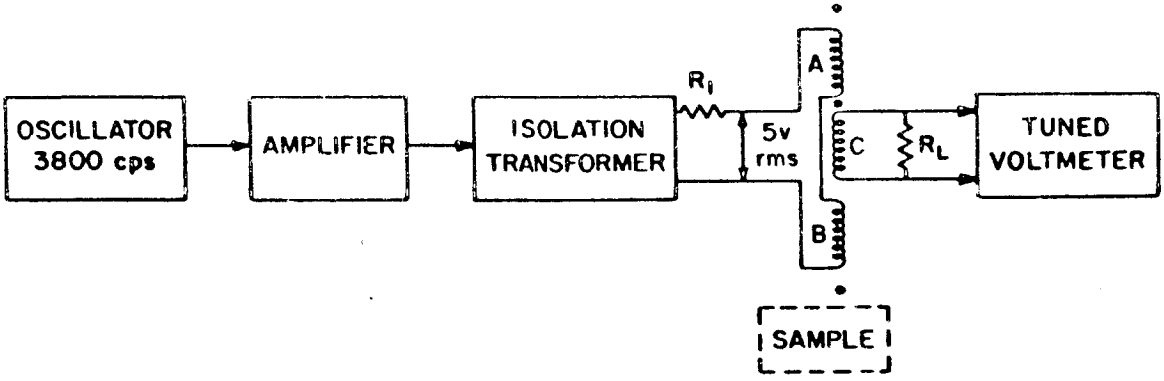

FIGURE 24. SYSTEM BLOCK DIAGRAM OF THE SURFACE MAGNETIC SUSCEPTIBILITY INSTRUMENT

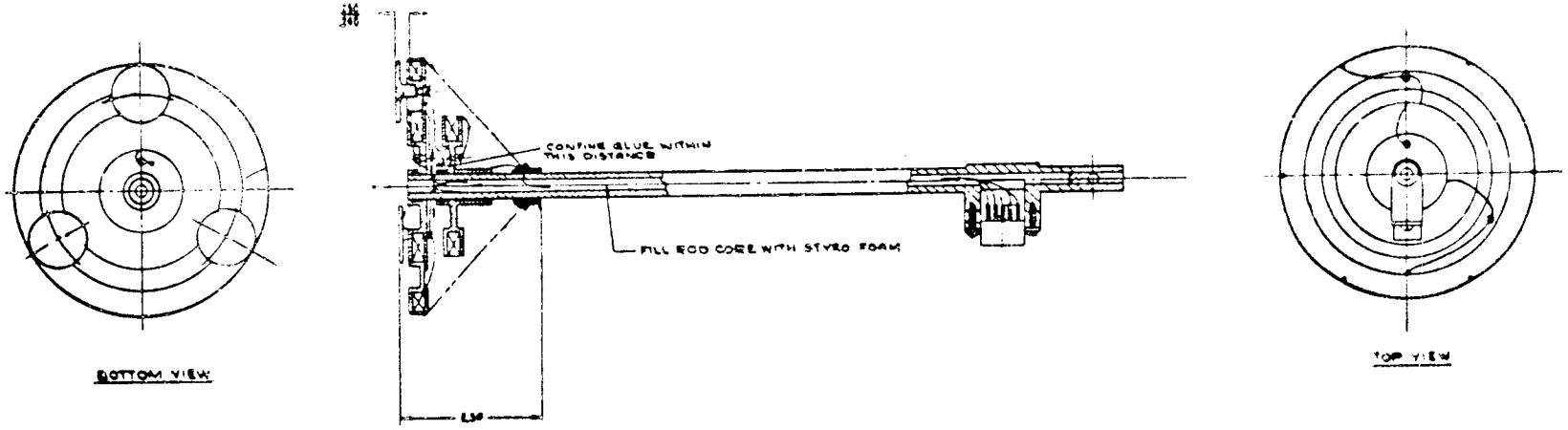

FIGURE 25. ASSEMBLY DRAWING OF THE SURFACE MAGNETIC SUSCEPTIBILITY INSTRUMENT

position the device a given distance above the test surface. The complete coil section is enclosed within an aluminized Mylar shield to minimize uneven temperature effects caused by solar radiation. The temperature of the device is determined by a thermocouple located in the holding rod between the upper and lower coils.

The outline and mounting dimensions for the Surface Magnetic Susceptibility Instrument are shown on TEI drawing No. 387-253-OM (Figure 25). The maximum height of the instrument is 12.025 inches and the maximum diameter 4.218 inches. The weight of the instrument is 0.575 lb, and the location of the center of gravity is indicated in Figure 26.

The electrical requirements of the instrument are 0.011 amp rms at 5 volts rms and 3800 cps.

5.3 Testing and Calibration

5.3.1 Results of Functional Tests. This section covers the calibration results obtained in the final acceptance tests seen prior to shipment of the magnetic susceptibility instrument. Details of the procedure are given in TEI Specification 387-253-97 (6).

The following samples were used to calibrate the Surface Magnetic Susceptibility Instrument:

1.	Ferric chloride solution	$S = 59.2 \times 10^{-6}$ cgs units
2.	1000 ppm (by volume) iron filings in sand	$S = 197 \times 10^{-6}$ cgs units
3.	3000 ppm iron filings in sand	$S = 591 \times 10^{-6}$ cgs units
4.	10,000 ppm iron filings in sand	$S = 1970 \times 10^{-6}$ cgs units
5.	30,000 ppm iron filings in sand	$S = 5910 \times 10^{-6}$ cgs units
6.	100,000 ppm iron filings in sand	$S = 19,700 \times 10^{-6}$ cgs units
7.	500,000 ppm iron filings in sand	$S = 98,500 \times 10^{-6}$ cgs units
8.	100% iron filings	$S = 197,000 \times 10^{-6}$ cgs units

The magnetic susceptibility, S, of the ferric chloride solution was determined by measuring the specific gravity of the solution and

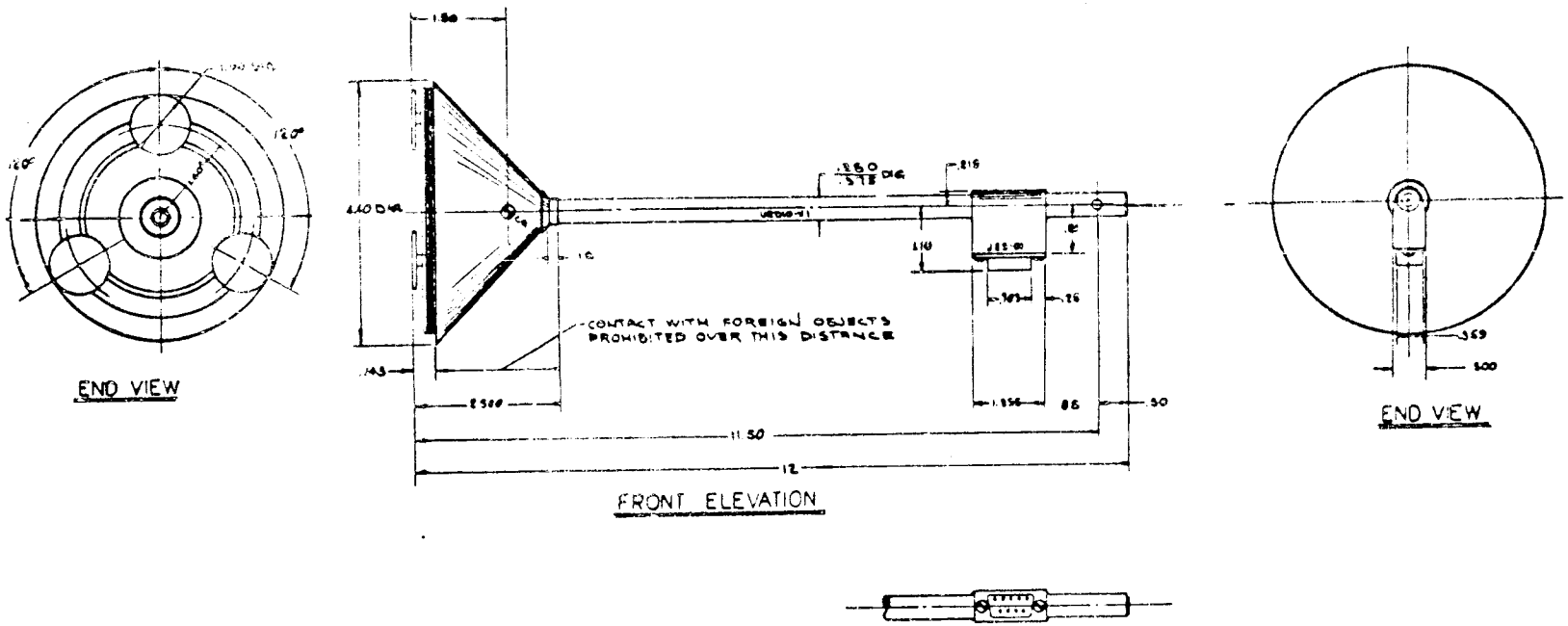

FIGURE 26. OUTLINE AND MOUNTING DIAGRAM OF THE SURFACE MAGNETIC SUSCEPTIBILITY INSTRUMENT

determining the percent of $FeCl_3$ in solution at the test temperature (7). The volumetric magnetic susceptibility was then determined by:

$$S = \chi pd$$

where S is the volumetric magnetic susceptibility, χ is the specific susceptibility of $FeCl_3$ (86.2×10^{-6} cgs units), p is the percent $FeCl_3$ in solution, and d is the specific gravity of the solution.

To determine the magnetic susceptibility of the mixtures of sand and iron filing the instrument was placed in turn on each of the mixtures as well as on the ferric chloride solution. The results were plotted with the abscissa in ppm iron filings in sand and the ordinate in units of output voltage. Then from the known parameters for the $FeCl_3$ (output voltage and volumetric susceptibility) a point was located on a second graph with the abscissa labeled in magnetic susceptibility units. The two curves were overlaid and the Fe-sand curve arranged so that, maintaining the same slope, it would pass through the point established by the $FeCl_3$. The remaining points were transferred to the second graph, and the correlation of ppm iron in sand to magnetic susceptibility was established.

To perform the calibration the samples were placed in an outdoor test area to minimize the effects of ac fields present within the laboratory. The instrument was connected as shown in Figure 27 and the null voltage measured by suspending the instrument 3 feet above the ground and away from any magnetic materials. A temperature measurement was also made in this position. The instrument was then placed on the smooth and level surface of each of the Fe-sand samples and five independent readings made of output voltage. A temperature reading was made on each of the samples. The measurement on the ferric chloride solution was made by placing the instrument on a polyethylene float resting on the surface of the solution. Finally the null voltage was again measured by suspending in air as before.

Measurements were also made with a test jig which allowed the instrument to be held on the surface at angles of 15°, 30°, and 45° from the vertical. This method of calibration was used to determine the response on uneven surface. Previous tests had been run with an uneven surface mold composed of a polyethylene sheet which had been heated and stretched to form various-sized hills and valleys. The mold was placed in the test sample container and filled with the sample material. The

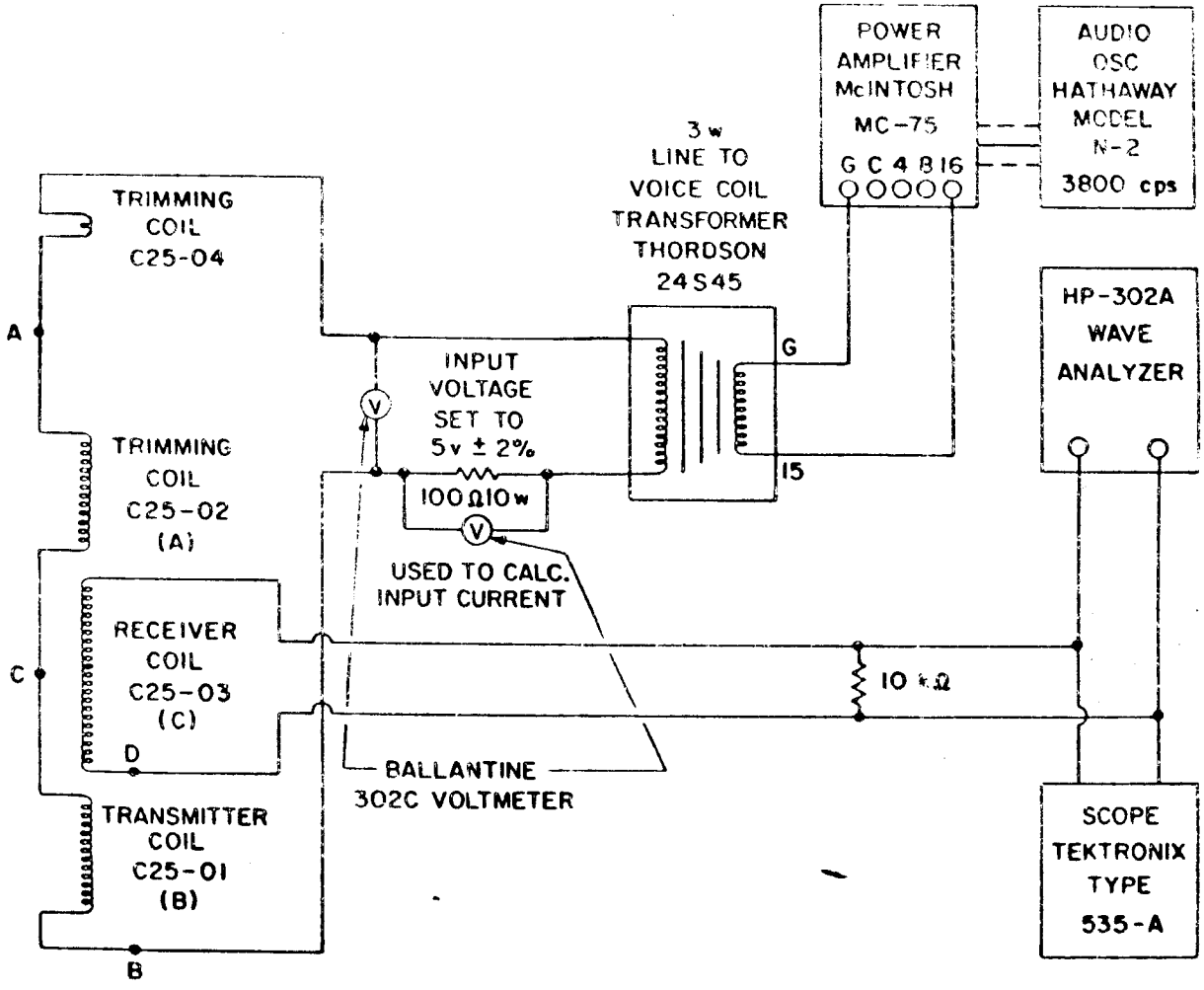

FIGURE 27. CALIBRATION SETUP

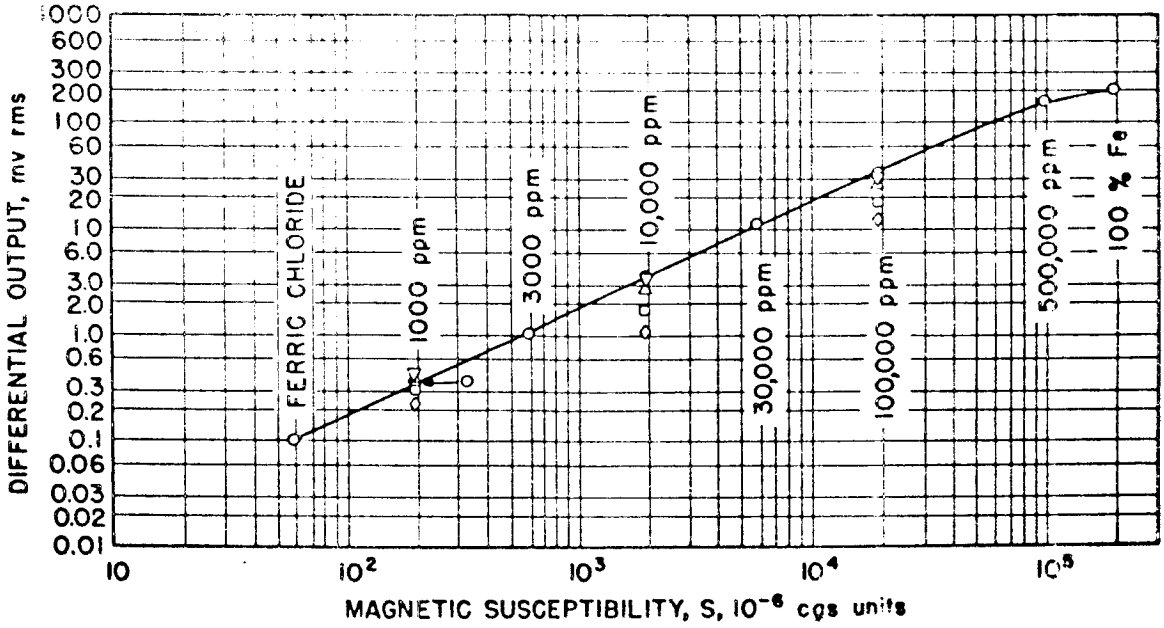

FIGURE 28. RESPONSE FOR EVEN AND UNEVEN SURFACES

○ EVEN SURFACES
▽ UNEVEN SURFACES, 0°
△ UNEVEN SURFACES, 15°
□ UNEVEN SURFACES, 30°
◇ UNEVEN SURFACES, 45°

AVERAGE OF NULLS IN AIR, 1.5 mv

instrument was positioned at various places on the mold and readings made. The repeatability of measurements was so poor, because of difficulty in placing the instrument at the exact position each time and in filling the mold exactly the same, that this method was discarded.

The chosen procedure can be used to determine response if the effective volume of the measured material of an uneven surface is known. That is, the device may be tilted so that a like amount of material will excite the instrument.

Test time allocation allowed for only three independent measures at each of four angles (0°, 15°, 30°, and 45°). Repeatability in the readings at each angle was within ±5% for the 1000 and 10,000 ppm Fe-sand mixtures but decreased to approximately ±16% for the 100,000 ppm mixture.

5.3.1.1 Accuracies obtained.

Figure 28 shows the differential (output minus null) response curve obtained. It can be seen that the curve for even surfaces is linear from 59.2×10^{-6} cgs units of magnetic susceptibility to approximately $50,000 \times 10^{-6}$ cgs units and continues to $200,000 \times 10^{-6}$ cgs units with very little roll-off. Repeatability of voltage readings on all of the samples was within ±5% of the average.

The curve for uneven surfaces is shown for information purposes to indicate the degree of error experienced.

5.3.1.2 Departures from JPL functional requirements.

The response of the instrument was not determined at a magnetic susceptibility of 10×10^{-6} cgs units because of a lack of suitable test samples.

The null voltage was 1.5 mv, whereas it was specified as 0.3 mv maximum. This was caused by adjusting so that the minimum null voltage would occur below the expected operating temperature of the instrument. In this way there would be no change in phase of the output signal throughout the temperature range as specified. The current was 11 ma rms for 5 v rms at 3800 cps input. The specified current was 10 ma rms.

5.3.1.3 Departures from JPL design specifications.
The only departure was in the use of turret-type terminals rather than fork-type.

5.3.1.4 General summary of scientific objectives obtained and experimental results.
The Surface Magnetic Susceptibility Instrument will measure magnetic susceptibility in the range from 59.2 to 197,000 x 10^{-6} cgs units. The response is linear up to approximately 50,000 x 10^{-6} cgs units and extends to 197,000 x 10^{-6} with a slight roll-off. The readings on each of the samples will repeat within ±5%.

5.3.2 Results of Developmental Tests. This section describes the testing program carried out in the scientific development of the surface magnetic susceptibility instrument. It covers the following tests:

1. Effects of temperature differentials on response.
2. Comparison of direct voltage measurements with the bridge-balance method.
3. Response of instrument at 1 and 5 kc for input voltages of 5, 12.7, and 25 volts rms.
4. Null sensitivity versus frequency.
5. Null sensitivity versus temperature.
6. Effectiveness of sun shield.
7. Capability of making conductivity measurements.

Failure reports are not given as such, but a discussion of the results obtained and the changes made is included.

5.3.2.1 Effects of temperature differentials on instrument response.
A developmental model surface unit was built identical with that used in the feasibility study. The device was placed on a test sample and exposed to uneven heating by an infrared heat lamp. The change in output voltage which resulted because of differential expansion and shift in the null balance was such that materials having susceptibility less than 300 x 10^{-6} cgs

units would be obscured within the null shift. It was therefore decided that a sun shield would be included to minimize the uneven heating effects.

5.3.2.2 Comparison of direct voltage measurement with the bridge-balance method.

Because of the complexity of performing a balance function remotely, especially by radio signals, the desirability of making a direct output voltage measurement was studied. The output coil was connected directly to a suitable load resistor (10 kohm), and the changes in output voltage experienced on the different samples were measured with an ac voltmeter. The input voltage was 25 v rms at 1 kc as used for the bread-board model. Figure 29 shows the comparison of the results obtained in this manner with those previously found with the bridge. It can be seen that the linear portion of the curve is extended by the direct measurement technique. The range of signals obtained was such as to be suitable for spacecraft handling, and therefore this method was used in all future testing.

5.3.2.3 Comparison of response at 1 and 5 kc for input voltages of 5, 12.7, and 25 volts rms.

In order to conserve energy the spacecraft contractor requested that the instrument be tested with lower input voltages and at higher frequencies. Therefore the device was tested at 1000 cps and 25 volts input, the feasibility test conditions, and at reduced voltages of 12.7 and 5 volts rms. The three test voltages were also applied at 5000 cps.

The results obtained are shown in Figure 30. It can be seen that the output voltage decreases approximately as the ratio of the input decreases. Increasing the frequency causes a slight rounding at the upper end as a result of the eddy current losses in the iron particles being greater at 5000 cps. From these data it was decided that the instrument would be operated with 5 v rms input at 3800 cps.

5.3.2.4 Null sensitivity versus frequency.

To define the frequency-stability requirements necessary for proper nulling of the instrument, measurements of output in air were made with the input varied ±0.1 and ±0.2 kc about a

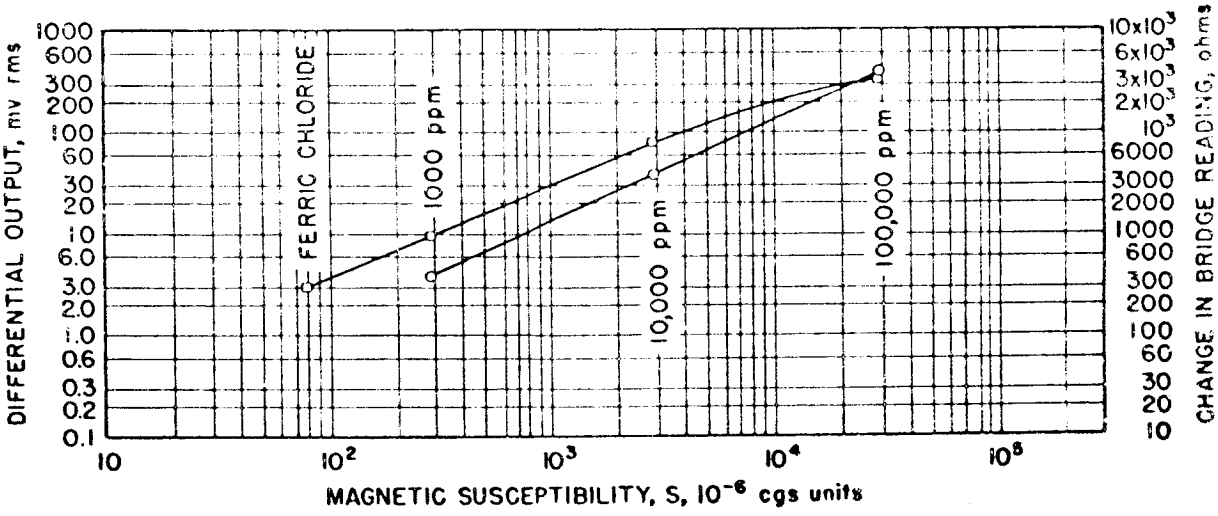

FIGURE 29. COMPARISON OF RESPONSE OF DIRECT VOLTAGE MEASUREMENT WITH BRIDGE-BALANCE METHOD

○ DIRECT VOLTAGE MEASURMENT □ BRIDGE-BALANCE METHOD

INPUT, 25 v rms AT 1000 cps

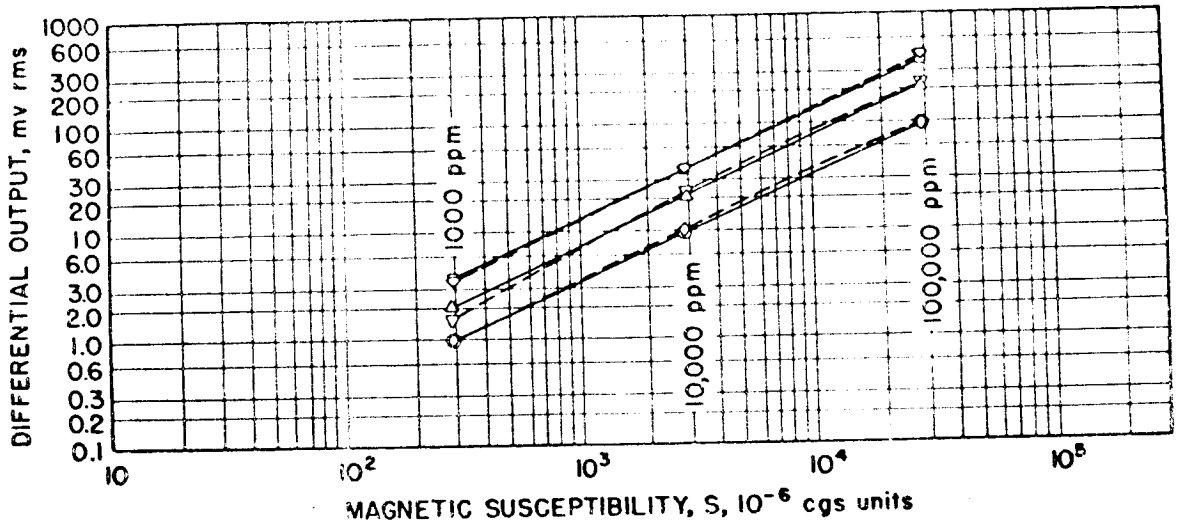

FIGURE 30. COMPARISON OF INSTRUMENT RESPONSE WITH INPUT VOLTAGE

□ 25 v rms, 1000 cps
△ 12.7 v rms, 1000 cps
○ 5 v rms, 1000 cps
◇ 25 v rms, 5000 cps
▽ 12.7 v rms, 5000 cps
◇ 5 v rms, 5000 cps

center frequency of 3.8 kc. The detector used was an untuned ac voltmeter. No noticable change in null output was experienced in either case. With these results the frequency-stability specification was set at ±0.2 kc for a 3.8-kc input frequency. In cases where a tuned detector is used the filter must vary directly with the input frequency for the above condition to exist.

5.3.2.5 Null sensitivity versus temperature.

An extensive series of developmental tests was carried out to improve the null-drift-with temperature relationship as found with the breadboard magnetic susceptibility instrument.

When the breadboard instrument was subjected to temperatures from 20 to 150°C the null voltage changed from 0.2 mv rms to approximately 60 mv rms. The change was so great that it was extremely difficult to measure any materials except those with large susceptibilities when the temperature of the instrument was above 100°C.

It was found that the holding rod was expanding to such a degree that the coils were not maintaining their relative spacings, and therefore the proper bucking was not taking place and the null was not remaining constant.

The first approach to the solution of the problem was to use a Pyrex glass holding rod because of its low coefficient of expansion. The result was a reduction in the null drift to 20 mv at 150°C. Further reduction was required in order that readings at the low end of the susceptibility scale could be made for all temperatures.

Further study of the epoxy-glass characteristics pointed out that the coefficients of expansion for the material varied according to the direction of fibers in the material. It was found that by proper choice of lengths and points of attachment the expansion of the rod and that of the upper coil form could be made to counteract each other, and the resultant null drift could be minimized. Empirical testing resulted in the scheme as used in the final assembly. Figure 31 shows the relative effectiveness of the various methods employed.

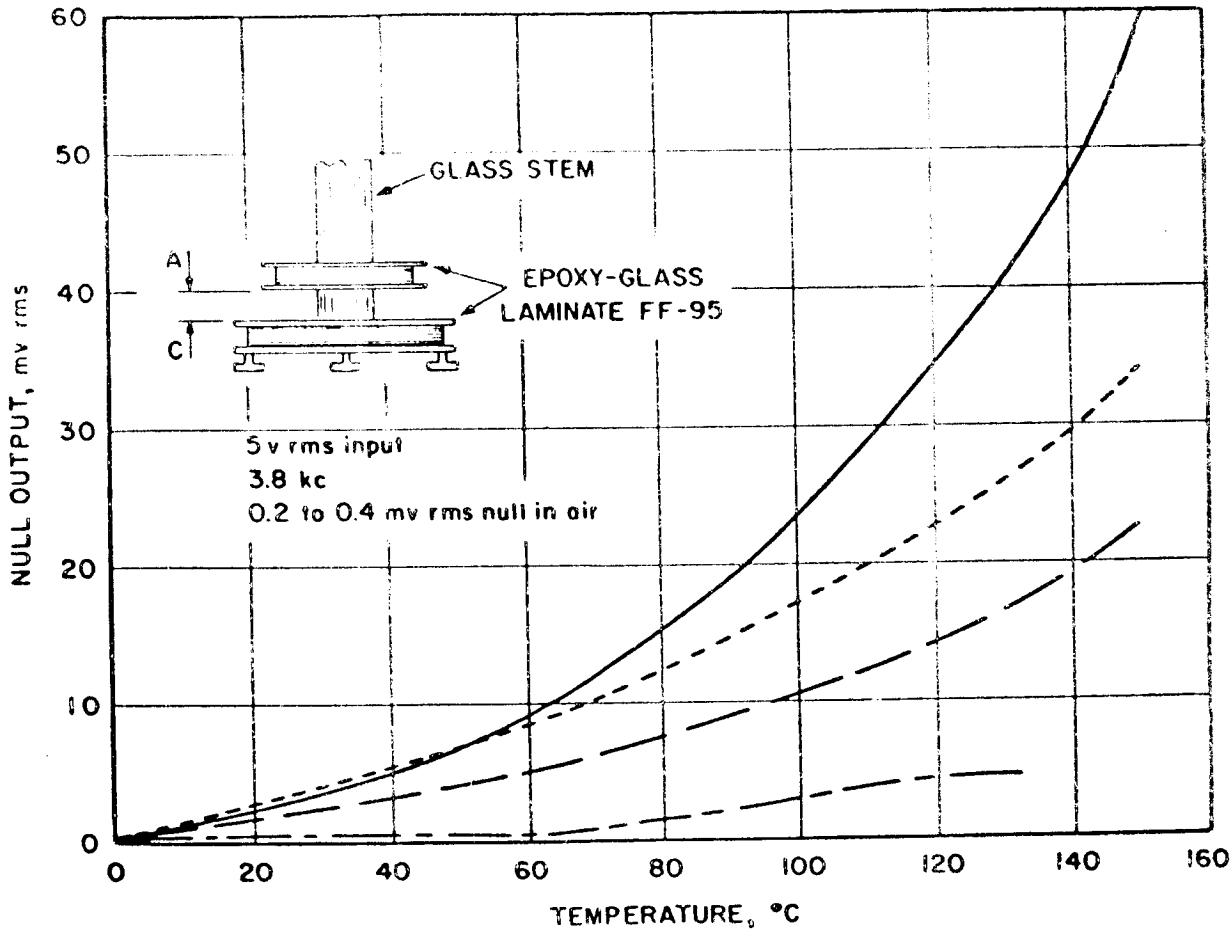

FIGURE 31. EFFECTIVENESS OF TECHNIQUES TO REDUCE NULL TEMPERATURE SENSITIVITY

——— ALL FF-95 CONSTRUCTION, A TO C = 0.82 cm
- - - - - - FF-95 AND GLASS STEM, A TO C = 1.43 cm
— — — FF-95 AND GLASS STEM, A TO C = 0.82 cm
— - — - — FINAL DESIGN, FF-95 WITH TEMPERATURE COMPENSATION

5.3.2.6 Effectiveness of sun shield.

A developmental model Surface Magnetic Susceptibility Instrument similar to the prototype device was instrumented with a number of thermocouples to determine the effectiveness of the aluminized sun shield and to verify that the position chosen for the location of the unit thermocouple was a suitable one. In all, 11 thermocouples were located at various points within the shielded area, and one was attached to the outside surface of the shield at the focus of the heat source and positioned 2 inches from the shield.

The instrument was then placed on a sample of 10,000 ppm iron filings in sand and a reading of output voltage made at ambient conditions. The heat lamp was energized and any change in output noted. All thermocouple outputs were monitored with a 12-position thermocouple switch and a recording potentiometer.

It was found that the output voltage did not change for approximately 5 min, during which the temperature as indicated by the thermocouple located outside the shield rose from 25 to 108.5°C and that indicated by the instrument thermocouple rose from 25 to 26.5°C. The change in output subsequent to this time followed the null drift as determined by a previous test such that by applying the proper correction factor the output remained constant for the 45-min duration of the test. During this 45-min period the instrument thermocouple indicated a temperature rise to 58°C, whereas the outside shield temperature stabilized at approximately 112°C after 6 min. It was also found that the maximum temperature reached by the inner surface of the Mylar shield at the focus was 75°C.

It was determined from this test that instantaneous changes in incident radiation on the shielded instrument would not cause a change in output signal. Long-term temperature changes could be followed by the instrument thermocouple and the necessary corrections to the output made.

5.3.2.7 Capability of making conductivity measurements.

Since it was known that the conductivity of a material influences

the phase of the output signal, the instrument was connected in the normal manner and measurement made on a number of Fe-sand samples and on iron slabs. It was determined that although the output would be saturated for 100% iron, the phase angle would vary according to the fused material present, that is, the conductivity. Sample phase-angle measurements are: 100% iron filings, 5°; boiler plate iron, 66.4°. In both cases the output voltage was approximately the same.

From these tests it was shown that the instrument could be used to measure not only magnetic susceptibility but also conductivity and thus indicate if the material being measured was of meteoritic origin.

5.4 Components Outline

5.4.1 Notation and Explanation of Deviations from JPL and HAC Preferred Parts Lists. There is only one purchased component included as part of the Surface Magnetic Susceptibility Instrument. It is the Cannon DEM 9PNM connector, which was specified by HAC.

5.4.2 Results of Component Tests. No tests have been carried out on the connector except to verify that it would not affect the instrument response when positioned at the prescribed place on the instrument.

5.5 Packaging Philosophy

The packaging of the Surface Magnetic Susceptibility Instrument was governed by the conditions of meeting the scientific requirements while holding size and weight to a minimum.

The epoxy-glass laminate was chosen for the structural material because of its nonmagnetic properties, high strength-to-mass ratio, low coefficient of expansion, and relative ease of fabrication.

The requirement that the upper coil be free for positioning relative to the lower coil pair during nulling, and that certain critical dimensions should be maintained to minimize temperature null drift, necessitated the collar arrangement used.

It was found in attaching the sun shield to the instrument that thermal stresses would affect the null output voltage when the shield was cemented

in place at both ends. Therefore, cementing was used at the lower end only and the upper end left free to move within a pair of collars at the top.

5.6 Theoretical Studies

The developmental work carried out on the Surface Magnetic Susceptibility Instrument was based on the feasibility study performed by Texaco's Research and Technical Department at Bellaire, Texas (5, 8, 9).

5.7 Environmental Test Results

5.7.1 Vibration Tests. The Surface Magnetic Susceptibility Instrument was subjected to sinusoidal vibration in the vertical position according to the following plan:

Frequency, cps	Level, g's	Time
10-40	2.5	6 min 45 sec
40-1500	8.5	2 min 10 sec
40-1500	5.0	11 min 20 sec
3-8	0.6-inch displacement	10 min
5-35	1.5	21 min 40 sec
35-48	3.0	3 min 20 sec
48-500	5.0	23 min 30 sec

These tests were run without the sun shield attached.
No failures occurred as a result of these tests.

5.7.2 Temperature-cycling Tests. In the course of the assembly procedure temperature cycling was carried out to varnish impregnate the coils properly and to relieve any stresses in the materials. The instrument was subjected to three cycles from -65 to + 150°C and held for a total of 3 hours at each temperature extreme.

No failures resulted because of these conditions.

5.8 Recommendations

None.

6. SURFACE DENSITY INSTRUMENT

URD 8

Control Item X239210

6.1 System Description

The Surface Density Instrument is designed to measure the density of the lunar surface at a place adjacent to the spacecraft. The experiment utilizes the gamma-gamma logging technique used for several years by the oil companies to determine the density of formations of the earth. In general, a radiation source (approximately 40 mc, Ir^{192}) is located a known distance from a Geiger-Mueller counter tube. The radiation is directed such that it impinges on the lunar material beneath the instrument. The shielding is arranged so that little radiation passes directly from the source to the detector. The density is derived from the knowledge that the radiation received from the source due to scattering is related to the density of the material subjected to the experiment (10).

Accurate measurements require that all background effects be accounted for. This is accomplished by taking readings with the source extended from and retracted into the shield. The source is positioned in or out of this shield by means of a solenoid mechanism actuated by earth commands.

Ambiguity in the double-ended density-versus-response curve is removed by making two measurements, one slightly above the surface. The instrument is lowered to the surface and supported on a set of legs. After the measurement the legs are released by means of an explosive pin puller, and the instrument falls to the surface, where a second measurement is made.

Temperature corrections to the data are made by measuring the temperature of the counter tubes with a thermocouple.

The instrument is also used to house a geophone employed as part of the acoustic velocity experiment.

6.2 Equipment Description

6.2.1 General. The over-all assembly of the Surface Density Instrument and acoustic sensor appears as shown in Figure 32.

The radioactive source (Ir^{192}) is carried in a sliding assembly with two positive positions, the apex of the forward cone shield and 1 inch inside

the cone shield. The cone shield is constructed of Mallory 1000 metal, a sintered tungsten alloy.

The source-indexing mechanism is contained within the tube connecting the cone shield with the geophone housing. It consists of a solenoid which imparts motion to a slide assembly containing a tooth and slot arrangement. The geophone housing acts as a carrier for the geophone or acoustic sensor and as a support for the elevating legs and their release mechanism. The elevating legs are released by an explosive-actuated pin puller and are secured before release by a 0.187-inch-diameter pin and four guide bushings. The Geiger-Mueller tube is mounted behind the geophone housing within a rear shield assembly also constructed of Mallory 1000 metal.

6.2.2 Dimensions and Weight. The outline and mounting dimensions for the Surface Density Instrument and acoustic sensor are shown on TEI drawing No. 387-234-OM (Figure 33). The maximum height of the instrument is 5.31 inches and the maximum width 3.56 inches. The maximum length of the instrument with radioactive source retracted is 10.87 inches, whereas with radioactive source extended the maximum length is 11.87 inches. In order for the source-positioning mechanism to operate, an additional 0.25 inch of movement is necessary. Therefore, a clearance envelope 12.12 inches in length is required to position the source.

The weight of the Surface Density Instrument and acoustic sensor is 3.21±0.1 lb. The location of the center of gravity of the instrument is indicated in Figure 33.

6.2.3 Power Consumption. Geiger-Mueller counter tube:

Voltage requirement, between 800 and 1000 v dc.
Actual set voltage for tube Serial No. 3162, 870 v dc.
Current requirement, 10 μa peak pulse.
Counting rate, 5 to 1500 counts/sec.

Source-positioning solenoid:

Voltage requirement for solenoid No. 1, 22+6-4 v dc.
Current requirement for solenoid No. 1, approximately 9 amp dc at -125°C with 28 v input; 2 amp dc at 125°C with 18 v input.
Pulse length, 100 msec minimum, 500 msec maximum.

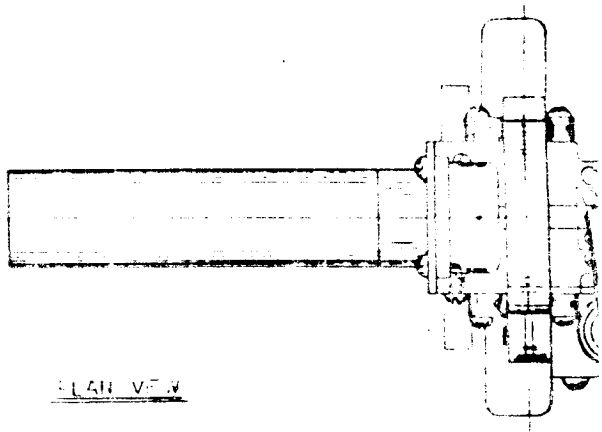

PLAN VIEW

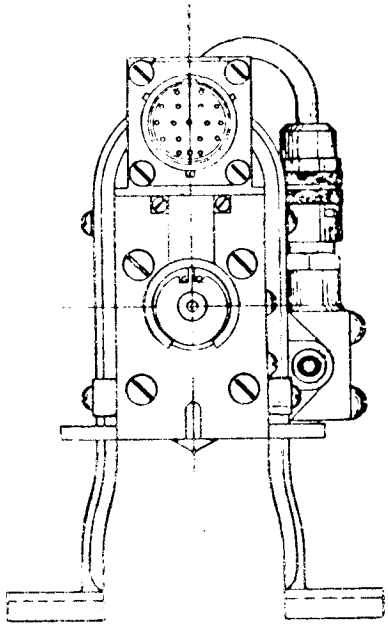

END VIEW

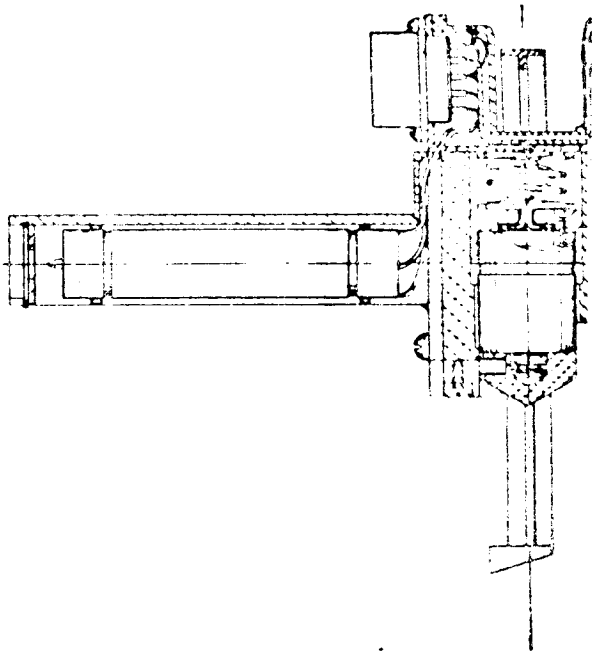

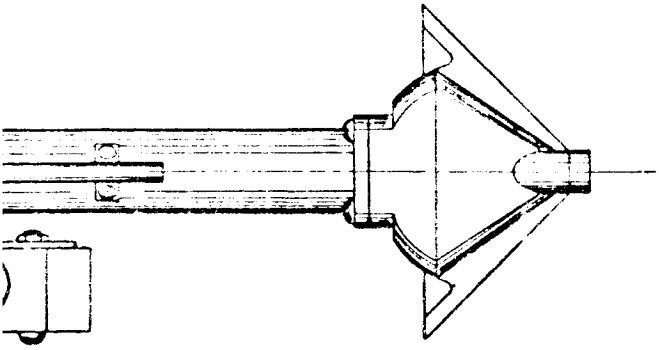

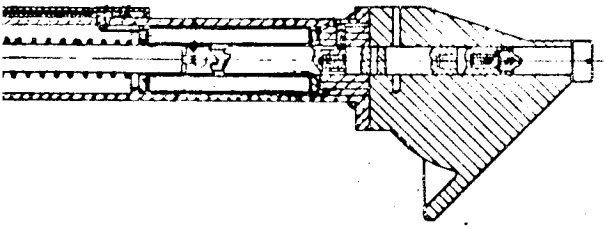

SECTION THRU

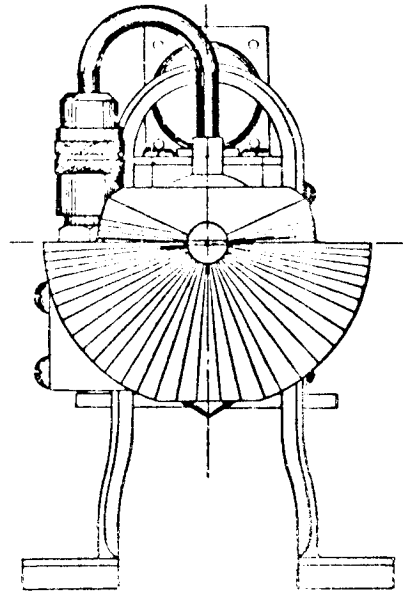

END VIEW

FIGURE 32. ASSEMBLY DRAWING OF THE SURFACE DENSITY INSTRUMENT

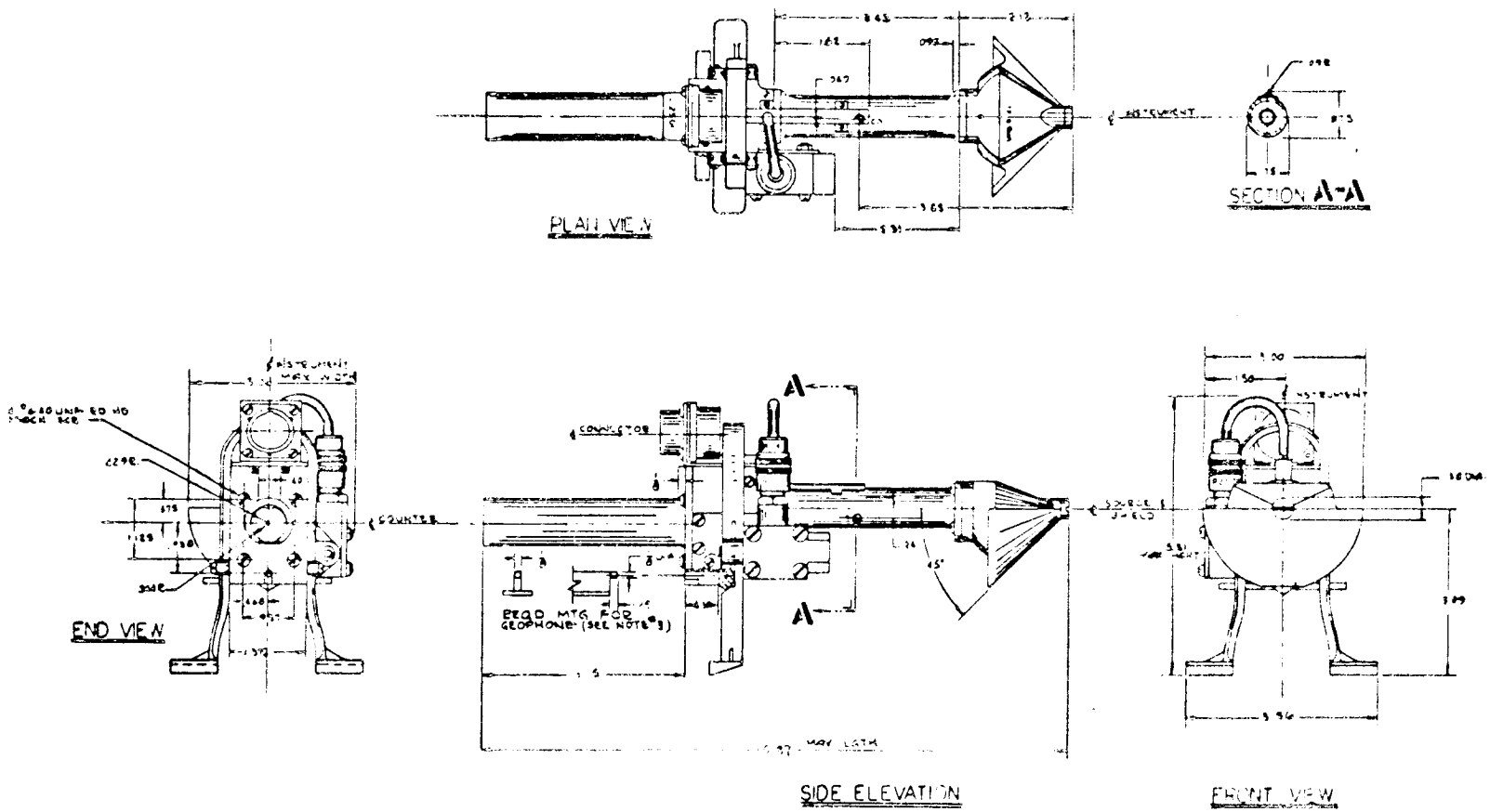

FIGURE 33. OUTLINE AND MOUNTING DRAWING OF THE SURFACE DENSITY INSTRUMENT AND ACOUSTIC SENSOR

Pin-puller squib:

Voltage requirement, 22+6-4 v dc.
Current requirement, 4 amp dc minimum for each bridge, 10 msec minimum.

Geophone:

Voltage requirement, none.
Current requirement, none.

6.3 Testing and Calibration

6.3.1 Results of Functional Tests.

6.3.1.1 Explosive-lowering device.

The test was conducted to determine the stability of the instrument as it fell from the raised to the level position when the legs were released (11). The test was run with a sand-filled inclined-plane test jig, which was set at 0°, 15°, and 20° to the horizontal.

The first test used a squib and pin-puller assembly as specified for the instrument. The device was placed on the test jig with the angle set at 0°. The squib was fired and the action of the instrument recorded on film. The remaining tests were run with a solenoid-activated pin-puller assembly because of the inaccessibility of the proper squib-pin-puller assembly and its prohibitive costs (approximately $150 each).

The procedure used in the test was to place the instrument with the legs in place on the inclined-plane test jig so that the longitudinal axis was parallel with the line of intersection of the inclined plane and the horizontal. The plane was adjusted to the desired angle and the solenoid mechanism activated. The attitude of the instrument after falling was then observed.

Upon completion of the tests at each of the angles, the instrument was rotated 180° and the procedure repeated. A motion-picture record was made of each of the drops.

a. Departure from JPL functional requirement or design specifications.
No detail requirements have been given.

b. General summary of scientific objectives obtained and experimental results
In all cases the instrument fell within the legs in an upright position.

6.3.1.2 Source-positioning solenoid.

The test was conducted to determine if the source would extend and retract upon application of 18 and 28 v dc to the solenoid mechanism (12). The test was run at ambient conditions. In both cases the source was positioned as required.

a. Departures from JPL functional requirement or design specifications
None.

b. General summary of scientific objectives obtained and experimental results
The source capsule may be extended from or retracted into the shield cone by a programmed signal from earth. No power is required to hold the source in either position once it has been indexed. This procedure allows for shielding of the source except when density measurements are being made.

6.3.1.3 Calibration of the assembled instrument.

This section covers the calibration results obtained in the final acceptance tests run prior to shipment of the Surface Density Instrument (13). Data are presented here for all sample materials on hand, whereas the acceptance test booklet contains results from only the six original samples.

The following samples were used to calibrate the Surface Density Instrument:

Sample	Density, g/cm^3
Balsa	0.17±0.0051
Lava	0.65±0.0072
Fluorapatite	2.68±0.0176
Rutile (TiO_2)	4.0±0.0300

Sample	Density, g/cm^3
Austin chalk	1.93±0.0136
Ohio sandstone	2.09±0.0124
Barium sulfate ($BaSO_4$)	4.26±0.0278
Iron carbonate	3.88±0.0237
Georgia granite	2.62±0.0150
Carthage marble	2.64±0.0172
Vermont granite	2.65±0.0152
Virginia slate	2.84±0.0162
Powdered iron	7.0±0.0452
Virginia greenstone	2.95±0.0167
Hematite	4.95±0.0343
Manganese hubnerite ($MnWO_4$)	6.80±0.0417
Limestone	2.27±0.0124
Zinc sphaterite	4.07±0.0249
Sand	2.64±0.0157
Kyanite	3.56±0.0287

The densities of the consolidated samples were found by measuring the dimensions to ±0.02 inch with a 24-inch machine divided scale and measuring the weight to ±0.25 lb with a 1000-lb-capacity platform scale.

The densities of the unconsolidated samples were found by weighing approximately 50 cm^3 of a material to ±0.05 g and then pouring the material into a burette partially filled with water. The change in volume was measured to ±0.5 cm^3 and then the density computed in grams per cubic centimeter.

The accuracies obtained for the samples are as shown in the preceeding listing.

The samples were placed in an outdoor test area in an environment with natural background only. The radioactive Iridium-192 source capsule was installed in the instrument and the instrument connected as shown in Figure 34. Measurements were made on each of the samples.

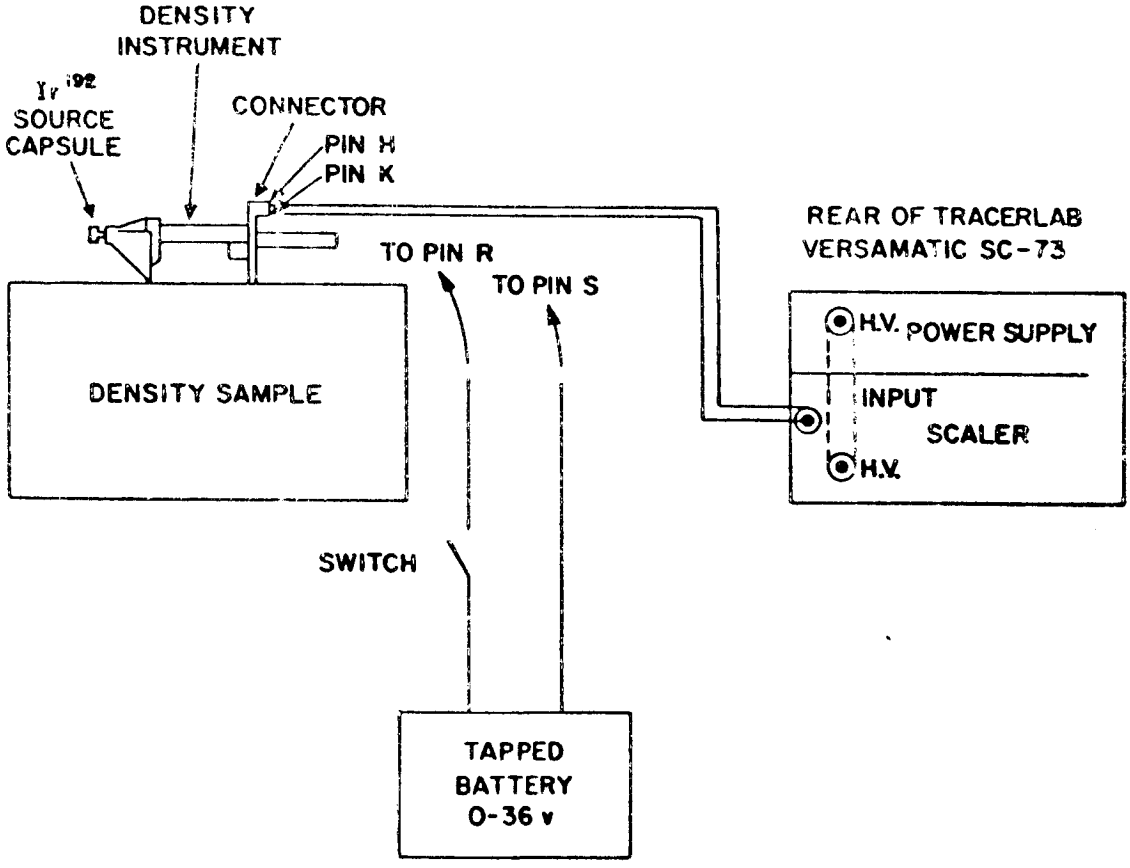

FIGURE 34. BLOCK DIAGRAM FOR DENSITY INSTRUMENT CALIBRATION

a. Accuracies obtained

Figure 35 shows the response curve obtained. It can be seen that all consolidated materials fall within 0.1 g/cm^3 of the curve. The response measured on the chalk (ρ = 1.93 g/cm^3) repeats within 3.5% or ±0.048 g/cm^3. All unconsolidated minerals except barium sulfate and manganese hubnerite fall well off the curve.

b. Departures from JPL functional requirements

Most unconsolidated materials do not fall within 0.1 g/cm^3 of the curve. An accuracy of 0.025 g/cm^3 was not attained at a density of 1.95 g/cm^3.

Lack of testing time and shortage of sample materials dictated that tests could not be run to determine accuracy on protuberances up to 10 cm.

Response of instrument at 0.1 g/cm^3 was not determined because of a lack of suitable test samples.

c. Departures from JPL design specification

No departures.

d. General summary of scientific objectives obtained and experimental results

It can be seen from the curve shown that the response was essentially linear from 0.65 to 4.0 g/cm^3. This linearity probably extends to the maximum point of the curve, which is approximately 0.2 g/cm^3. Materials with densities between 0. and 0.2 g/cm^3 presumably lie on a straight line passing through the point established by the balsa wood sample (ρ = 0.17 g/cm^3). Readings above background are still detectable out to a density of 6.80 g/cm^3. The change in response which takes place when the instrument is raised on its legs is also shown. It should be noted that the reading increased on the balsa, although development tests had indicated that it should decrease. This change over that experienced for the developmental model is probably due to scattering taking place from assemblies which were not present in the previous model, such as the connector housing, the geophone and its housing, and the pin-puller assembly.

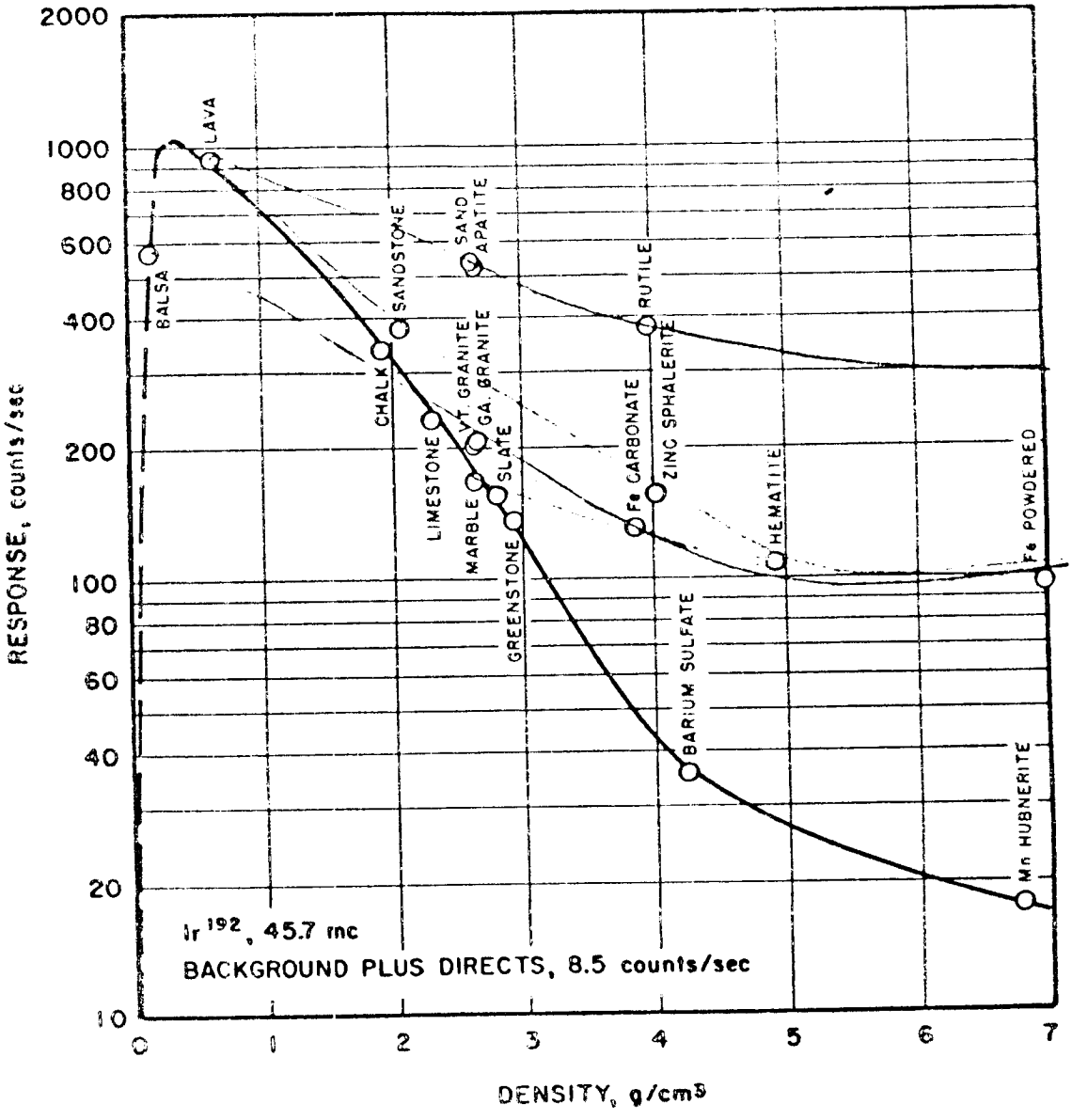

FIGURE 35. CALIBRATION CURVE OF THE SURFACE DENSITY INSTRUMENT

The remaining discussion concerns the response obtained on the unconsolidated materials. In all cases the unconsolidated materials except barium sulfate and manganese hubnerite fell to the right of the curve; that is, the measured density was less than the calculated density. This characteristic can be explained in part by recalling the method used to calculate the sample densities. In the case of the consolidated materials the densities were obtained by determining the weight and physical dimensions of the stones, and thus the density is bulk density.

The densities of the unconsolidated materials were found by the displaced-water method of determining volume and thus are specific densities. This method of measuring the unconsolidated materials was chosen because of the difficulty in repeating a volume measurement for a powdered or granulated material with any degree of precision since the amount of trapped air was not constant. The degree of scattering and absorption of the radioactive energy and thus the response of the instrument, however, is a function of the electron density of the material, and since some air is present, the net result is an averaging of the heavier mineral density and the lighter air density. It is not understood at the present time why the barium sulfate and manganese hubnerite fall on the extension of the curve defined by the consolidated samples. Further work is required to define accurately the above phenomenon so that the necessary compensating factors may be applied to the measurements obtained.

6.3.2 Results of Developmental Tests.

6.3.2.1 Leg-dropping mechanism.

a. Outline of tests conducted
The following tests were performed on the leg-dropping mechanism of the Surface Density Instrument and acoustic sensor to evaluate performance.

1. Mechanism actuated with a solenoid-actuated pin puller.

2. Mechanism actuated with an explosive-actuated pin puller.

The tests outlined above were conducted at 26°C.

b. Failure reports
The instrument would not fall freely within the legs with the 18-8 stainless-steel guide pins as shown in Figure 32.

c. Summary of corrective measures employed
The 18-8 stainless-steel guide pins were replaced with guide bushings fabricated from TFE Teflon.

d. Summary of experimental results
In all tests following the incorporation of the Teflon guide bushings the instrument fell freely within the legs.

6.3.2.2 Source-indexing mechanism

a. Outline of tests conducted
The function of the source-indexing mechanism is to move the radioactive source 1 inch upon a command from the spacecraft and return it to its initial position upon a second command from the spacecraft. The mechanism is to hold the source in either of its two extreme positions without power consumption. In the actual mechanism a solenoid imparts linear motion to a slide assembly containing the source. A series of teeth, in a rachet-type configuration, and a spring provide the holding arrangement. The teeth work against an indexing pin: this combination provides the proper rotary alignment of slots, pin, and teeth to accomplish the actual positioning of the mechanism.

The tests performed during the development of this mechanism were designed to eliminate the following modes of failure:

1. Failure of the indexing core due to mechanical failure or damage to the teeth.

2. Failure of the indexing pin due to impact.

3. Failure of the solenoid due to excessive current flow through the windings.

The mechanism was to operate from an unregulated bus at 22+6-4 volts dc through a temperature range of -65 to 150°C.

The extreme conditions for operation therefore were as follows:

1. At 18 volts dc (22 - 4 volts) and 150°C when the resistance of the windings was a maximum, the voltage a minimum, and therefore the solenoid force a minimum.

2. At 28 volts dc (22 + 6 volts) and -65°C when the resistance of the windings was a minimum, the voltage applied a maximum, and therefore the solenoid force a maximum.

Since the force provided by the solenoid must compress a spring for the mechanism to operate, the spring was chosen at condition 1. The maximum force which was provided by the spring could be no greater than the minimum force provided by the solenoid under the specified conditions. At condition 2 the force provided by the solenoid was in excess of the force absorbed by the spring and provided the worst condition for mechanical failures.

An area of 0.21 $in.^2$ was available for the solenoid windings. Figures 36 and 37 are the result of calculated values of length and resistance of the windings which could be fitted into this area; 28-gauge wire was chosen as it would supply the necessary ampere-turns without an excessively large current flow through the windings.

The following tests were performed on the developmental model of the source-indexing mechanism (Figure 38).

1. At 150°C and 18 volts dc tests were performed matching the spring force to the force provided by the solenoid.

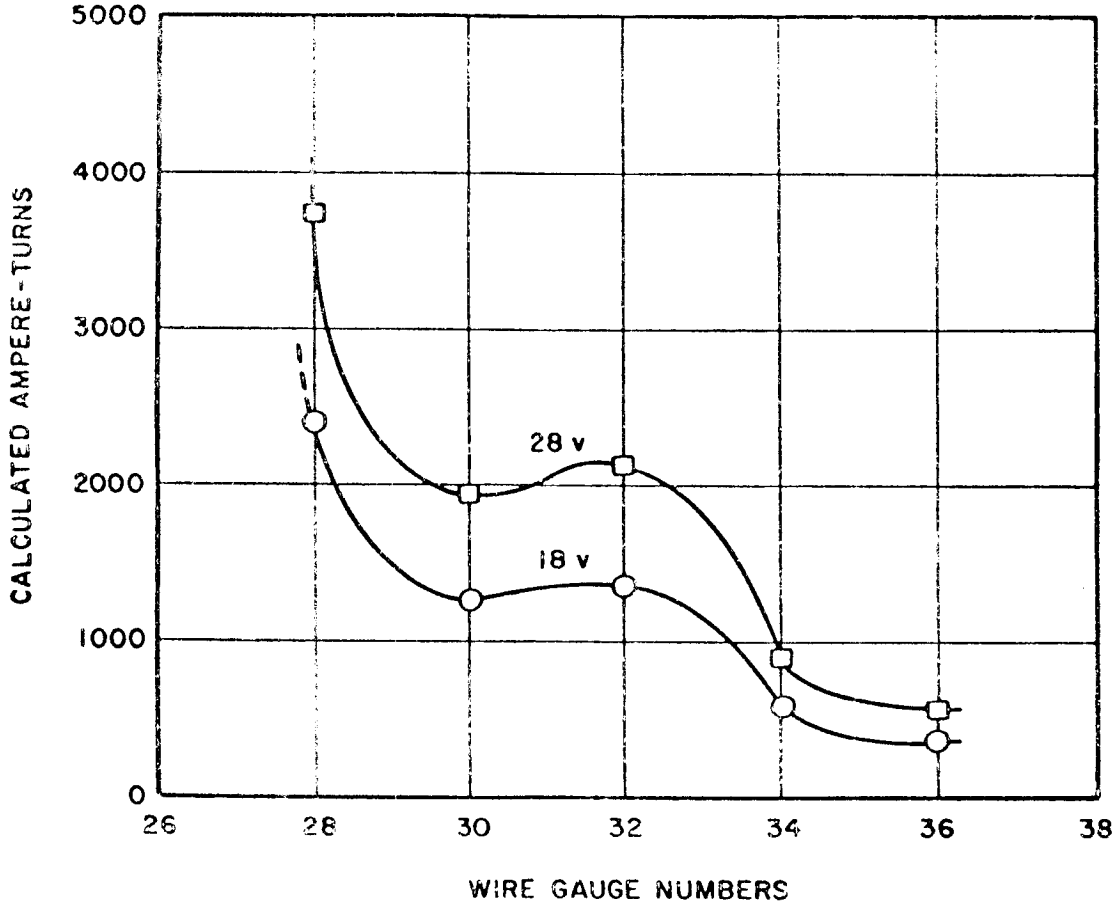

FIGURE 36. EFFECT OF WIRE GAUGE NUMBER ON SOURCE-POSITIONING SOLENOID PERFORMANCE AT 20°C

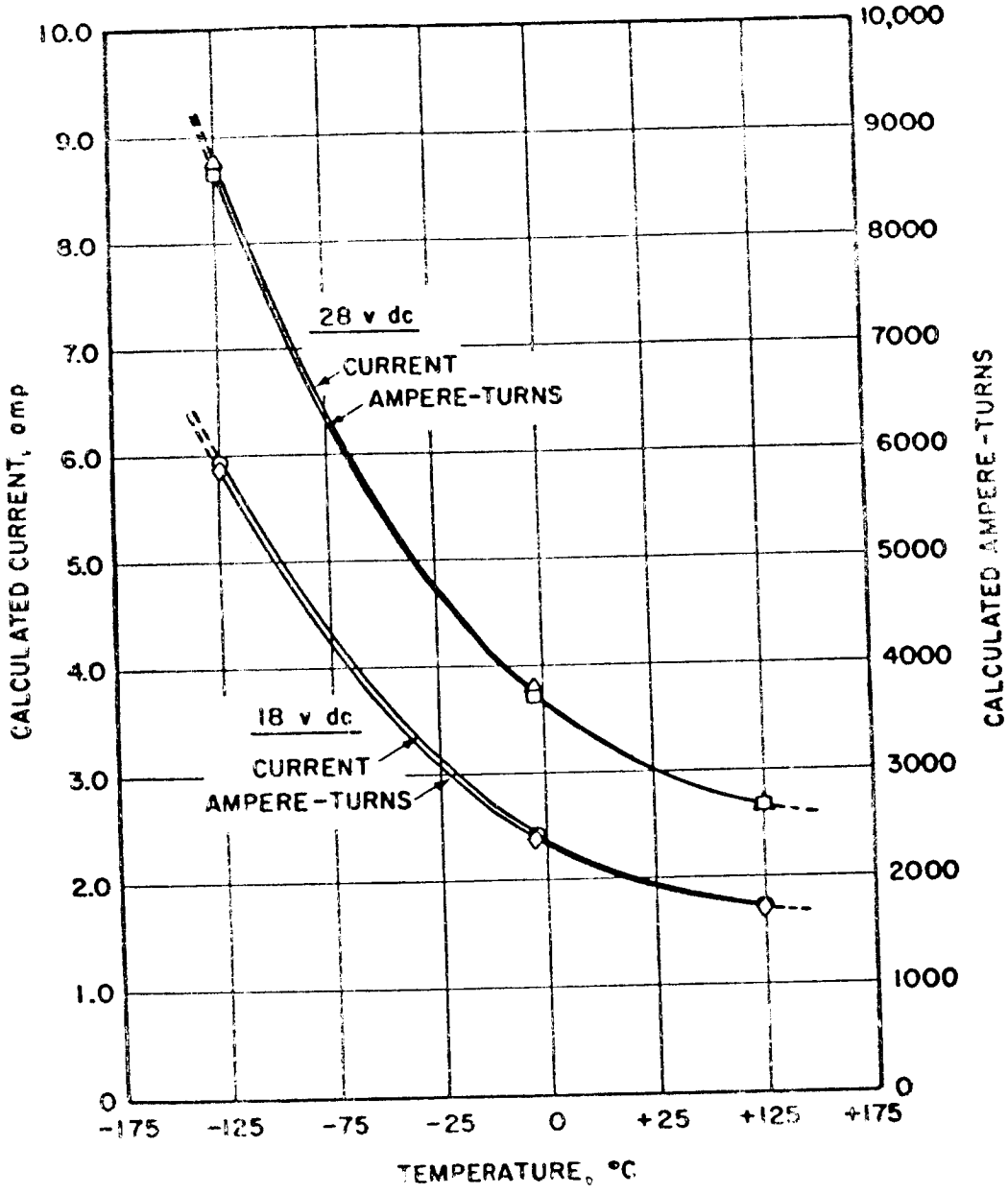

FIGURE 37. EFFECT OF TEMPERATURE ON SOURCE-POSITIONING SOLENOID PERFORMANCE FOR 990 TURNS, 28 GAUGE WIRE

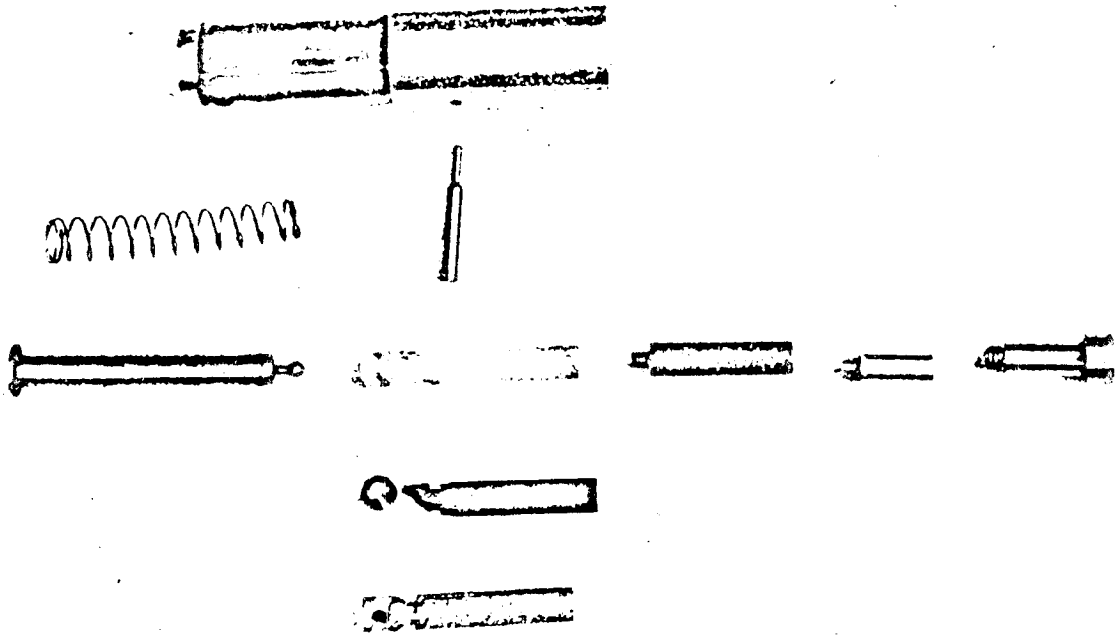

FIGURE 38. DEVELOPMENTAL MODEL OF SOURCE-POSITIONING MECHANISM

2. The source-indexing mechanism was then tested under the following conditions:

   (a) 150°C and 18 volts dc
   (b) 150°C and 28 volts dc
   (c) 26°C and 18 volts dc
   (d) 26°C and 28 volts dc
   (e) -65°C and 18 volts dc
   (f) -65°C and 28 volts dc

In order to eliminate the possibility of cold welding under hard vacuum conditions and to provide a dry lubricant, the Mallory 1000 portions of the slide assembly were coated with TFE Teflon 0.002 inch thick.

In addition to the tests outlined above the following test was conducted:

1. The windings were immersed in liquid nitrogen (-195.8°C) and allowed to reach equilibrium.
2. The windings were removed from the liquid nitrogen to 26°C ambient temperature, and immediately a voltage of 28 volts dc was applied to the windings.
3. This voltage was applied for 22 sec.

b. Failure reports

Two failures occurred during the developmental testing, both involving the indexing core. The first of these (Figure 39) was the mechanical failure of one tooth and occurred at 26°C with 28 volts dc applied to the windings. The material was Nylon 101. The second failure occurred (Figure 40) with an identical indexing core fabricated with Nylatron GS. This failure occurred at -65°C with 28 volts dc applied to the windings. No other failures were observed.

c. Summary of corrective measures employed

Since the observed failures were the result of excessive solenoid force, which developed from the change of applied voltage and environmental conditions, the indexing core was strengthened by increasing the amount of material between the teeth and the ball socket. No further

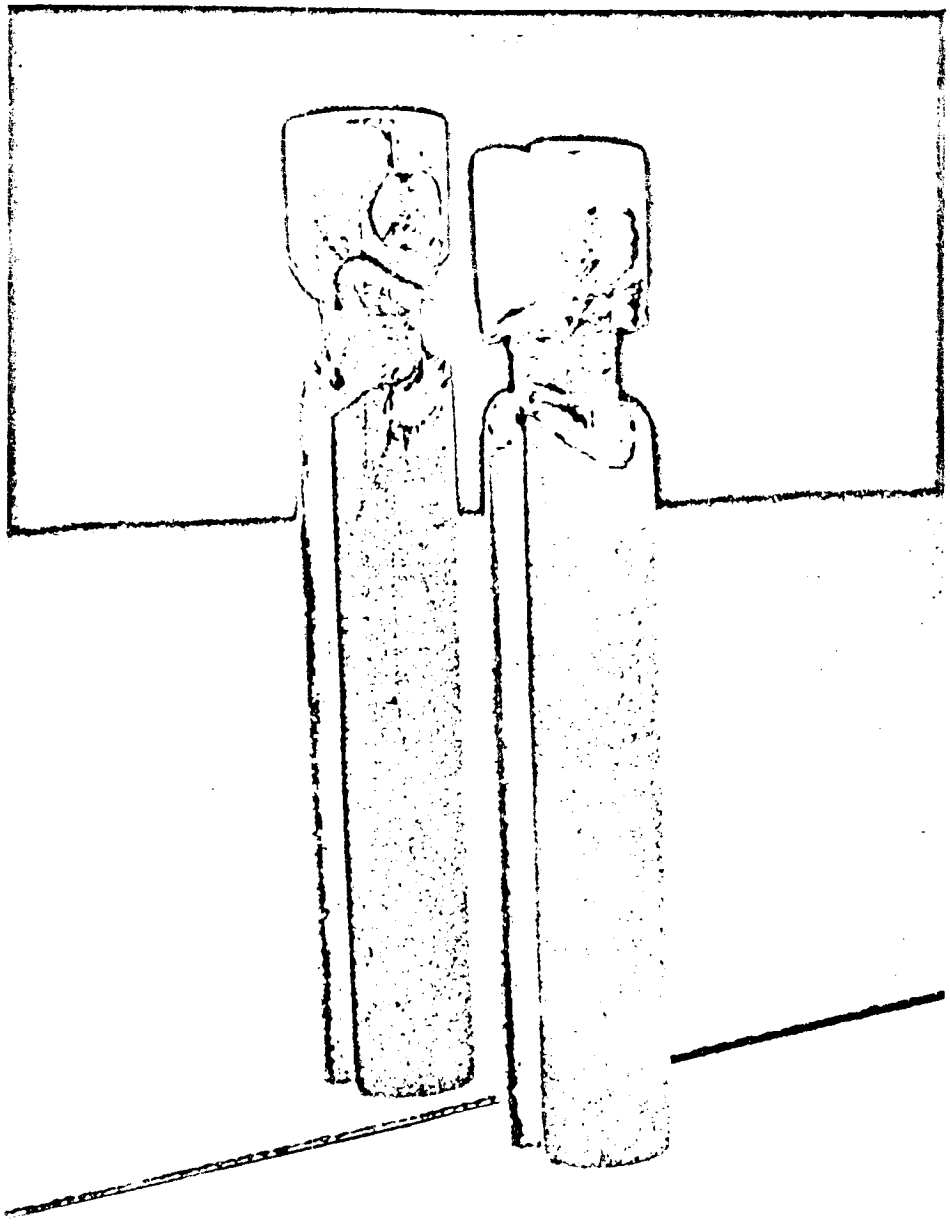

FIGURE 39. INDEXING CORE — MECHANICAL FAILURE OF ONE TOOTH AT 26°C AND 28 VOLTS DC

MATERIAL, NYLON 101

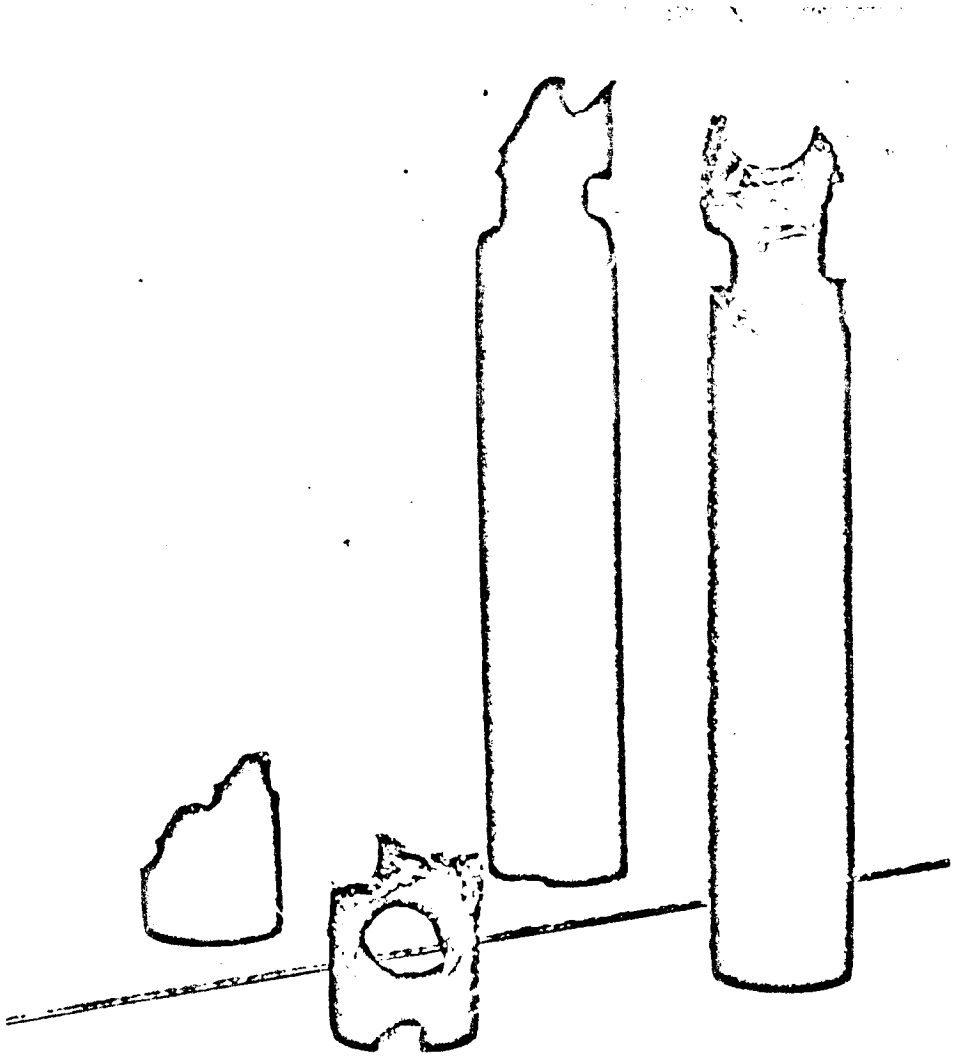

FIGURE 40. INDEXING CORE — MECHANICAL FAILURE AT BALL SOCKET AT -65°C AND 28 VOLTS DC

MATERIAL, NYLATRON GS

failures were observed after this change was incorporated.

d. Summary of experimental results
The source-indexing mechanism will operate satisfactorily with applied voltages of 22+6-4 volts dc within a temperature range of -65 to 150°C.

6.3.2.3 Geophone housing.

a. Outline of tests conducted
Tests were performed at 150°C to insure that sufficient clearance was available between the geophone cap and the interior walls of the geophone housing to allow free sliding of the geophone assembly within the housing.

b. Failure reports
Sufficient clearance was not allowed with the geophone cap as originally given.

c. Summary of corrective measures employed
The outside diameter of the geophone cap in assembly was reduced to provide the necessary clearance.

d. Summary of experimental results
Subsequent tests substantiated that sufficient clearance was incorporated in the design to allow free sliding of the geophone assembly within the geophone housing at 150°C.

6.3.2.4 Scientific development.
This section describes the testing program carried out in the scientific development of the Surface Density Instrument. It is broken down to cover shielding-material comparisons, establishment of test-area requirements, comparisons of response obtained for different radioactive source materials, optimization of source-shield cone angle, effects on response due to shield removal, response of multiangle cone shape, method for removal of response curve ambiguity, and radiation field strength measurement surrounding the device.

Since in general the test results did not lend themselves to failure analysis, the sections covering failure reports and

corrective measures employed have been deleted. The results obtained and the incorporated changes are discussed.

a. Transmission tests for shielding comparison of lead and Mallory 1000

The apparatus was setup as shown in Figure 41. Counting-rate measurements were made as 1/8 inch pieces of first lead and then Mallory metal were placed in front of the collimated source container. Figure 42 shows that for the straight portion of the curve Mallory 1000 is about 10% more efficient as a shielding material than lead. That is, 1/2 inch of Mallory 1000 will provide the same shielding as 3/5 inch of lead. From these results and because of superior mechanical properties, Mallory 1000 metal was specified for all shielding sections.

b. Determination of the degree of scattering within test laboratory

A G-M counter tube was connected to the scaler power supply in the normal manner and a collimated radioactive source placed a given distance away. A comparison of the response was made as the source was positioned at three different distances. The results are shown below:

Distance, in.	Response, counts/sec
30	3069
60	1044
90	495

The source was 31.6 mc of iridium-192. By the inverse-square attenuation law and the 30-inch reading as standard, the counting rate should have been:

Distance, in.	Response, counts/sec
30	3069
60	768
90	341

These data indicate that scattering from the walls and ceiling significantly affect the response and point out the need for testing in outdoor areas.

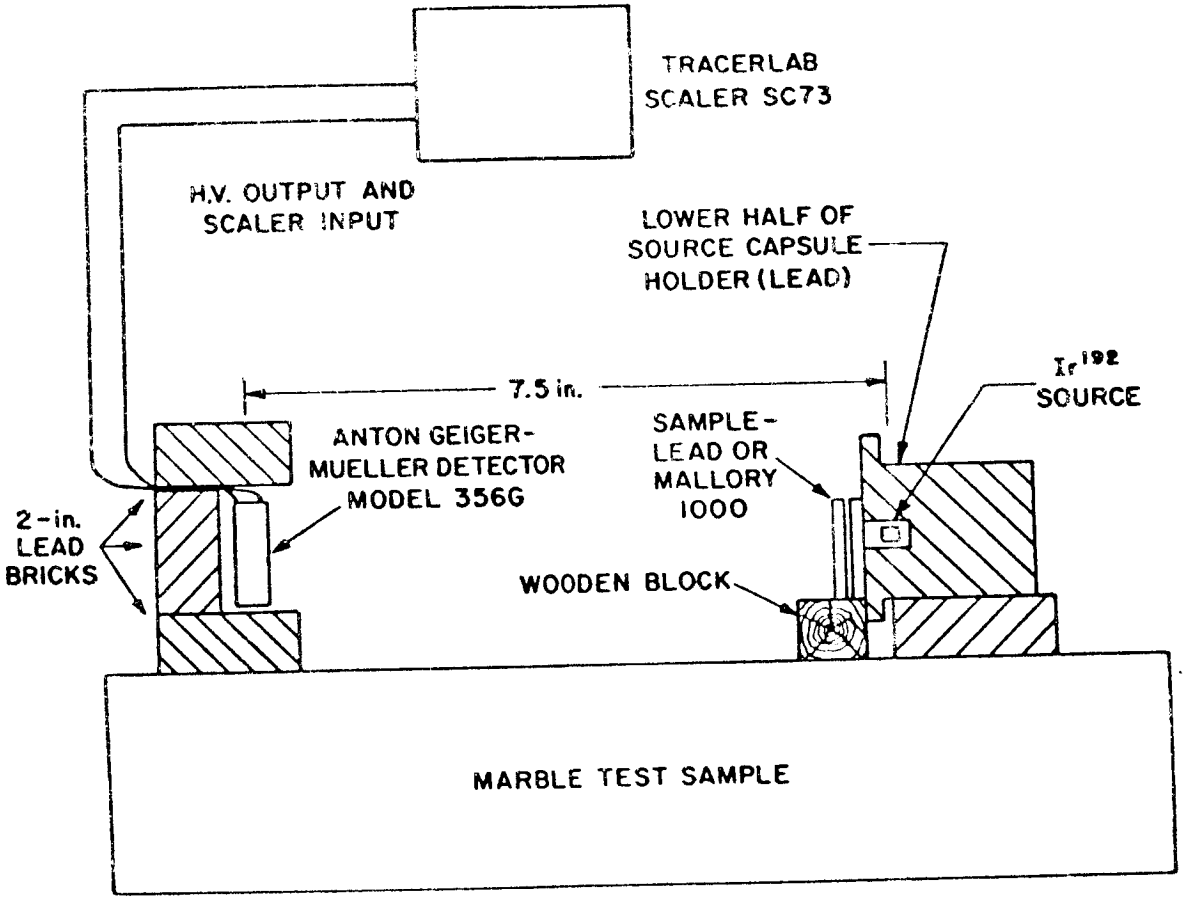

FIGURE 41. TEST SETUP—SHIELDING COMPARISON OF LEAD AND MALLORY 1000 METAL

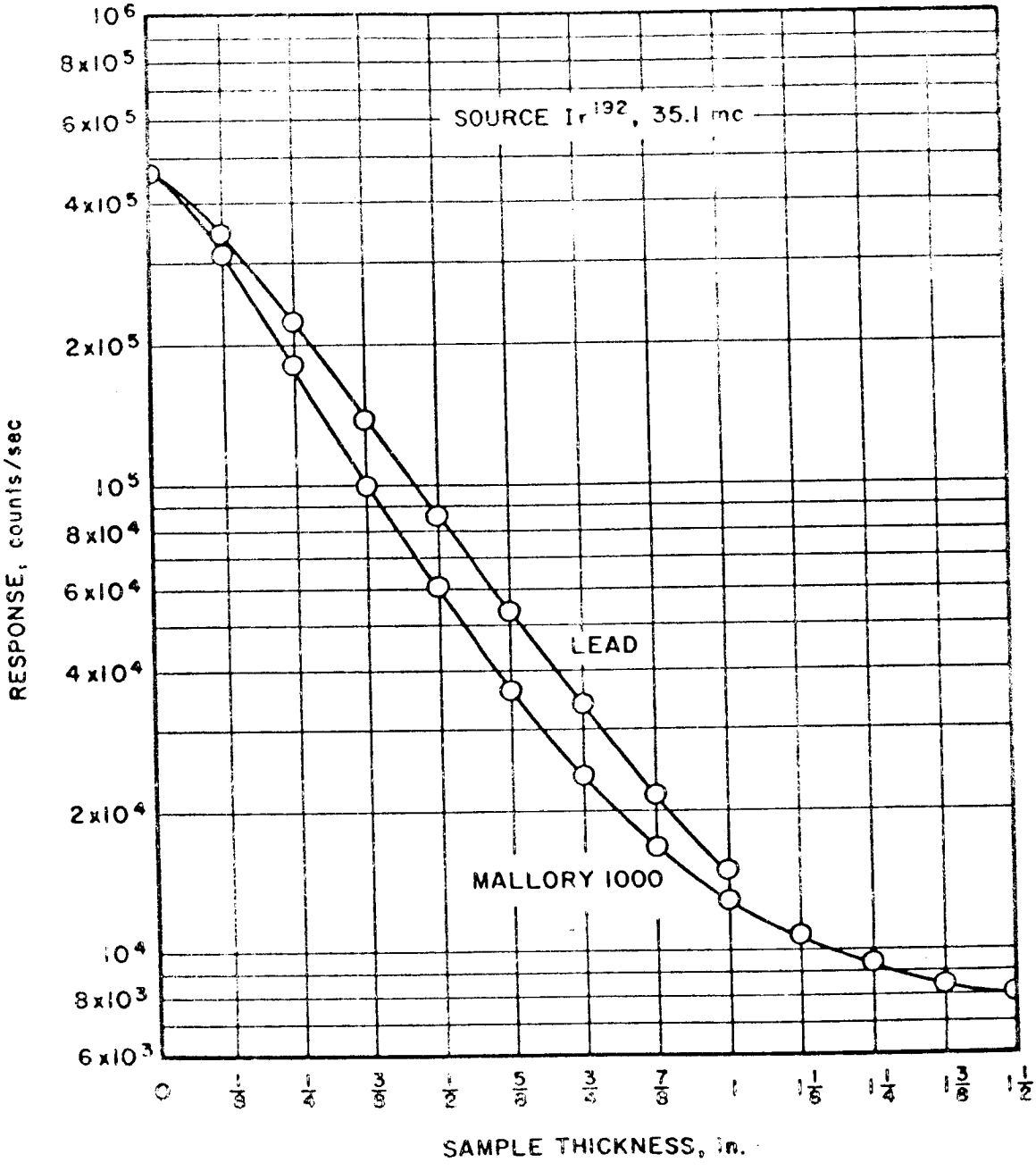

FIGURE 42. SHIELDING COMPARISON OF LEAD AND MALLORY 1000 METAL

c. Radioactive source comparison with breadboard density instrument

A lead model density device similar to that used at Texaco Bellaire Laboratories was constructed and connected to the scaler power supply. Response measurements were made on the lava, chalk, and marble samples to compare the iridium-192 source with the cesium-137 used in the breadboard development work. The data obtained are plotted in Figure 43 along with the response curve as given in the Texaco Bellaire Laboratories report (14).

The instrument using the iridium-192 source produced a substantially higher counting rate and a slope nearer the ideal 45° and thus was specified for the prototype instrument. An additional advantage of this compound is that its half-life is 74 days as compared with 30 years for cesium-137, and therefore the danger of lunar contamination is reduced.

d. Optimize source shield cone

Utilizing a lead developmental model density instrument, tests were run to determine which source cone angle would provide the best compensation for the instrument when placed on simulated surface protuberances. Source cone half-angles (from centerline) of 26°, 36°, and 46° were used with the instrument placed on simulated protuberances of 1, 2, and 3 inches. The resultant data obtained from the tests on lava, chalk, and marble are shown in Figures 44, 45, and 46. The curves are best analyzed by noting any major deviations in response for the various cone angles at different heights of the instrument on the lava, chalk, and marble samples. It can be seen that the 26° and 36° cone shapes have large deviations for certain combinations of instrument position and sample material. The 46° cone shape provides the least deviation and was chosen (45°) to be used on the prototype model.

e. Effects of shield material removal on instrument response

A Mallory metal developmental instrument was constructed

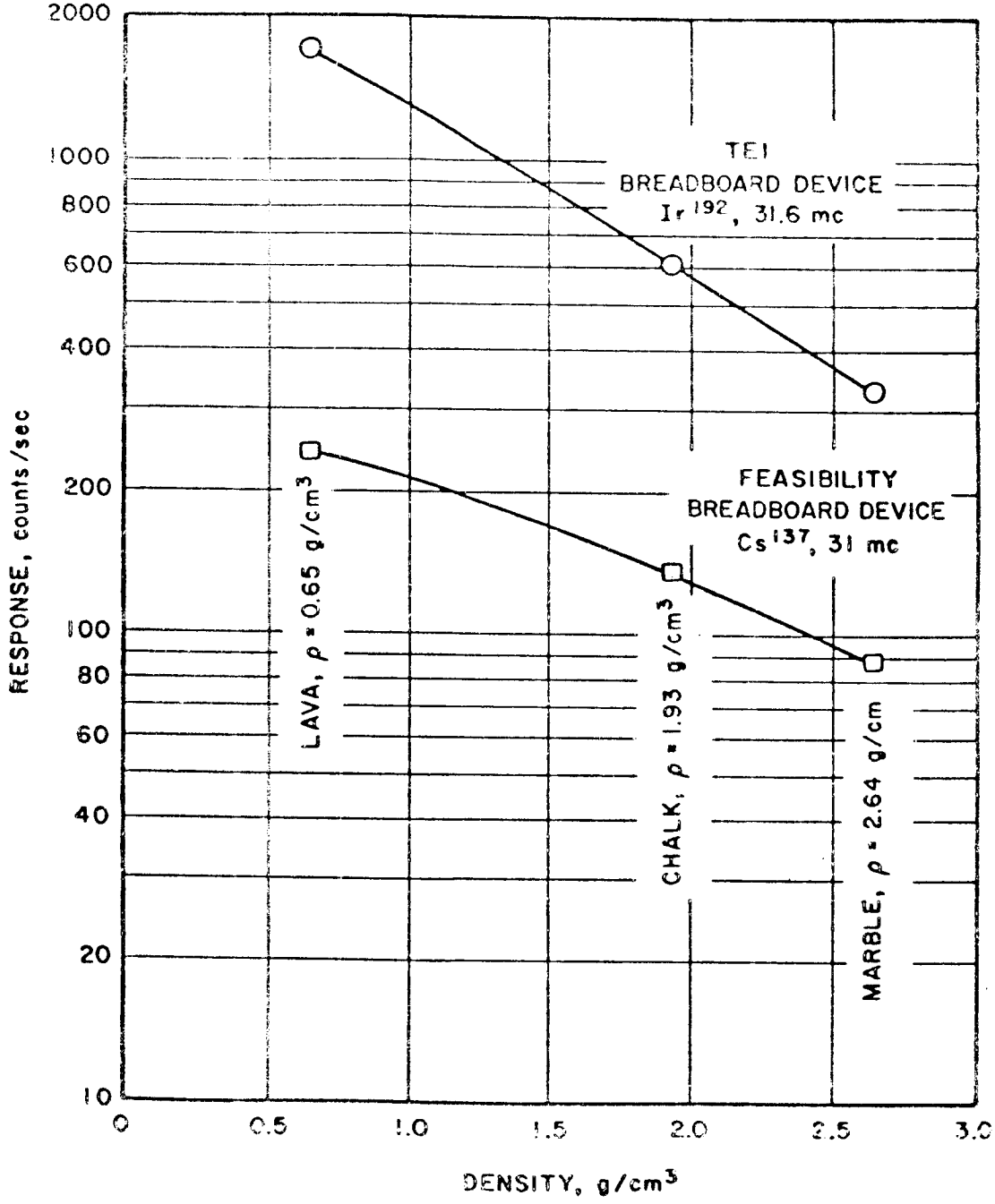

FIGURE 43. COMPARISON OF RESPONSE FROM IRIDIUM-192 AND CESIUM-137 SOURCES WITH BREADBOARD DEVICES

1.17 Mev

Compton Transition

Compton - 6 = .137 - - - .661 Mev

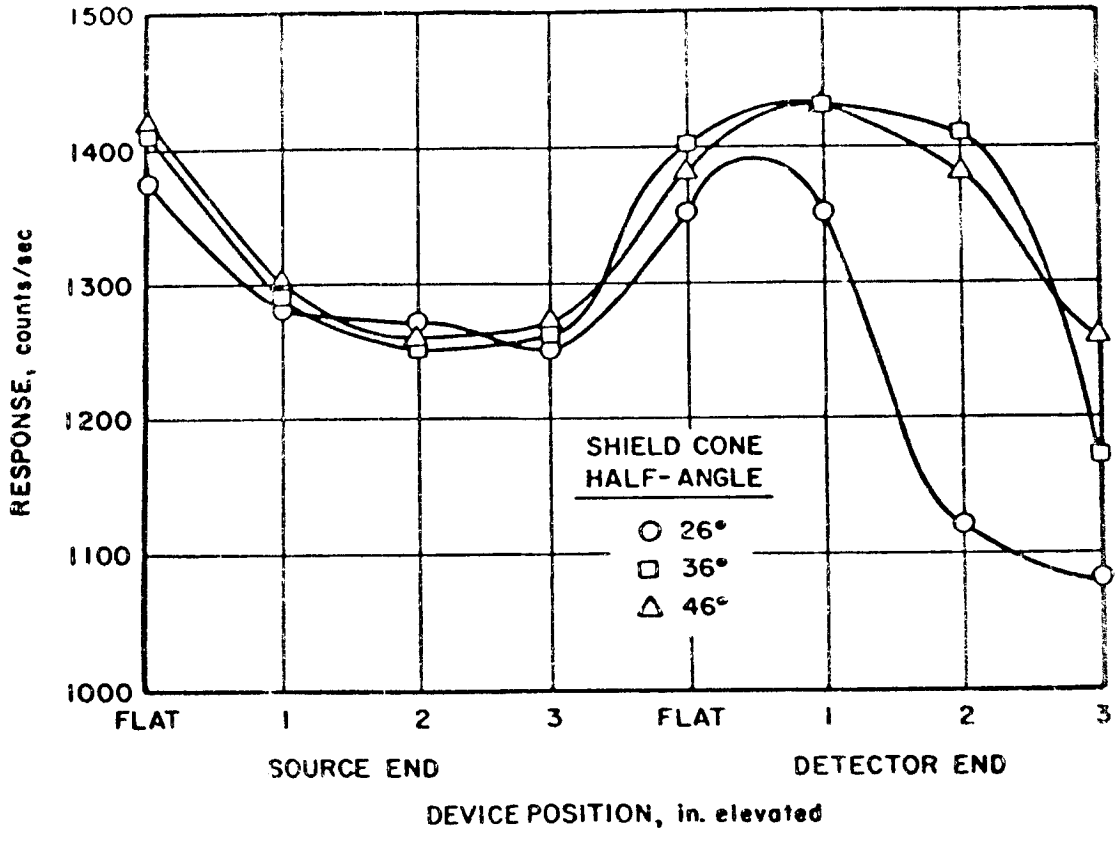

FIGURE 44. RESPONSE OF DEVELOPMENTAL MODEL DENSITY INSTRUMENT ON LAVA SAMPLE FOR VARIOUS SHIELD CONE HALF-ANGLES

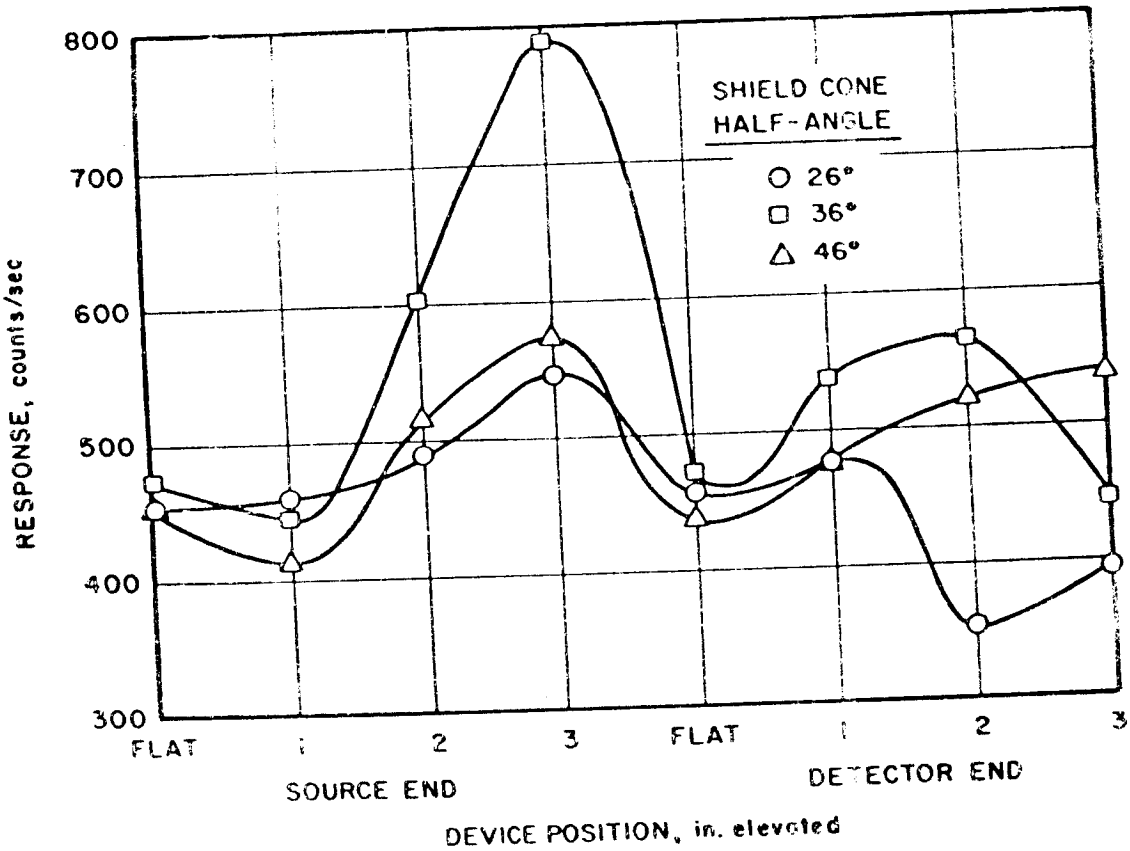

FIGURE 45. RESPONSE OF DEVELOPMENTAL MODEL DENSITY INSTRUMENT ON CHALK SAMPLE FOR VARIOUS SHIELD CONE HALF-ANGLES

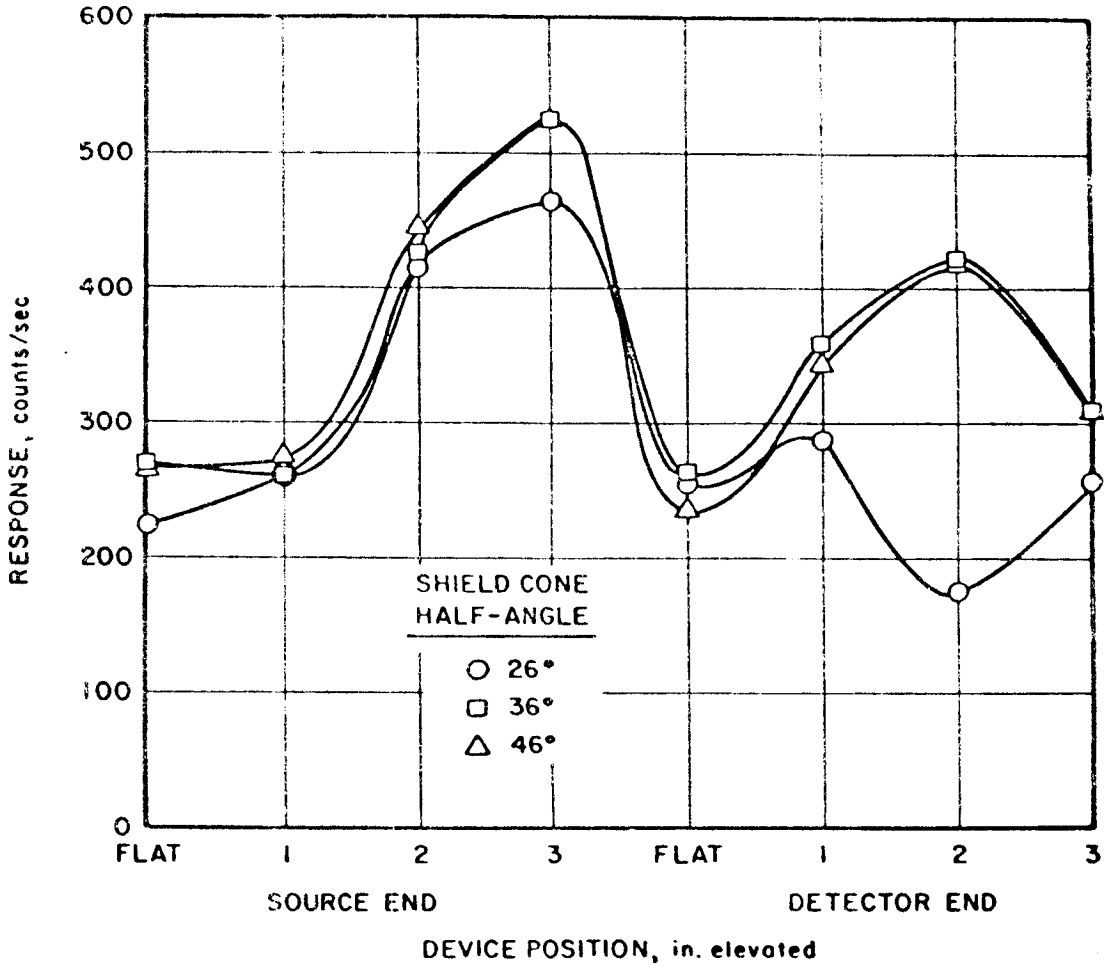

FIGURE 46. RESPONSE OF DEVELOPMENTAL MODEL DENSITY INSTRUMENT ON MARBLE SAMPLE FOR VARIOUS SHIELD CONE HALF-ANGLES

similar to the lead breadboard unit, and tests were run to determine the amount of shielding which could be removed without materially affecting the instrument response. The results obtained are shown in Figure 47. The indicated changes were incorporated into the prototype unit.

f. Response of multiangle cone.
In order to reduce weight further, a multiangle cone was fabricated to provide the 45° half-angle on the lower section as required for proper functional operation and a 22.5° half-angle on the upper section to provide the necessary shielding for the other sensitive instruments located on the spacecraft. The results obtained indicate that the functional requirements were not compromised by removing shielding from the upper section of the cone. A later change requiring additional spacecraft shielding necessitated a redesign which resulted in the final configuration as shown in Figure 32.

g. Determination of height above surface required to raise the instrument to remove ambiguity in response curve
The Mallory metal developmental model with wire leg assembly was positioned on the balsa wood and lava samples with the counter tube end of the instrument level and raised 1, 2, and 3 inches above the normal position and the change in counting rate between the raised and level positions recorded. The results are shown in Table 18.

Figure 48 shows the change in response obtained for measurement made on balsa, lava, chalk, marble, and barium sulfate with the density instrument in the level position and then with the detector end raised an additional 3 inches.

From these data it was determined that a two-position measurement could remove any ambiguity in the response curve.

h. Radiation field strength around instrument
The developmental model density instrument with the 22.5°-45° half-angle cone shield was placed on the ground in the

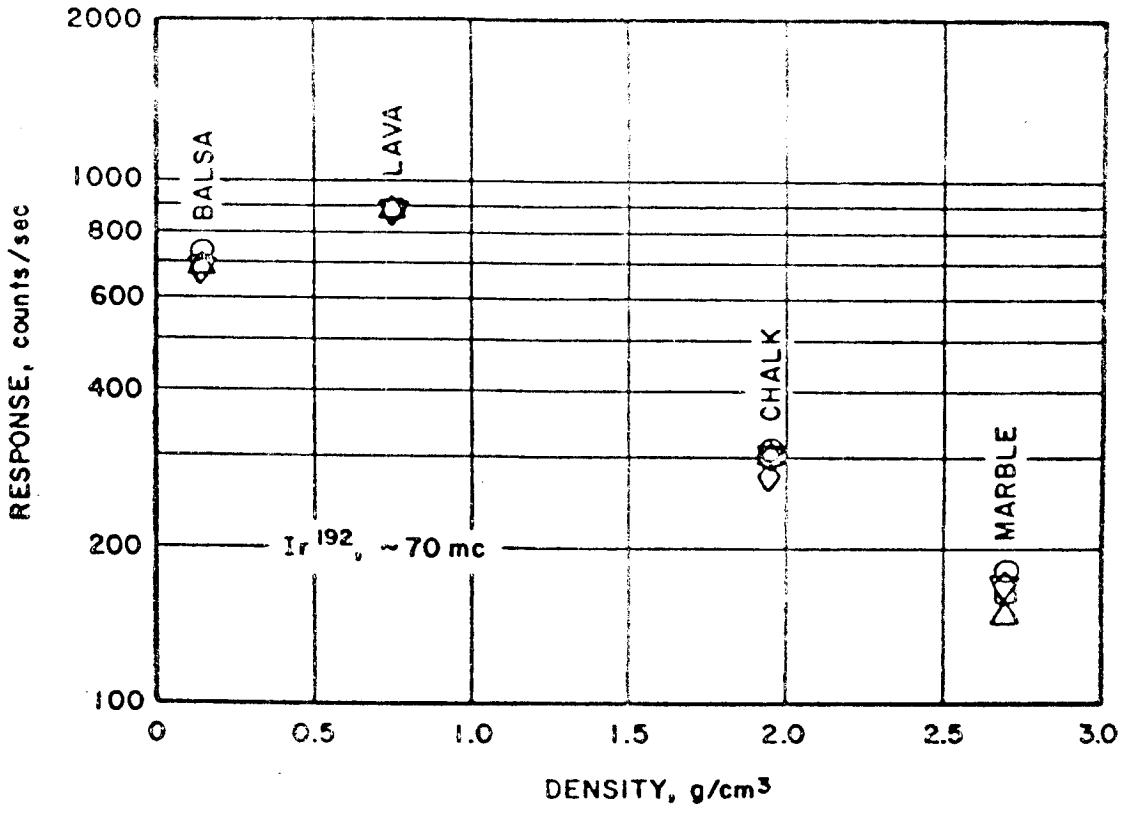

FIGURE 47. EFFECT OF SHIELD REMOVAL ON INSTRUMENT RESPONSE

△ START OF TEST
◇ SIDES REMOVED FROM REAR SHIELD
○ TOP RIM REMOVED (180°)
□ 0.020 IN. REMOVED FROM TUBE WALL
▽ 0.040 IN. REMOVED FROM TUBE WALL

TABLE 18

CHANGE IN INSTRUMENT RESPONSE ON BALSA AND LAVA WITH COUNTER TUBE RAISED 1, 2, AND 3 INCHES ABOVE NORMAL

Material	Instrument Position	Response	
		counts/min	av counts/sec
Balsa	Level	41,762	
		41,713	
		41,374	
			695
	Detector up 1 in.	42,058	
		41,908	
		41,374	
			694
	Detector up 2 in.	40,536	
		40,631	
		40,437	
			675
	Detector up 3 in.	38,569	
		38,161	
		38,412	
			640
	Level	42,242	
		42,257	
		42,501	
			705
Lava	Level	52,593	
		52,650	
		52,536	
			876
	Detector up 1 in.	53,866	
		53,380	
			893
	Detector up 2 in.	58,484	
		58,187	
			972
	Detector up 3 in.	56,877	
		56,387	
			943
	Level	53,581	
		53,895	
			895

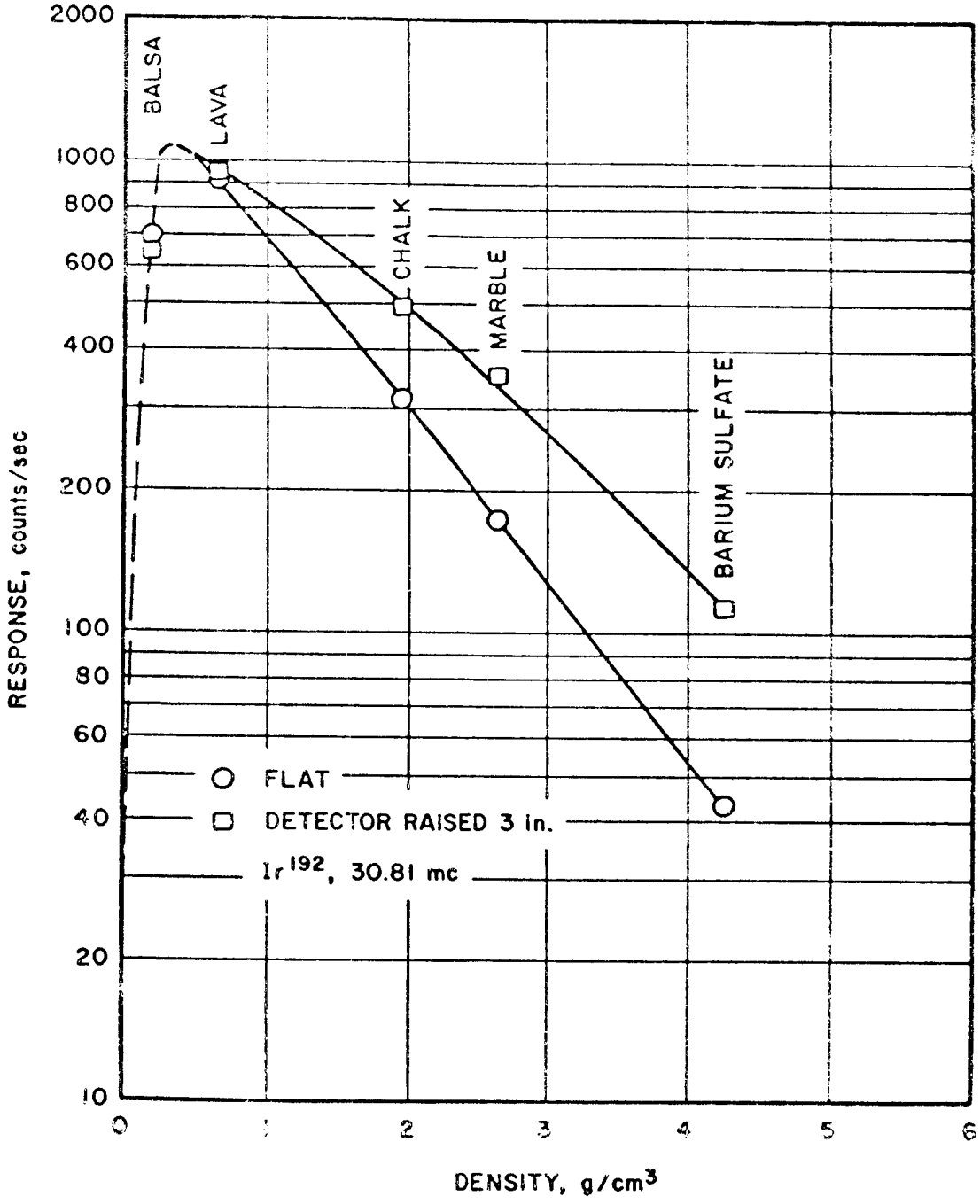

FIGURE 48. EFFECTS OF TWO-POSITION MEASUREMENTS ON INSTRUMENT RESPONSE

center of three concentric circles with radii of 5, 10, and 20 ft. An Anton No. 356 counting tube was positioned at various angles around the circles and at different heights to measure the counting rates due to a 40 mc iridium-192 source mounted in the density instrument. The purpose was to see if sufficient shielding was provided to protect the sensitive area of the spacecraft from excessive radiation fields.

The results obtained are shown in Figures 49 and 50 for the source in the exposed and retracted positions.

The field-strength requirement at the time of the test was that the counting rate be less than 0.01 mr/hr for a 1 cm^2 area 344 inches from the source situated within the shaded area of the cone. The data obtained indicated that the level would be approximately 0.003 mr/hr with the source exposed and 0.00065 mr/hr with source in the shielded position.

6.4 Components Outline

6.4.1 Notations and Explanation of Deviation from JPL and/or HAC Preferred Parts List. There are seven purchased components included in the Surface Density Instrument as follows:

1. Connector - Bendix Pigmy PTS02A-14-18(005)
2. Connector - Bendix Pigmy PTS06A-84S(300)
3. Squib - Per HAC Spec. No. 236182-1
4. Pin Puller - Per HAC Spec. No. 236170
5. Geiger-Mueller counter tube - Anton No. 356
6. Geophone - Hall-Sears Model HS-J
7. Radioactive Source - Technical Operations sealed source

The connectors are JPL/HAC approved. The squib and pin puller are being qualified by HAC. All other components are special and do not fall under classifications within the approved parts list of JPL/HAC. Therefore, limited qualification testing was performed prior to inclusion of these parts in the prototype instrument.

6.4.2 Results of Components Tests.

6.4.2.1 Geiger-Mueller counter tube.

An Anton No. 356 Geiger-Mueller counter tube similar to that utilized in the feasibility study was subjected to the tests described below to determine if it would survive the environmental tests as specified by HAC (15).

a. Outline of Tests Conducted - First tube

1. Static acceleration

(a) 10 g for 4 min
(b) 5 g for 8 min

2. Vibration - sinusoidal (two planes)

(a) Nominal 1.3 g from 5 to 10 cps for 18 min
(b) 1.3 g from 10 to 35 cps for 16 min
(c) 3.0 g from 35 to 48 cps for 4 min
(d) 5.0 g from 48 to 500 cps for 25 min

3. Vibration - random and combined sinusoidal (two planes)

(a) 15 g rms wga 15 to 1500 cps for 10 sec
(b) 10 g rms wga 15 to 1500 cps for 3 min
(c) 4.5 g rms wga 15 to 1500 cps plus 4.5 g superimposed sinusoidal 40 to 1500 cps for 7 min

4. Temperature cycling 25 to -65°C and 25 to 150°C for total of 4 hours at each temperature

5. Cooling to liquid-nitrogen temperature

b. Failure reports

The tube used in the qualification tests (Serial No. 6132) successfully survived all static acceleration and vibration tests and the temperature-cycling tests. It was not subjected to the liquid-nitrogen survival tests.

From these results and from the knowledge that no other vendors had off-the-shelf tubes which could fulfill the dimensional and scientific requirements, and since that time did not allow for tube development, the tube was specified for use in the prototype model. Tube No. 6132 was delivered as part of the surface prototype instrument.

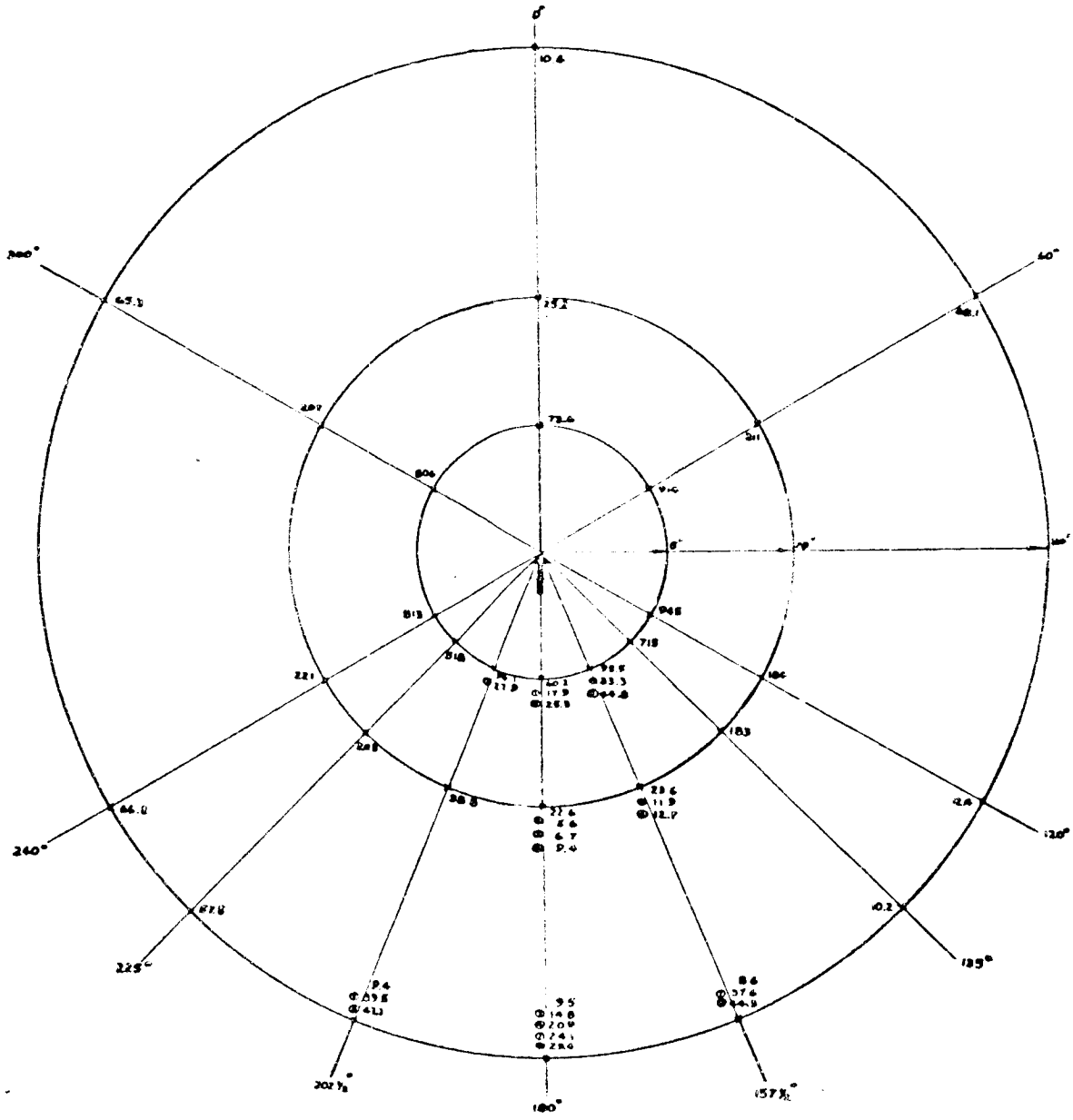

FIGURE 49. RADIATION FIELD STRENGTH VERSUS DISTANCE — SOURCE EXPOSED

RESPONSE IS IN COUNTS PER SECOND
CIRCLED NUMBERS INDICATE COUNTER TUBE HEIGHT ABOVE SURFACE

200 counts/sec ≅ 1 mr/hr
ACTIVE CROSS-SECTIONAL AREA OF COUNTER TUBE, ~7.7 cm²
Ir^{192}, 40 mc

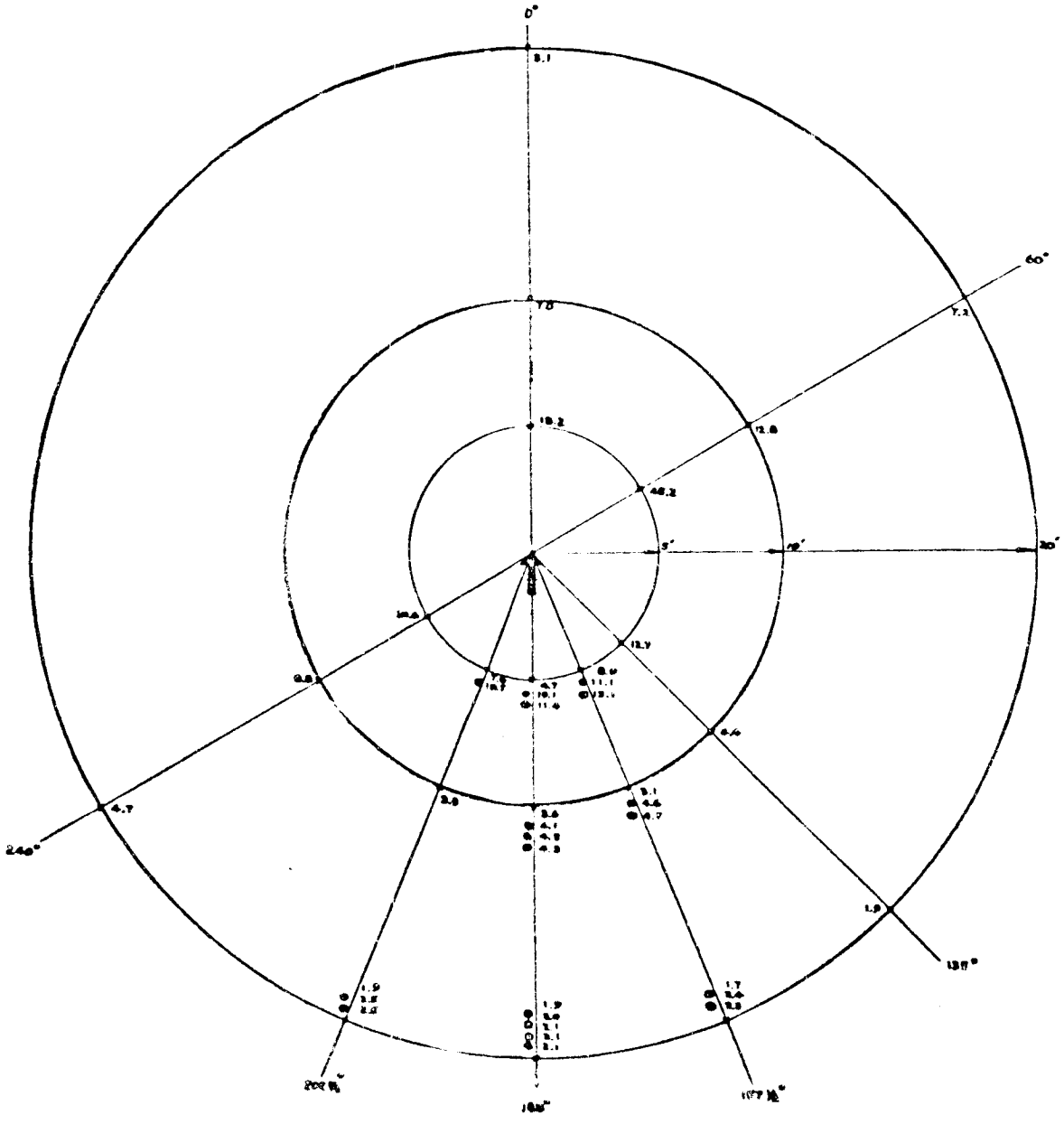

FIGURE 50. RADIATION FIELD STRENGTH VERSUS DISTANCE— SOURCE RETRACTED

RESPONSE IS IN COUNTS PER SECOND

CIRCLED NUMBERS INDICATE COUNTER TUBE HEIGHT ABOVE SURFACE

200 counts/sec ≅ 1 mr/hr

ACTIVE CROSS-SECTIONAL AREA OF COUNTER TUBE, ~7.7 cm^2

Ir^{192}, 40 mc

An outline of the tests conducted on future tubes and failures reports are given below.

Tube No. 6139 was submerged in liquid nitrogen after having been wrapped in a polyethylene bag. The tube failed. The cause of failure was found to be cracked glass at seal-off end and separated ground wire.

Anton tubes No. 12 and No. 20 were subjected to sinusoidal vibration of 10 g's from 20 to 3000 cps for 20 min. Both tubes failed. Failure was caused by cracked ceramic seals at exit point of anode wire.

All of the above tubes utilized pigtail leads as a means for connecting to the tube. In all cases the anode or cathode wire separated from the tube as a result of excessively high pressure used in crimping the wire in the holder.

At this point a source inspection was held at the vendor's plant to determine possible cause for tube failure. The inspection revealed an unusually lax quality control practice and a poor state of housekeeping. It was recommended that the pigtail leads be replaced with solder lugs so that TEI might attach the wires as required. The vendor assured us that any faulty tubes would be replaced but made no attempt to improve reliability.

The tube history for subsequent tubes is given below:

1. Tube No. 100 was run through the temperature-cycling test. The tube failed because of poor high temperature characteristic.

2. Tube No. 101 would not function upon receipt.

3. Tube No. 6202 withstood temperature-cycling tests, but the plateau characteristic did not meet acceptance test specifications.

4. Tube No. 6207 successfully passed limited vibration test and all acceptance tests except it was not subjected

to liquid-nitrogen survival. The tube was used in the Subsurface Density Instrument.

Other tube manufacturers, Amperex Electronic Corporation and EON Corporation, were contacted so that a second source of more reliable tubes could be found. Both organizations were interested in designing tubes to our specification. Amperex was chosen to deliver ten tubes on an approval basis. Three prototype tubes have been delivered and are presently undergoing qualification tests. Amperex was chosen because of their experience in building high-reliability tubes for use in well logging and because of their manufacturing techniques and quality assurance practices. It may be advisable to have EON supply tubes as a backup source. No tubes are presently being purchased from Anton-Lionel.

6.4.2.2 Geophone.

See Acoustic Velocity section of this report for test results.

6.4.2.3 Radioactive source.

Fabrication of sealed radioactive source capsules is controlled by AEC regulations. Wipe tests as specified by the National Bureau of Standards will be performed at the required intervals to determine if the capsules are intact (16).

6.5 Packaging Philosophy

Basically the philosophy employed in the mechanical packaging of the Surface Density Instrument and acoustic sensor was as follows:

1. Attempt to contain the instrument within a minimum envelope while maintaining dimensions critical for the scientific experiments.
2. Keep the total mass of the instrument as small as possible.
3. Provide for ease of maintainability.
4. Insure that the instrument would function as required under the expected environmental conditions.

Two dimensions were critical for the density experiment. These were the distance between the source, when extended, and the Geiger-Mueller tube and the elevation of the Geiger-Mueller tube above the surface when the instrument was in its elevated position. From the first of these the over-all length of the instrument was fixed, from the second the over-all height. Stability requirements determined the width of the legs and, therefore, the over-all width of the instrument.

Of the total weight of 3.21 lb the material necessary in shielding the radioactive source comprised 2.23 lb or 69.5% of the total weight. The geophone, or acoustic sensor, incorporated within the instrument added 0.13 lb to the necessary scientific weight. Therefore, packaging operations controlled only 0.85 lb of the total weight or 26.5% including structure and mechanisms.

Ease of installing replacement parts was provided whenever such an arrangement would not adversely affect the operation or structural soundness of the instrument. In most instances the operations required consisted of the removal of threaded fasteners.

Functional tests were performed on all moving parts under the critical environmental conditions to insure their satisfactory operation.

6.6 Theoretical Studies

The developmental work performed for the Surface Density Instrument was based on feasibility studies carried out at the Texaco Bellaire Laboratories. Results of these studies may be found in their reports (9, 10, 14, 17).

6.7 Environmental Test Results

6.7.1 Purchased Components. The environmental tests conducted on the purchased components are described in the components outline section.

6.7.2 Assemblies. Testing carried out for the assemblies is described in the developmental tests section.

6.7.3 Complete Instrument. No environmental tests have been run on the completely assembled instrument.

6.8 Recommendations

1. In order to reduce weight and system complexity the leg and leg release assemblies should be removed from the instrument. Detail comments are given in Appendix F, an internal memorandum dated 4 April 1962.

2. A cover should be added to the cone shield section to enclose the source when in the extended position. Details are given in an internal memorandum dated 4 April 1962 (Appendix G).

3. Detail studies should be carried out to define response characteristics on unconsolidated materials.

4. The solenoid low-temperature operating requirement should be limited to that of the counter tube (225°K) to improve reliability by lessening the danger of impact damage to the index mechanism.

5. Positional-stability requirements should be established for the instrument.

7. SURFACE PENETRABILITY INSTRUMENT

URD 28, 29, and 30

Control Item X239235

7.1 System Description

The Surface Penetrability Instrument consists of a piezoelectric-type accelerometer with a specifically shaped impact tip. It is to be mounted on a pivoted-arm bracket (HAC) and dropped, one from each of three spacecraft legs, causing the impact tip to strike the lunar surface at about 4 ft/sec. Two of these tips are compound conical tips and one is hemispherical: the conical tip offers the better information upon impact with a hard material, such as rock, whereas the hemispherical tip gives somewhat better results in sand.

The output of the instrument, then, is the deceleration-time history of its impact with and penetration of the lunar surface. From this record several distinguishing characteristics may be obtained:

a. Pulse height, maximum or mean, in units of acceleration.

b. Pulse width, in units of time.

c. Characteristic shape, including bounce, harmonics, etc.

d. Slope or rate of deceleration, in units of acceleration per unit time.

e. Velocity and displacement histories, obtained by successive integrations of the curve.

Thus the lunar surface material is to be classified in terms of equivalent earth material by the comparison of its characteristics to those obtained in the laboratory.

7.2 Equipment Description

The physical parameters of the penetrometers are as follows:

a. Dimensions, over-all: 1.00 inch in diameter by 1.712 inches in length, depending upon the thickness of the HAC bracket (assumed 0.038 inch).

b. Weight: conical-tip models (URD 28 and 29) weight, 42.5 grams (0.094 lb). Spherical-tip model (URD 30) weight, 45 grams (0.099 lb). Total weight, 130 grams (0.287 lb).

c. Electrical connector required: Microdot Series 32 screw-type or Endevco 3090 low-noise cable assembly.

The dimensions and center-of-gravity locations are shown in Figure 51. The materials are as follows:

a. Accelerometer case: Type 303 stainless steel.

b. Accelerometer stud: Type 416 stainless steel with magnesium oxide insulation.

c. Tip base: 2024-T4 aluminum, clear sulfuric acid anodized.

d. Hardened tip (conical): M-2 HSS hardened to Rc 60-65

The accelerometers are Endevco Corporation Model 2233M11 with a modified 2980B insulating stud.

The accelerometers do not consume power; they are piezoelectric devices. The Endevco 2620 charge amplifier used with the accelerometer (not TEI furnished) requires +28.5 volts dc ±9% and draws 25 ma or 0.714 watts.

7.3 Testing And Calibration

7.3.1 Results of Functional Tests. The penetrometer final acceptance tests were reported to JPL as our TM-1330 (18). This report will not show all the oscillograms in TM-1330, although some of the data will appear here.

In general, these tests were carried out on the test fixture shown in Figure 52. They were performed on man-made materials for maximum reproducibility, on natural materials to study characteristic deceleration curve shapes, and at high and low temperatures and under vacuum conditions to simulate environment. Oscilloscope traces of the instrument deceleration were photographed and the deceleration in g's (maximum value of a mean line) and the width of the pulse at the base line in milliseconds were measured and recorded.

7.3.1.1 Accuracies obtained.
Tables 19 and 20 show that the repeatability of maximum deceleration and pulse width on man-made materials varied from 3.9% (maximum variation from average) on gum rubber to 0.1% on aluminum. On natural materials 25% was not uncommon, as can be seen from Table 21.

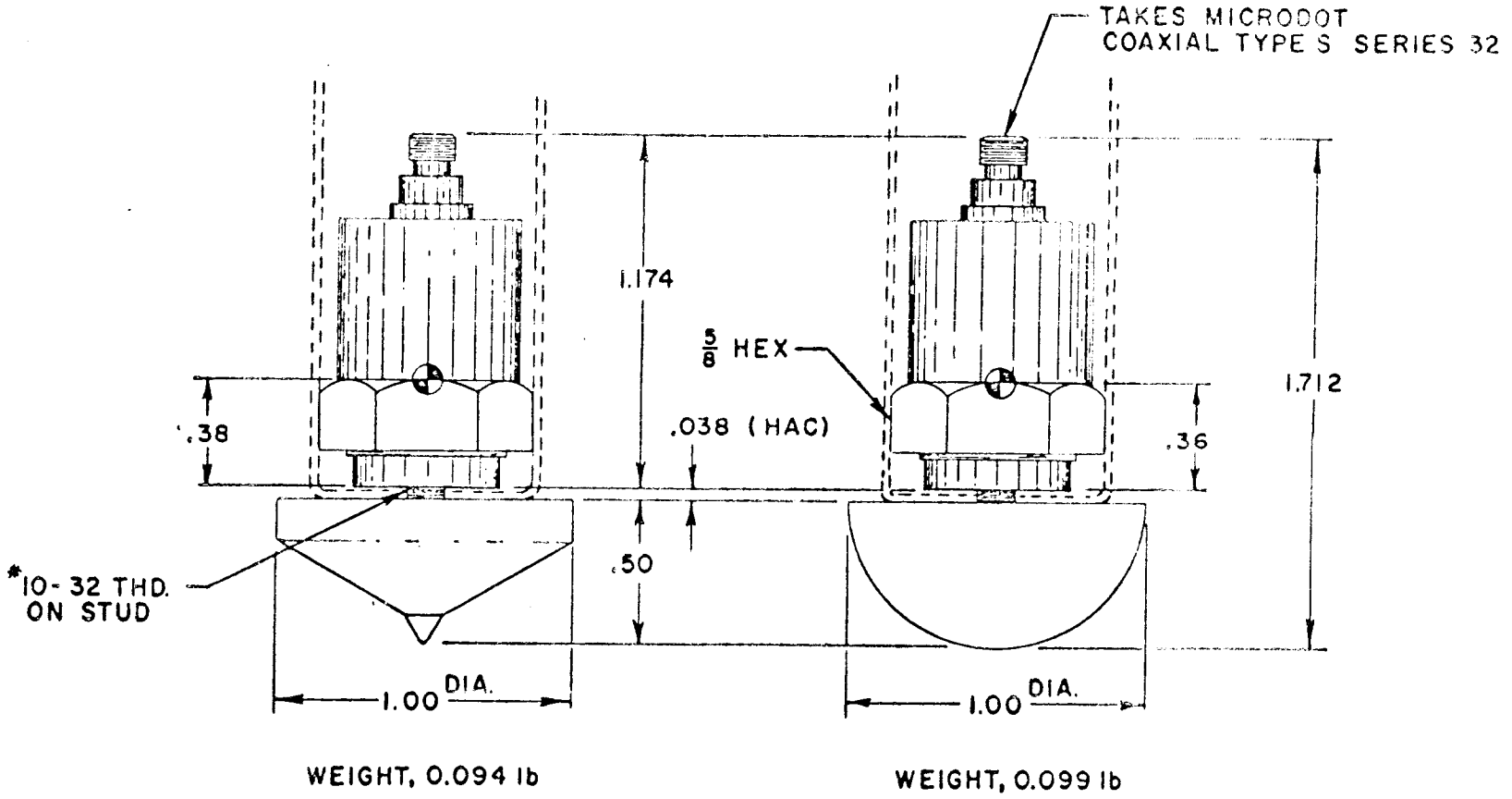

FIGURE 51. SURFACE PENETRABILITY INSTRUMENT

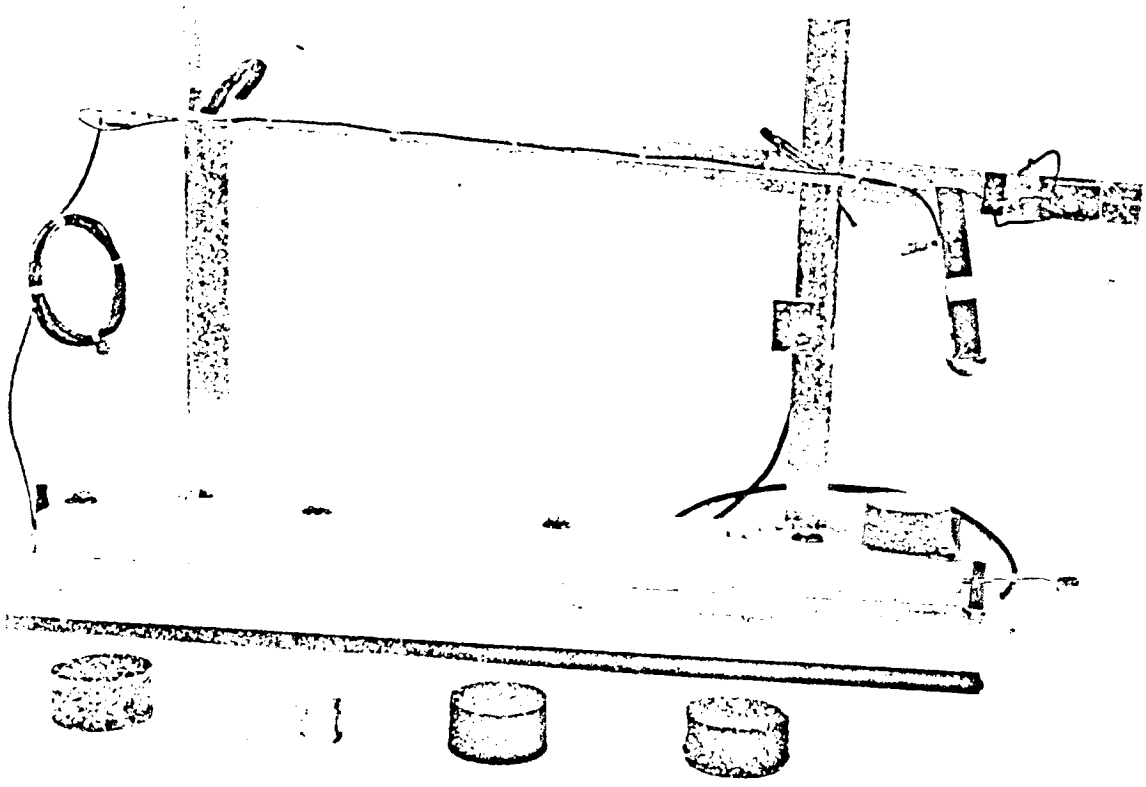

FIGURE 52. PENETROMETER TEST FIXTURE

TABLE 19

TYPICAL PULSE DIMENSIONS ON MAN-MADE MATERIALS

3-inch Drop Height — Room Temperature

Material	Tip	Pulse Height, Earth g's	Pulse Width, msec
Urethane Foam	Conical	12.1	14.9
		12.5	15.8
	Spherical	9.72	17.7
		9.92	17.8
Gum Rubber	Conical	42.5	7.99
		41.7	8.05
	Spherical	62.2	4.84
		62.6	4.83
Lead	Conical	156	1.06
		154	1.01
Aluminum	Conical	324	0.442
		325	0.437
Mild Steel	Conical	751	0.218
		747	0.216
Tool Steel	Conical	2400	0.18
		2400	0.16

TABLE 20

PARTIAL RESULTS OF PENETROMETER CALIBRATION TESTS

Run 1/29/62-2/3/62

	Pulse Height, g's			Pulse Width, msec		
Accelerometer Serial No.	DA58	DA59	DA60	DA58	DA59	DA60
Gum Rubber, Spherical Tip	62.6	62.6	59.9	4.86	4.39	4.86
	62.0	63.1	59.3	4.88	4.90	4.85
Aluminum, Conical Tip	318	314	303	0.435	0.540	0.427
	325	319	304	0.425	0.530	0.429
Mild Steel, Conical Tip	718	774	771	0.224	0.242	0.236
	719	771	771	0.224	0.241	0.239

TABLE 21

TYPICAL PULSE DIMENSIONS ON NATURAL MATERIALS

3-inch Drop Height — Room Temperature

Material	Tip	Pulse Height, Earth g's	Pulse Width, msec
Pumice (Powdered)	Conical	3.33	17.8
		2.32	18.0
Pumice (Powdered)	Spherical	6.53	15.3
		6.35	17.8
Sand	Conical	12.5	12.7
		12.3	11.3
Sand	Spherical	7.93	15.9
		8.55	17.8
Lava	Conical	80	3.2
		93	2.6
Lava	Spherical	210	1.1
		180	1.1
Austin Chalk	Conical	223	0.742
		226	0.722
Marble	Conical	586	0.339
		472	0.360
Quartz	Conical	2000	0.13
		1800	0.17

It should be noted that the band is wide (2 to 2000 g's or three orders of magnitude) and that repeatability will probably be of secondary importance to characteristic form as useful information.

7.3.1.2 Departures from JPL functional requirements.
JPL has expressed a desire for a 5% band of repeatability of maximum deceleration and pulse width or 2.5% variation from average on man-made materials and 10% on natural materials. We have been unable to attain this accuracy thus far. It is believed that the major deviation is due to variations in the test materials.

7.3.1.3 Departures from JPL design specification.
We are aware of no departures.

7.3.1.4 General summary of scientific objectives obtained and experimental results.
The ability has been demonstrated to produce a signal that represents the deceleration history of the instrument as it strikes a surface. From this signal can be obtained the characteristic curve form of the particular material under test along with a calibrated pulse height and width, which are measures of the maximum deceleration and the time length of pulse.

Repeatability between instruments has been shown to be generally within a 10% band on man-made materials and within a 25% band on natural materials.

It may be noted from Figures 53 and 54 that the deceleration varies linearly with the drop height up to a point. Then in unconsolidated material, such as sand, when the drop height becomes high enough to cause the penetrometer to bury itself to its maximum diameter, the curve changes slope. Similarly, when the tip begins to chip or flake a consolidated material, such as marble, the slope changes.

The instrument has been operated successfully at a pressure of 10^{-3} mm Hg. Unconsolidated materials follow different patterns. Powdered pumice becomes much softer in a vacuum;

i.e., the g value goes down. In sand, however, the opposite is true: the vacuum causes the sand to resist penetration. This can be seen in Table 22.

The penetrometer is relatively insensitive to temperatures from -60°C to 125°C as can be seen from Table 23.

7.3.2 Results of Developmental Tests. The original work on the penetrometer was done at Texaco's Research and Technical Department at Bellaire, Texas, under JPL Contract N-33552 and was reported in their Partial Report No. 9 (19).

The design at the time that TEI entered the program consisted of essentially the same accelerometer unit with a steel 60° tip. It was enclosed in a vertical hollow tube and was released at the top and allowed to slide the length of the tube and strike the test surface.

The decision had already been made that the unit would be dropped from a pivoted arm and that one hemispherical and two compound-angle conical tips would be used. TEI had only to design these units and develop the test and calibration hardware and procedures.

7.3.2.1 Outline of tests conducted.

a. Tests were made to prove the performance of the hemispherical and compound conical tip when they were first made.

b. Tests were run to find a set of test samples, man-made and natural, that would give a maximum range of deceleration values to reasonable intervals. At the same time an attempt was made to select the most homogeneous of all the materials for use in the repeatability studies.

c. Tests were made to select the amplifier to be used and also to desensitize the accelerometer to prevent the amplified signal from being clipped on the harder materials and yet retain maximum allowable sensitivity for signal strength on low-deceleration materials.

d. The calibration and final acceptance tests had to be developed. This program turned out to be the most time consuming of all the tasks.

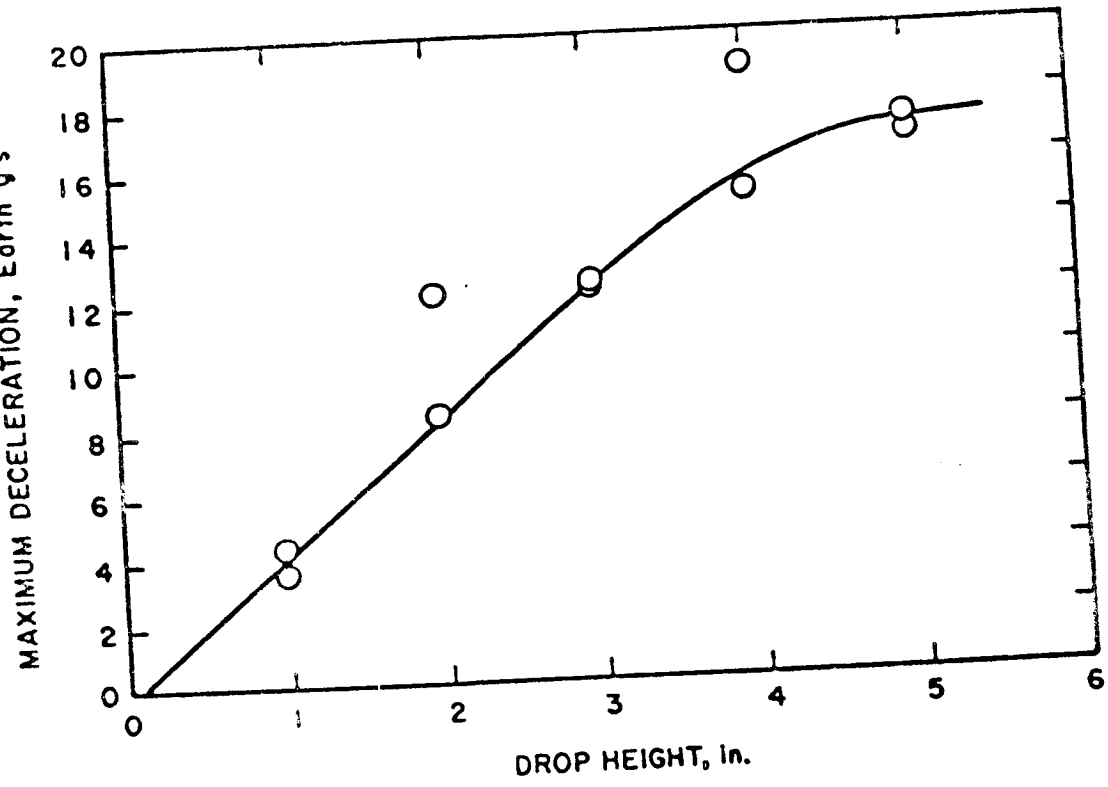

FIGURE 53. PENETROMETER VARIABLE-DROP-HEIGHT TESTS IN SAND

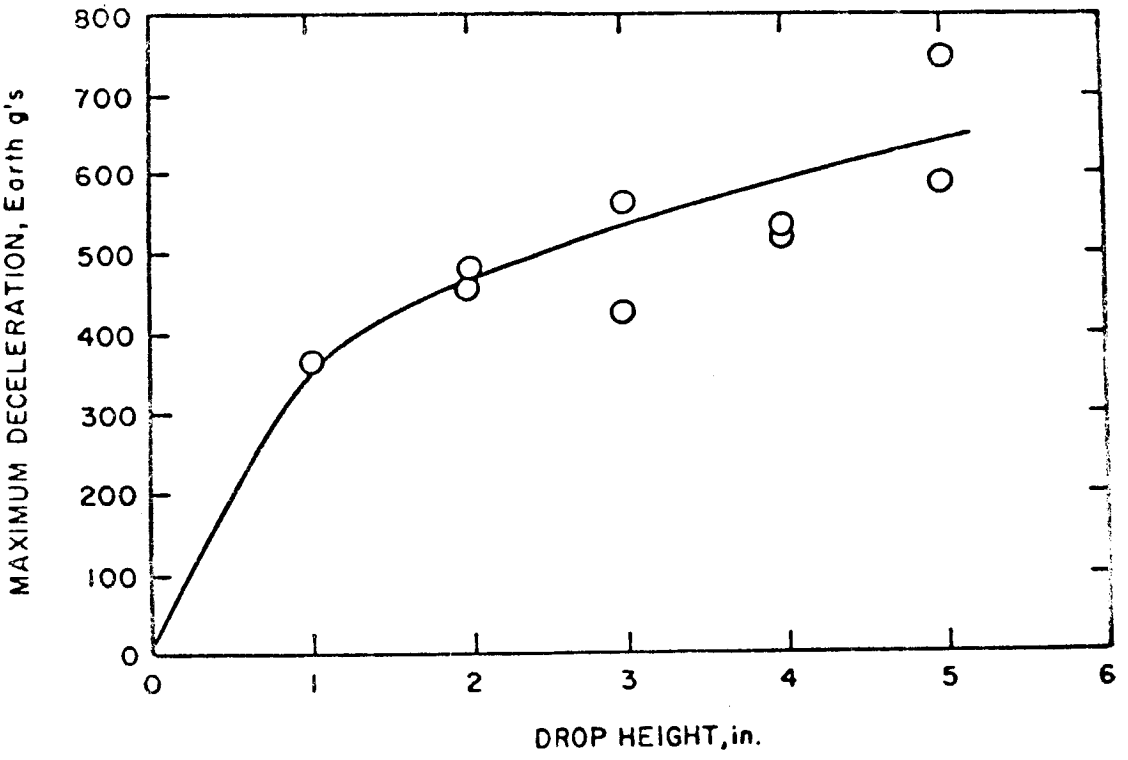

FIGURE 54. PENETROMETER VARIABLE-DROP-HEIGHT TESTS ON MARBLE

TABLE 22

TYPICAL PULSE DIMENSIONS IN VACUUM

3-inch Drop Height Room Temperature

Material	Tip	Pressure, mm Hg	Pulse Height, Earth g's	Pulse Width, msec
Pumice (Powdered)	Conical	760	6.65	12.5
			7.88	15.4
		10^{-3}	4.19	17.5
			3.95	12.7
	Spherical	760	9.50	12.5
			8.87	10.0
		10^{-3}	3.63	18.0
			3.47	22.8
Sand	Conical	760	8.72	12.2
			7.87	11.0
		10^{-3}	13.8	6.7
			14.6	6.5
	Spherical	760	6.07	16.7
			7.38	15.7
		10^{-3}	11.2	4.4
			16.1	3.9
Lava	Conical	760	82	3.5
			55	2.4
		10^{-3}	71	3.6
			73	3.2
	Spherical	760	130	1.4
			130	1.4
		10^{-3}	170	1.7
			170	1.5

TABLE 23

TYPICAL PULSE DIMENSIONS AT TEMPERATURE EXTREMES

3-inch Drop Height — Spherical Tip on Gum Rubber

Temperature	Pulse Height, Earth g's	Pulse Width, msec
-65°C	62.7	5.09
	62.2	5.03
Room	62.6	4.86
	62.0	4.88
125°C	61.1	4.89
	62.0	4.92

7.3.2.2 Failure reports.

No component failures have been experienced; however, since it was felt that the accuracy of repeatability should be greatly improved, a great deal of work was done in attempting corrective practices.

7.3.2.3 Summary of corrective measures.

In an attempt to improve repeatability several modifications were made on the test fixture:

a. The unit was pinned at the correct drop height.

b. The pivot bearing was replaced with a flexure.

c. The release mechanism was modified to improve alignment of the penetrometer.

d. The diameter of the oscilloscope trigger spring wire was reduced to minimize any force on the dropped unit.

e. The mass and rigidity of the test fixture were increased.

f. The calibration techniques were refined.

7.3.2.4 Summary of experimental results.

The procedures and techniques of calibration have been greatly improved, although the repeatability has not improved to the same extent. The greatest single improvement resulting from the effort is the increased quality assurance.

The man-made test samples chosen for calibration were urethane foam, gum rubber, hard rubber, aluminum, and mild steel.

The Endevco 2620 Charge Amplifier was chosen as reported in a memorandum titled "Feasibility of Using a Charge Amplifier with the Penetrometer," which is included in this report as Appendix H.

The Penetrometer Final Acceptance Test Report (18) and the Penetrometer Checkout and Calibration Procedure, included as Appendix I, indicate the developed test and calibration procedures.

7.4 Components Outline

7.4.1 Notation and Explanation of Deviation from JPL and/or HAC Preferred Parts List. The electrical connector on the accelerometer does not comply; no miniature coaxial connector does. The manufacturers felt that the connector, however, is a great deal more reliable than a pigtail. Two companies stated this opinion, both based on past experience.

7.4.2 Results of Components Tests. The purchased components have been satisfactory in every case. The Penetrometer Test Booklet, which will accompany each set of instruments, will show the TEI acceptance tests run on the accelerometers.

7.5 Packaging Philosophy

The only requirements of the penetrometers are that the tips be securely attached to the accelerometers and that they be shaped so as to give them the best possible chance of striking the lunar surface, even in a severe depression.

The hardened tip is set in its base under pressure, and both tips are torqued through the bracket and insulating stud (since the accelerometer is case grounded) to insure good coupling. The diameter of the assembly is kept to a minimum to lessen the chance of the point being held off the test surface by premature contact by some other part of the instrument. This philosophy is also carried out by the HAC bracket.

7.6 Theoretical Studies

No such studies were performed.

7.7 Environmental Test Results

Environmental tests were made both on the components as component acceptance tests (see Penetrometer Checkout and Calibration Procedure, Appendix I) and on the instruments for the Penetrometer Final Acceptance Test (18).

7.7.1 Report of the Survival of the Instrument under Conditions of Its Particular Environment. The instrument has survived, one at a time, liquid nitrogen temperature, 150°C, and 10^{-5} mm Hg vacuum.

It has been operated at -65° and 125° at 10^{-3} mm Hg vacuum.

7.7.2 Failure Report. There have been no instrument failures.

7.8 Recommendations

1. The penetrometer test fixture should be mounted on a heavy plate to lessen the effect of using a small and therefore high-natural-frequency test sample.

2. The accelerometers should be recalibrated with their modified insulating studs by the manufacturer after their acceptance tests but before calibration.

3. In view of the similarity of results with the spherical and conical tips on low-deceleration surfaces, such as sand, the spherical tip should be abandoned and replaced by either a single 60° point or by the compound point used on the other two instruments.

8. SURFACE ACOUSTIC VELOCITY INSTRUMENT

URD 24 and 25

Control Item X239220 and X239221

THE MISSING PAGES IN THIS DOCUMENT ARE BLANK
AND, THEREFORE, WERE NOT REPRODUCED

8.1 System Description

This experiment was designed to determine the sonic velocity of the lunar surface along two overlapping paths by recording the time that elapses between the generation of a seismic wave by an electrically fired explosive squib and its arrival at each of two detectors placed in known positions relative to the source position.

The source shown in Figure 55 is designed to be lowered to the lunar surface from the spacecraft, from which it must be acoustically decoupled, where it will, upon command, fire six explosive squibs in succession. It is desirable to put as much of the explosive energy as possible into the seismic wave, but a certain amount of the energy must be used to stabilize the source.

The seismic detector, or geophone, is a velocity-sensitive device which generates a voltage when its spring-suspended coil is moved in its magnetic field. One of these devices, shown in Figure 56, is dropped from a leg of the spacecraft, and the other is an integral part of the density device, which is lowered to the surface from an extended boom approximately in line with the source and first sensor and some distance away. They must also be acoustically insulated from the spacecraft.

An accelerometer in the subsurface sonde will be used as a seismic wave detector and will also pick up waves generated by the surface source.

8.2 Equipment Description

The over-all size of the acoustic source is 3.95 inches in diameter by 3.03 inches high. Its weight without squibs is 0.348 lb, and with six of the squibs used for testing its weight is 0.488 lb. Since this unit was built to take a squib with a 3/8"-20 thread and it has since been decided that a 1/2" - 20 thread squib will be used, this weight may change. The power required depends also on the squib selection, which has not been made at present.

The first acoustic sensor will fit in a cylinder 1.28 inches in diameter by 2.62 inches high. Its weight is 0.191 lb, and it consumes no power, being a voltage-generating device.

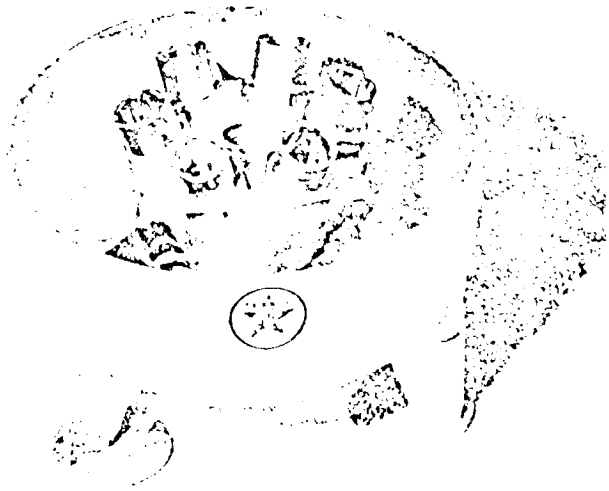

FIGURE 55. ACOUSTIC SOURCE

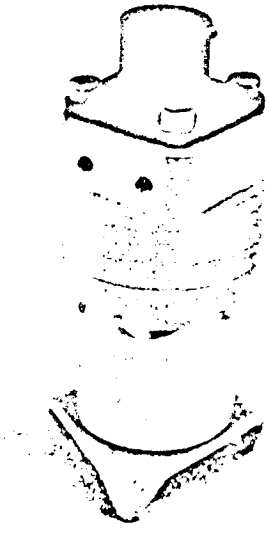

FIGURE 56. ACOUSTIC SENSOR NO. 1

These parameters along with center-of-gravity location of the source and first sensor are shown in Figure 57.

The second acoustic sensor is described in the surface-density section; it makes use of a geophone identical to the one used as the first sensor. Likewise, the subsurface sensor is described in a separate report.

The source holder material is 6061-T6 aluminum welded with 4043 wire. The assembly is clear anodized, and the feet are coated with epoxy and silicon carbide grit.

The sensor is copper and nickel plate on steel with clear anodized 2024-T4 aluminum cap and tripod. Fasteners are 18-8 stainless steel.

8.3 Testing and Calibration

8.3.1 Results of Functional Tests. The final acceptance and functional test program for the sonic-velocity experiment was carried out at the Jet Propulsion Laboratory between 12 February and 19 March 1962 by JPL personnel with the help of personnel from Texaco. The final report written by JPL on this program will cover the functional tests.

8.3.2 Results of Developmental Tests. Practically all of the testing done at Texaco Experiment Incorporated was devoted to developing the acoustic source and determining a satisfactory explosive charge size. The acoustic sensor as developed by the feasibility study and bread-board development program at Texaco Research and Technical Department in Bellaire, Texas, was quite satisfactory, but the source did not perform well in the vacuum chamber and therefore had to be redesigned on this contract. This is reported in Bellaire's Partial Report No. 10 dated 21 August 1961 (20).

The acoustic source had to be strong enough and stable enough to withstand the six shots without failure or overturning and at the same time couple efficiently with the lunar surface. The resulting source was able to withstand six shots on sand in a vacuum of 10^{-3} mm Hg.

It is necessary to match the size of the explosive charge to the size of the hole in the bottom of the source bowl since this hole determines the amount of the generated blast energy that will be used to hold the source down and the amount that will be passed through to generate the seismic

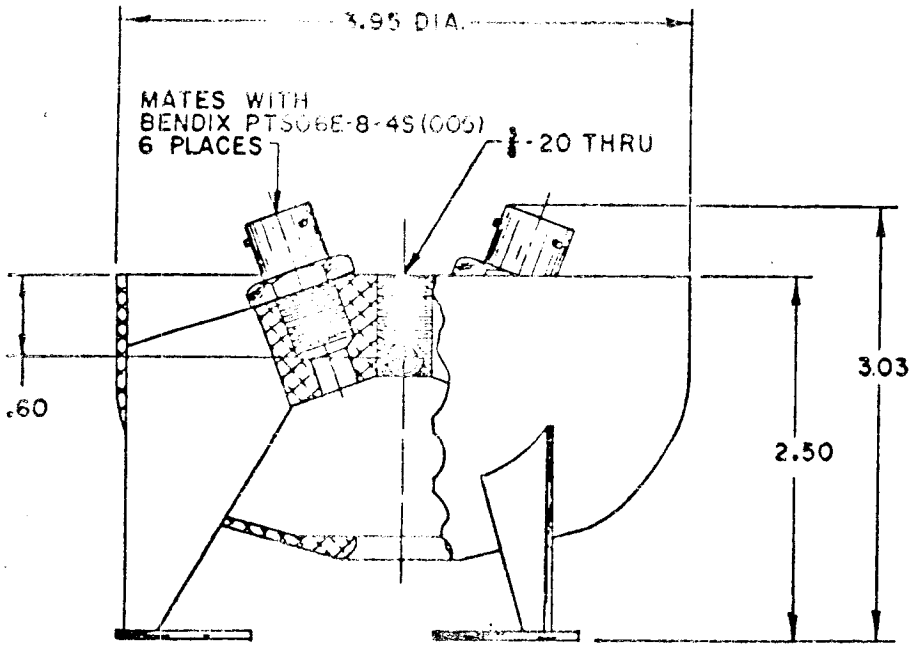

WEIGHT, 0.488 lb

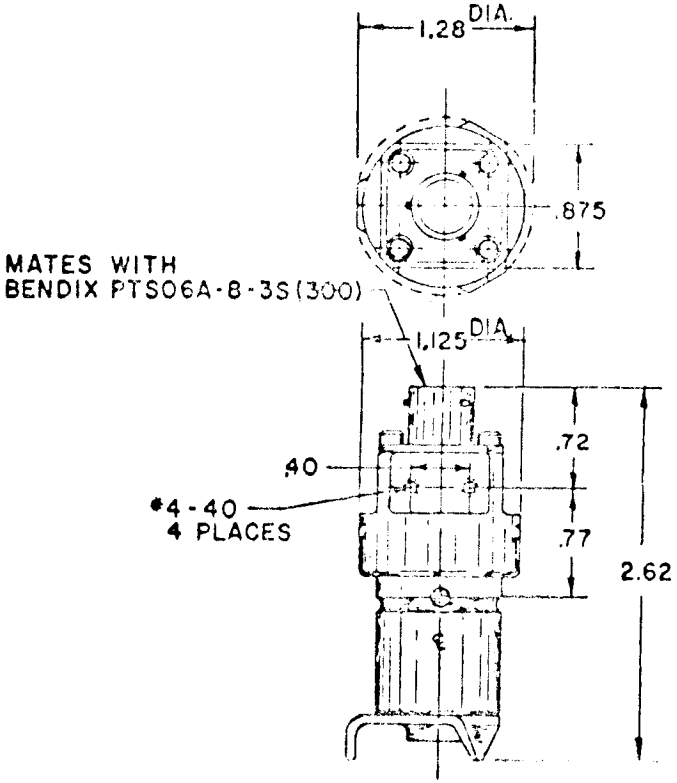

WEIGHT, 0.191 lb

FIGURE 57. ACOUSTIC SOURCE AND FIRST ACOUSTIC SENSOR

wave. This was determined by starting with a small hole and sucessively testing and enlarging until the source left the surface when fired. When the final squib selection is made, the size will be more exactly bracketed by firing the source spring-suspended in a vacuum chamber.

A reasonable source size was determined by relative signal strength in a range of materials as the equivalent of 2 grains of Hercules Hi-Temp powder.

8.4 Components Outline

The geophones were purchased as a stock item and came with cadmium-plated cases. Between the stripping and replating operation and the acceptance tests only two units out of the original 10 remained usable. Steps will be taken to improve this by the use of specifications to the manufacturer. Geophone acceptance test procedure is shown in Appendix J. Squib selection and qualification will be the responsibility of JPL.

8.5 Packaging Philosophy

The source must be strong enough to withstand its blast, stable enough to remain upright, and designed to put a maximum portion of its blast energy into the seismic wave.

The metal thicknesses required for welding are quite sufficient to withstand the blast stresses. The shape is such that the feet are tripod and as far apart as the assigned envelope would allow. The feet are grit coated to give additional purchase on sloping terrain. The bowl catches a portion of the blast wave coming from the squib and reverses its direction; the resulting reaction holds the unit against the thrust generated by the squib. The major portion of the blast passes through the hole in the bottom of the bowl and strikes the ground, generating the required seismic wave. The bowl must be far enough from the ground to prevent any pressure build-up underneath the bowl; this situation is also helped by making the radial path divergent so that the gases can expand as they move out.

The sensor must be acoustically coupled to the ground but not to the spacecraft. The tripod base on the sensor was selected by JPL as being satisfactory. The aluminum cap serves as an attachment point for the HAC bracket and the electrical connector and as a shield for the connecting wires.

All fabricated parts on both units are aluminum to conserve weight and anodized to prevent corrosion. Fasteners are stainless steel.

8.6 Theoretical Studies

A short mathematical study of acoustic waves in the lunar surface was made and reported in Texaco Experiment Incorporated TM-1325 (21).

8.7 Environmental Test Results

Both the source and sensor have been operated at temperatures of -50°C and 150°C and in a vacuum of 10^{-3} mm Hg but under only one condition at a time. No failures were observed, but satisfactory operation of the source will depend upon the squibs, which have not been specified.

8.8 Recommendations

None.

9. SUMMARY OF QUALITY ASSURANCE PRACTICES EMPLOYED

The quality assurance practices employed during the manufacture of the Surface Geophysical Instrument included the following:

1. Incoming Acceptance Tests of Purchased Components
Incoming acceptance tests were performed on the following purchased components according to the applicable documents:

Component	Applicable Document
Counter Tube	387-234-99, Counter Tube—Incoming Acceptance Test (22)
Geophone	387-234-97, Geophone—Incoming Acceptance Test (23)
Accelerometer	387-241-99, Accelerometer Acceptance Test (24)
Interferometer Spectrometer	387-212-89, Acceptance Test Procedure—Interferometer Spectrometer (1)
Thermostat	387-224-97, Thermostat Acceptance Test (25)

2. Inspection of Manufactured Parts
All manufactured parts were inspected to assure compliance with the engineering drawings.

3. Acceptance Tests of Manufactured Components
Acceptance tests were performed on the following manufactured components according to the applicable documents:

Component	Applicable Document
Penetrometer Steel Points	387-241-89, Penetrometer—Material Acceptance Test (26)
Penetrometer Conical Points	387-241-97, Inspection Procedure—Conical Points (27)
Density Source Positioning Solenoid	387-234-91, Source Positioning Solenoid Acceptance Test (12)
Density Explosive Lowering Device	387-234-89, Explosive Lowering Device Acceptance Test (11)

4. In-process Inspection

During the assembly of the surface instruments each subassembly was checked upon completion. The cognizant engineer for the particular instrument observed each step and assured compliance to the engineering drawings. Solder joints were inspected with a stereoscopic microscope at 10x magnification to assure quality of workmanship. Mating parts were visually checked upon assembly. All welds were inspected for quality by x-ray and dye-penetration methods.

5. Checkout of Completed Instrument

Each completed instrument was checked according to the following applicable documents:

Instrument	Applicable Document
Surface Density Instrument and Acoustic Sensor	387-234-94, Checkout Procedure—Surface Density Instrument and Acoustic Sensor (28)
Surface Magnetic Susceptibility Instrument	387-253-99, Inspection Procedure—Surface Magnetic Susceptibility Device (29)
	387-253-97, Checkout and Calibration Procedure—Surface Magnetic Susceptibility Device (6)

Surface Thermal Diffusivity Instrument	387-224-99, Checkout Procedure — Surface Thermal Diffusivity Instrument (30)
Surface Penetrability Instrument	387-241-95, Checkout Procedure — Penetrometer (31)

In addition, all instruments were checked according to Specification 387-241-87, Final Inspection Procedure (32), before delivery. The acoustic source was proof-tested by firing two squibs simultaneously.

The quality assurance on the interferometer spectrometer as performed by Block Associates, the instrument manufacturer, is rather limited at this time. Their quality assurance effort is presently performed by designers and fabricators. However, steps have been taken to institute an acceptable quality assurance program at Block Associates. Time and availability of qualified personnel are the only limiting factors.

10. REFERENCES

(1) "Acceptance Test Procedure—Interferometer Spectrometer," Texaco Experiment Incorporated Specification 387-212-89.

(2) "I-4 Interferometer Spectrometer, Manual of Theory and Operation," Block Associates, Inc., 27 October 1961.

(3) "Design, Development, and Construction of an Interferometer Spectrometer for Use as a Lunar Temperature Instrument," Block Associates, Inc., 28 April 1962.

(4) "Lunar Physical Parameters Study. Partial Report No. 8. Design Calculations—Measurement of Thermal Diffusivity," Texaco Inc. Research and Technical Dept., Bellaire, Texas, 8 May 1961.

(5) "Lunar Physical Parameters Study. Partial Report No. 7. Measurement of Electrical Properties on Lunar Surface—A Feasibility Study," Texaco Inc. Research and Technical Dept., Bellaire, Texas, 15 December 1960.

(6) "Checkout and Calibration Procedure—Surface Magnetic Susceptibility Device," Texaco Experiment Incorporated Specification 387-253-97.

(7) C. D. Hodgman, Ed., Handbook of Chemistry and Physics, 34th Ed., Cleveland, Chemical Rubber Publishing Co., 1952.

(8) "Lunar Physical Parameters Study. Partial Report No. 11. Breadboard Tests of the Surface Magnetic Susceptibility Coils," Texaco Inc. Research and Technical Dept., Bellaire, Texas, 20 September 1961.

(9) "Measurement of Lunar Physical Parameters, Feasibility Study. Final Report," Texaco Inc. Research and Technical Dept., Bellaire, Texas, 15 December 1960.

(10) "Lunar Physical Parameters Study. Partial Report No. 1. Measurement of Lunar Surface Density—A Feasibility Study," Texaco Inc. Research and Technical Dept., Bellaire, Texas, 31 August 1960.

(11) "Explosive Lowering Device Acceptance Test," Texaco Experiment Incorporated Specification 387-234-89.

(12) "Source Positioning Solenoid Acceptance Test," Texaco Experiment Incorporated Specification 387-234-91.

(13) "Calibration Procedure—Surface Density Instrument," Texaco Experiment Incorporated Specification 387-234-93.

(14) "Lunar Physical Parameters Study. Partial Report No. 15. Breadboard Tests of the Surface and Subsurface Density Measuring Devices," Texaco Inc. Research and Technical Dept., Bellaire, Texas, 20 September 1961.

(15) S. J. Vernon, "Environmental Requirements, Surveyor Type Approval Tests Sub-Systems and Assemblies," Hughes Aircraft Co. No. 224810, Rev. A, 16 June 1961.

(16) "Protection Against Radiations from Sealed Gamma Sources," U. S. Dept. of Commerce, National Bureau of Standards, Handbook 73, 27 July 1960.

(17) "Lunar Physical Parameters Study. Final Report. Breadboard Models of Surface and Downhole Equipment," Texaco Inc. Research and Technical Dept., Bellaire, Texas, 10 October 1961.

(18) "Penetrometer Final Acceptance Test Report," Texaco Experiment Incorporated TM-1330, 26 February 1962.

(19) "Breadboard Penetrometer Hardness Measurement," Texaco Inc. Research and Technical Dept., Bellaire, Texas, Partial Report No. 9, 15 June 1961.

(20) "Lunar Physical Parameters Study," Texaco Inc. Research and Technical Dept., Bellaire, Texas, Partial Report No. 10, 21 August 1961.

(21) R. L. Wolf and R. E. Canup, "A Theoretical Study of the Propagation and Attenuation of Acoustic Waves in the Lunar Surface," Texaco Experiment Incorporated TM-1325, 9 February 1962.

(22) "Counter Tube—Incoming Acceptance Test," Texaco Experiment Incorporated Specification 387-234-99.

(23) "Geophone—Incoming Acceptance Test," Texaco Experiment Incorporated Specification 387-234-97.

(24) "Accelerometer Acceptance Test," Texaco Experiment Incorporated Specification 387-241-99.

(25) "Thermostat Acceptance Test," Texaco Experiment Incorporated Specification 387-224-97.

(26) "Penetrometer—Material Acceptance Test," Texaco Experiment Incorporated Specification 387-241-89.

(27) "Inspection Procedure—Conical Points," Texaco Experiment Incorporated Specification 387-241-97.

(28) "Checkout Procedure—Surface Density Instrument and Acoustic Sensor," Texaco Experiment Incorporated Specification 387-234-94.

(29) "Inspection Procedure—Surface Magnetic Susceptibility Device," Texaco Experiment Incorporated Specification 387-253-99.

(30) "Checkout Procedure—Surface Thermal Diffusivity Instrument," Texaco Experiment Incorporated Specification 387-224-99.

(31) "Checkout Procedure—Penetrometer," Texaco Experiment Incorporated Specification 387-241-95.

(32) "Final Inspection Procedure," Texaco Experiment Incorporated Specification 387-241-87.

(33) A. I. Brown and S. M. Marco, Introduction to Heat Transfer, 3rd Ed., New York, McGraw-Hill Book Co., Inc., 1958.

11. APPENDIX

A. Miscellaneous Information on the Interferometer Spectrometer

March 15, 1962

J. J. Thomas/E. L. Brown
Jet Propulsion Laboratory
4800 Oak Grove Drive
Pasadena, California

Subject: JPL Contract No. 950155 - Your Telegram dated March 8, 1962

Gentlemen:

This letter is to answer the questions you asked in your telegram of March 8, 1962.

1. The modulation efficiency (H) of the Iota Beamsplitters is in the range of 0.25 to 0.35. Laborious calculations, however, prevent the specific modulation efficiency for a particular instrument at this time. Since this number varies with the tel[illegible]m coating on the KRS-5 substrate, measurements on rea[illegible]tings will have to be made and will be forthcoming from Block in the near future.

2. The transmission constant (Q_ψ) has not been computed for the Iota optics. It can be calculated knowing the reflection loss per surface of KRS-5. This measurement will shortly be computed by Block and will be forwarded to you.

3. The throughput (θ_0) is 0.0094 steradian-cm^2 as shown on the ray tracing included with this letter.

4. The noise equivalent power (N) may be computed from $N = \sqrt{S_D \Delta F_\psi}/D^*$. S_D and ΔF_ψ are known but lacking information on D^* (see 7 below) this information will have to be derived from Block at a later date.

5. The field semiangle (γ) is 6°19' as shown on the ray tracing.

6. The maximum convergence semiangle (γ') is also shown and is 45° at the detector.

7. The noise equivalent power from the detector (D*) is given in terms of how much it exceeds a resistor of the same resistance as the flake. In this particular case, Barnes's information on its bolometer flake is 1.38 times the flake resistance, which is 0.242 megohms at 25°C. Thus only the equivalent noise of a similar resistor needs to be known.

8. The mirror constant velocity period (T) is 0.294 sec.

9. The spectral resolution ($\Delta\psi$) is 71 cm^{-1}.

10. The total wavelength measuring interval of the Iota-001 is 5-30 microns.

Applying the above information to solve for NEPD we have:

$$NEPD = \gamma^2\sqrt{T}/H0_0\lambda^2\sqrt{S_D}\, D^* Q_\psi$$

$$= (0.0383)^2\sqrt{0.294}/(0.35)(0.0094)\sqrt{0.01}\, D^* Q_\psi$$

Since D* and Q_ψ are not presently known, the NEPD cannot be computed. We hope to have this information shortly. However, Neils Young of Block Associates has suggested that in order to determine the instrument function it is not practical to multiply together all the factors which you bring up.

It is useful, however, to remember what factors do affect the instrument function so that peculiarities (for example, the possibility of a temperature-dependent reversible instrument function) can be traced to the correct factors. For example, such a temperature dependence, which we are presently trying to determine here at TEI, would not be blamed on changes of throughput - but rather on changes of D*.

The instrument function should be obtained from repeated and numerous spectra for many instrument as well as source temperatures. The correct instrument function is then obtained by repeated application of blackbody tables. The instrument function will, in general, be a function

of the instrument temperature only—but it may be found that it depends upon other factors such as supply voltage. If so, then only through severe testing can we find this out and do something about it.

11. Method of obtaining temperature from Iota recorded interferogram.

To measure an unknown temperature within the limits of our device, we first make a series of tests with known blackbody temperatures, thus calibrating our device and from there work backwards.

To do this we make use of a blackbody radiator, knowing its temperature. With the sensing head detecting the known blackbody spectral radiance we make an interferogram. The output of the postamplifier is fed into a tape recorder, recording at least 100 sweeps in 33 seconds. We take this tape, form a loop, and play it back into our wave analyzer. Of course, with the instrument on the moon telemetered digitized information will be received. This in turn will be fed into an analog computer where with combined known data the computer will solve for the desired information.

The wave analyzer in turn will select a particular frequency from the band of frequencies being fed into it. With the tape loop being played back at a faster rate than recorded rate, the frequencies will be averaged out giving spectral resolution equivalent to one sweep; but it will be within the capabilities of the wave analyzer to "see" this resolution due to the wave analyzer passband. Taking this information from the wave analyzer and feeding it into an X-Y recorder the relative intensity of different frequencies over a known band of frequencies is recorded. With this "interferogram" we normalize its amplitude with the response calibration of the tape recorder. Then using $F_\psi = \psi B/T$, we calculate the wave numbers per the autocorrelated frequencies of the Iota output. Along with this information we plot the per cent full-scale amplitude versus wave number. This curve plotted, we will call the Iota measured response curve. Through the use of selective infrared pass band filters we calibrate our interferogram versus the autocorrelated frequencies. Later, we will have a transparent grid that will

directly convert the autocorrelated frequencies into wave numbers (ψ) and per cent full scale to facilitate ease of plotting.

Now with the temperature of the bolometer and blackbody known, we plot the theoretical blackbody spectral radiance, computed from a set of tables, for each temperature. This is done by solving λ for each N_λ for the bolometer and blackbody temperature. From the tables we see that for a particular λ at temperature T for the bolometer we have a value for the spectral radiance of the blackbody. We do this also for the blackbody temperature for each N_λ. With this information we subtract each value of spectral radiance to obtain ΔN_λ. Solving for λ^2 for each N_λ we find ΔN_n by using $\Delta N_n = \lambda^2 \Delta N_\lambda$. Then we plot this calculated difference radiance curve just above the Iota measured response curve. Now the ratio of these two curves, the Iota measured response curve versus the theoretical calculated difference curve gives the total absolute response curve of the Iota.

This total absolute response curve of the particular Iota will, of course, be unique in that it contains all of the peculiarities of the instrument. Any deviation, of course, will have been determined, compared, and calibrated before this response curve. Of course, many trials and tests will determine these factors.

With this information we are now ready to measure an unknown blackbody temperature. Really all we do is to work backwards. With the information being received from the Iota we feed it into our wave analyzer where the relative amplitudes of the spectral components will be plotted into an interferogram. Of course, when this is being received from the moon, all data processing will be carried out by a computer. In this case though we divide the total absolute response curve by the Iota measured response curve. This gives the calculated difference radiance curve. Knowing the bolometer temperature, we may readily solve for the temperature of the blackbody.

Example:

This will explain the process by which an unknown blackbody temperature may be determined by use of the Iota. Only here we will just give an example of <u>one</u> wave number of the entering radiation.

From the interferogram using $F_\psi = \psi B/T$

We see that for F_ψ = 100 cps, $\psi = \frac{100 \times 0.294}{279 \times 10^{-4}}$

$= 1053 \text{ cm}^{-1}$

1) For this wave number we find its amplitude in per cent full scale assuming full-scale deflection of the recorder is 30 mv/10 in. Its amplitude is 70% of full scale; therefore this would correspond to 0.70 x 30 = 21 mv on the Iota measured response curve provided the tape recorder response is 1:1.

2) Assuming the blackbody temperature is 400°K and the bolometer temperature is 300°K, we see from the tables that the theoretical spectral radiance of blackbody $N_1\lambda$ for 300°K is 9.972. Also from the tables we see that the spectral radiance of blackbody of $N_2\lambda$ for 400°K is 35.79.

   Since ψ = 1053, 9.5μ = λ

3) $\Delta N_\lambda = N_{2\lambda} - N_{1\lambda} = 25.818$

   Since $\lambda^2 = (9.5)^2 = 90.25 \times 10^{-8} \text{ cm}^2$

4) Then $\Delta N_n = 90.25 \times 10^{-8} \times 25.818 = 2.330 \times 10^{-3}$ μw/cm-sr.

5) Dividing this quantity into the Iota measured response we get .009 v/μw/cm-sr.

This value then is one point plotted on the total absolute response curve for the Iota; with this curve we can now work back to solve for the blackbody temperature.

Example:

From the Iota measure response curve transmitted back we do as we did before, i.e., solve for per cent full scale at 100 cps:

1) This equals 21 mv.

2) Dividing this by the total absolute response value corresponding to 100 cps or 1053 cm^{-1} wave numbers we have 2.33×10^{-3} μw/cm-sr.

Since λ^2 is 90.25×10^{-8} cm^2

3) We solve for $\Delta N_\lambda = 25.818$

Now we know the bolometer temperature and therefore its blackbody spectral radiance; solving for

4) $N_{2\lambda} = N_{1\lambda} + 25.818 = 9.972 + 25.818 = 35.79$

5) Looking at the tables for $\psi = 1053 = 9.5\mu$ we see that 35.79 corresponds to a blackbody spectral radiance of 400°K or the temperature of the unknown blackbody.

I hope that this information will help answer your questions which you asked. Realizing that this information is hardly complete in the sense of absolute values, we hope that after many tests these specific numbers will become less important as bits of information and that the over-all information and accuracy will be paramount in striving for absolute accuracy.

Sincerely,

TEXACO EXPERIMENT INCORPORATED

R. E. Canup

Supplement

The symbol convention to be used by us in all future correspondence on and discussions of theoretical calculations concerning interferometer spectrometers shall be as follows: Block's convention is shown and is also used in this, but it will be discontinued by us henceforth.

Block Convention	Our Convention	
$N\lambda$	$N\lambda$	Absolute spectral radiance of a blackbody in terms of wavelength bandwidth.
N_ψ	N_n	Absolute spectral radiance of blackbody in terms of wavenumber bandwidth.
λ	λ	Wavelength
ψ	n	Wave number
F	ν	Frequency of infrared radiation
F_ν	F	Audio frequency

This convention for the most part conforms to that used in "Tables of Blackbody Radiation Functions" written by Mark Pivovonsky and Max R. Nagel and published by the Macmillan Company. The convention choice was made because this book will be used for computing correction curves and finally temperatures of blackbodies at unknown temperatures. Please refer to the above book for more detailed definitions of the terms and for definitions of other terms.

IOTA - OPTICS LAYOUT

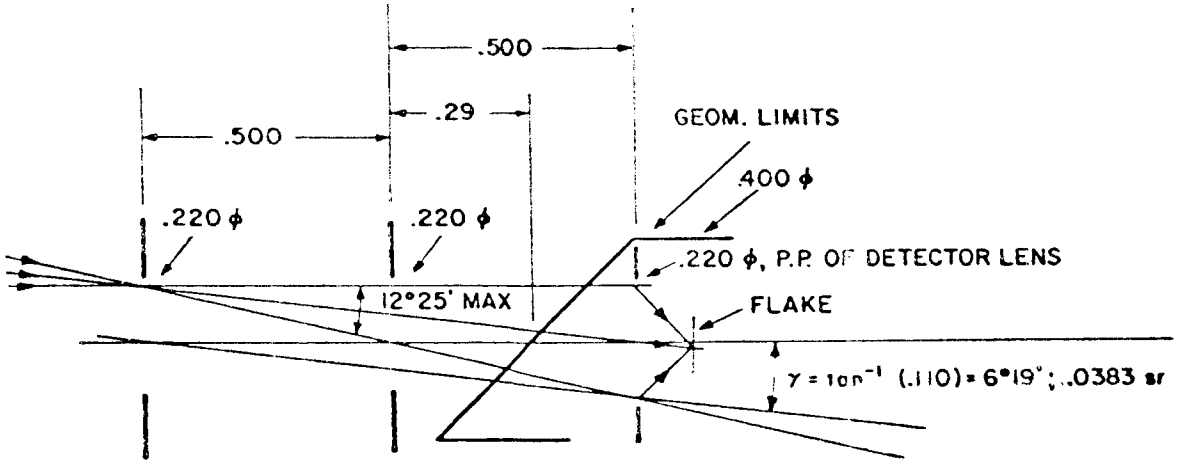

THROUGHPUT $\theta_0 = (0.0383)(0.110)^2 \pi (2.54)^2 = .0094$ cm²-sr

[CHECK: $\theta_0 \cong S_1 S_2 / l^2 = (0.2455)^2/(2.54)^2 = 0.00935$ cm²-sr]

FOR CONVERGENCE SEMIANGLE $\gamma' = 45°$ AT DETECTOR (1.84 sr)

$S_d = (0.0094)/(1.84) = 0.00511$ cm² = 0.511 mm²

MINIMUM SIZE FLAKE TO ACCOMMODATE THIS IS $(4/\pi)\sqrt{0.511}$

= 0.91 mm square

$M \cong \tan 45°/\tan 6°19' = 9.09$; $1/M = 0.110$ FROM P.P. TO FLAKE

E.F.L. OF DETECTOR LENS, F = 0.99"

FREE APERTURE ≥ 0.220" ϕ

B. Data Reduction Information from Tests of the Interferometer Spectrometer

April 11, 1962

J. J. Thomas/E. L. Brown
Jet Propulsion Laboratory
4800 Oak Grove Drive
Pasadena, California

Subject: JPL Contract No. 950155 - Data reduction information from tests of Interferometer Spectrometers

Gentlemen:

Enclosed are six (6) copies each of the temperature calculations using the spectrograms obtained during the acceptance tests of the Block Interferometer Spectrometers. These spectrograms are in the test booklets sent to you earlier, but we are including additional copies with the calculations to keep confusion to a minimum.

The temperature calculation for each instrument is as follows:

1) Instrument total absolute response (TAR) is calculated using the spectrogram obtained when the instrument was viewing a 150°C blackbody or in the case of URD 27 a 127°C blackbody.

2) The temperature is calculated using the spectrogram obtained when the instrument was viewing a blackbody warmer than the bolometer by approximately 20°C.

3) The temperature is calculated using the spectrogram obtained when the instrument was viewing a blackbody colder than the bolometer by approximately 20°C.

4) The temperature is calculated using the spectrogram obtained when the instrument was viewing a blackbody somewhat colder than the bolometer. (Later discussions will clarify the "somewhat" used here.)

5) For URD 27 an additional temperature was computed for the blackbody approximately 20°C colder than the bolometer.

6) For URD 11 an additional computation was made for both blackbody warmer than bolometer by 20°C and for blackbody colder by approximately 20°C.

The errors in calculated temperatures vs. measured temperature are as follows:

	Degrees of Error		
Calculation No.	URD 9	URD 11	URD 27
1	TAR	TAR	TAR
2	7	8	0
3	36	9	8
4	12	35	27
5	--	--	2.5
6a	--	11	--
6b	--	2	--

Calculation numbers correspond to the temperature calculations enumerated above. These numbers are marked on the calculation sheets and the corresponding spectrograms.

Some of the errors are quite large; however, reasonable explanations for the errors are as follows:

1) Temperature control of blackbody was manual excepting thermostatic control of highest temperature. Manual control prevented stabilization of blackbody temperature. This manual control gives random error of underterminable magnitude.

2) Sensor temperature was not known to the required accuracy as explained in our letter of April 4, 1962 (improperly calibrated resistance thermometer).

3) Averaging of spectrograms was not used because:

   a) the frequency response of the available tape recorder is not adequate.

   b) time limitations during performance of acceptance test did not allow us to obtain sufficient data.

COMMENT: Since the tape recorder was not used, the time required to complete one spectrogram was six minutes. This combined with manual temperature control caused considerable blackbody temperature drift during the measuring interval.

4) The spectrogram average value was obtained manually. The error caused by this method of averaging is undeterminable.

5) Erroneous information for smaller wave-number signals is caused by the wave analyzer (zero mark of wave analyzer is too near the desired information).

The following steps are being taken to correct the errors outlined in the preceding paragraphs 1 through 5.

1) Automatic control of blackbody temperature has been installed and is now being tested. With this system, we should be able to hold the blackbody temperature to within one degree at any one temperature in the range between -50 and +250°F.

We are trying different blackbody designs to determine, if possible, the error that could develop from emissivity, thermocouples imbedded in the blackbody surface, etc.

2) We have written for Block Associates a test procedure to insure the accurate calibration of the temperature sensing device in the sensor head. This procedure includes the measuring of the regulation of the 12V bus, linearity of the series resistor, resistance change versus temperature of the resistance thermometer, time variation dependancy in output, etc.

3a) A tape recorder has been ordered that will more than satisfy the requirements necessary to record the output of the interferometer. This will allow averaging 100 spectrograms for a more accurate determination of temperature.

b) Utilizing this tape recorder will reduce the measurement time from six (6) minutes to 33 seconds, thus minimizing any temperature drift of the blackbody.

4) We are in the process of locating and purchasing a digital device which will convert the wave analyzer output into bits of information which will in turn be fed into our computer for automatic

temperature computation. This will allow us to make many calculations in a relatively short period of time. This system will probably be ready when we test the third set of instruments.

For the second set of instruments, we will still have to do much of our averaging by hand; but filter networks may reduce this error somewhat. We are anticipating the reduction of the sources of error now present to a tolerable amount, that is, to the error caused by the noise threshold imposed by the bolometer itself.

5) The solution to this problem of the zero mark of the wave analyzer is to remove this zero reference mark entirely from the spectrogram. If we use suitable optical interference filters, audio tuning forks (which we now have) for markers the spectrogram can be very accurately calibrated without having to use the zero mark of the wave analyzer as a reference mark.

With the above techniques on future tests, we should be able to measurably reduce the computation errors now present.

So far, all of our tests and data reduction have indicated to us that this system of measuring temperature with the interferometer spectrometers will ultimately perform as well as we expected.

Sincerely,

TEXACO EXPERIMENT INCORPORATED

R. E. Canup

C. Determination of the Equilibrium Temperature of the Solar Shield

The portion of direct solar energy which is absorbed by the shield is represented by

$$q_{su} = \sigma E_{su} A F_{asu} T_{su}^4 \qquad (33)$$

where

q_{su} = solar energy absorbed, kcal/hr

σ = Stefan-Boltzmann constant, kcal/hr-m^2-°K^4

E_{su} = absorptivity of the shield for solar radiation (0.26)

A = area of the shield (0.0594 m^2)

F_{asu} = configuration factor, $(r/R)^2 \cos \alpha = 18.7 \times 10^{-6}$

where r = radius of sun

R = distance from the sun to the surface

α = angle of incidence when maximum area is subjected to solar radiation

T_{su} = temperature of the surface of the sun (6000°K)

The energy which is radiated into space by the shield, q_{sh}, is represented by

$$q_{sh} = \sigma F_{et} F_{at} A_1 (T_1^4 - T_2^4)$$

where

F_{et} = emissivity of the outer surface of the shield in the infrared range at 300°K (0.80)

F_{at} = 1 (since the surface is radiating in all directions into space)

A_1 = area of the shield (0.0594 m^2)

T_1 = absolute temperature of the shield

T_2 = absolute temperature of space (40°K)

The energy which is radiated from the lower surface of the shield is represented by

$$q_{sh_1} = \sigma F_{eb} F_{ab} A_1 (T_1^4 - T_3^4)$$

where

F_{eb} = emissivity of the lower surface of the shield (0.05)

F_{ab} = 0.8 from chart (33)

T_3 = absolute temperature of the inner shield (120°K)

The temperature of the shield will increase until thermal equilibrium exists where

$$q_{su} = q_{sh} + q_{sh_1}$$

Substitution and rearrangement give

$$T_1^4 = \frac{E_{su} F_{asu} T_{su}^4 + F_{et} F_{at} T_2^4 + F_{eb} F_{ab} T_3^4}{F_{et} F_{at} + F_{eb} F_{ab}}$$

$$T_1 = 294°K$$

D. Determination of Energy Transfer between the Heater Plate and Lunar Surface

The maximum energy transferred from the heater plate to the lunar surface is represented by

$$q_{hp} = \sigma F_e F_a A (T_1^4 - T_2^4) \qquad (33)$$

where

q_{hp} = energy radiated from the heater plate to the lunar surface

σ = Stefan-Boltzmann constant (4.96×10^{-8} kcal/hr-m^2-°K^4)

F_e = factor to allow for the departure of the two surfaces from complete blackness, a function of the emissivities E_1 and E_2 where E_1 is the emissivity of the heater plate radiating surface (0.94) and E_2 is the emissivity of the lunar surface (1); this value of E_2 will assume that all of the heat radiated to the lunar surface will be conducted away

$$F_e = E_1 E_2 = 0.94$$

F_a = configuration factor, a function of the configuration of the surfaces, is found in reference 33. Considering the surfaces to be disk shaped and connected by nonconducting reradiating walls, a value of 0.8 is found for F_a

A = area of the radiating surface (0.0506 m^2)

T_1 = temperature of radiating surface (400°K)

T_2 = temperature of the lunar surface (120°K)

q_{hp} = 48.0 kcal/hr = 55.3 watts

If factors F_a and F_e are not considered, the maximum power required would be:

$$q_{hp} = \sigma A (T_1^4 - T_2^4)$$

$$= 72.3 \text{ watts}$$

As the lunar surface approaches the temperature of the heater plate, the energy transferred between the two will be reduced. Figure 58 shows the change in power requirements of the device as the temperature of the lunar surface increases.

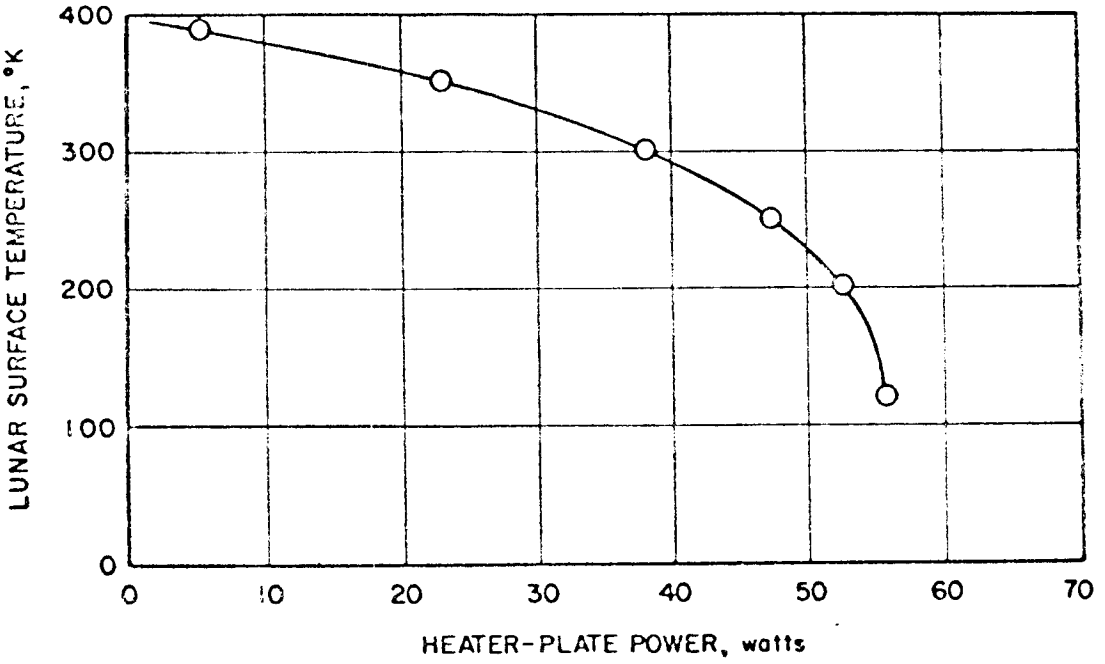

FIGURE 58. EFFECTS OF LUNAR SURFACE TEMPERATURE ON HEATER-PLATE POWER REQUIREMENTS

E. Determination of the Heater-plate Conductor Configuration

The conductor will take the form of an Archimedes spiral having the equation:

$$r = a\theta$$

$$d\theta = dr/a$$

where

r = radius

a = constant which determines the pitch

θ = angle in radians

The length of the arc, l, is given by

$$l = r\theta$$

$$dl = rd\theta$$

and substituting for $d\theta$:

$$dl = rdr/a$$

$$l = \frac{1}{a}\int_{r_1}^{r_2} rdr = \frac{1}{2a}\begin{bmatrix}4.9\\0.62\end{bmatrix} r^2 = 11.8/a$$

$$a = \frac{\text{spacing between center lines of the Cu segment}}{2\pi}$$

$$= \frac{W + c}{2\pi}$$

where W is the width of the segment and c is the clearance (0.015 inch); thus

$$W = 2\pi a - 0.015$$

The resistance of the conductor, R, which is 3.5 ohms at 293°K, is represented by

$$R = \rho l/S$$

where

ρ = resistivity (0.678 ohm-in.)

l = length (11.8/a)

S = cross-sectional area or tW, where t is the thickness of the conductor (0.003 inch)

Substituting, rearranging terms, and solving for a give

a = 0.01227 inch

W = 0.06209 inch

l = 961.7 inches

R = 3.500 ohms

F. Memorandum Recommending Removal of Surface Density Instrument Elevating Legs

4 April 1962

TO: R. E. Canup

FROM: R. Clinard

SUBJECT: Elevating Legs—Surface Density Instrument, Removal of

Early testing carried out in the feasibility study for the surface density instrument indicated that the response curve obtained was double valued, and thus an ambiguity would exist as to which side of the curve a sample material should fall. It was found that the ambiguity could be resolved if a second set of readings were made with the counter tube end of the instrument raised a few inches above the surface. This results in a decrease in the effective or measured volume causing an increase in counting rate for the heavier material and a decrease in counting rate for the materials to the left of the maximum point of the curve (ρ = 0.3 g/cm^3). This technique was demonstrated using a development model surface density instrument. The resultant data were as follows:

Material	Density, g/cm^3	Counting Rate Change
Balsa	0.17	7.8% decrease
Lava	0.65	5.0% increase
Chalk	1.93	58. % increase
Marble	2.64	100. % increase
Barium Sulfate	4.26	160. % increase

Note: These results obtained with counter tube end raised 3 inches

As a result of these tests it was decided that a set of legs would be attached to the density instrument so that two-position measurements could be made. The instrument would land in the raised position, a reading would be taken, the legs would be released by means of an explosive pin puller, and a second reading made.

The results obtained for the first prototype surface density instrument with the legs attached were as follows:

Material	Density, g/cm^3	Counting Rate Change
Balsa	0.17	4.7% increase
Lava	0.65	5.9% increase
Chalk	1.93	59. % increase
Marble	2.64	106. % increase
Barium Sulfate	4.26	134. % increase

It can be seen from these data that the counting rate did not decrease for balsa wood as before. This probably resulted due to scattering taking place from such added assemblies as the legs themselves, the pin puller housing, or the geophone and housing.

Prior to initiating a development program to determine exactly what factors materially affect the response and how the instrument could be modified to correct the problem, some thought was given to the desirability of deleting the legs all together. The advantages and disadvantages of removing the legs are listed below.

Disadvantages

1. Resolve the ambiguity in the response curve. Without the legs there will be an uncertainty involved if the lunar density is between approximately 0.1 and 0.3 g/cm^3.

Advantages

1. Simplify fabrication and assembly. The following pieces would be eliminated:

	Req'd	Name	Weight, lb
	1	Adaptor, Connector, Pin Puller	.0055
	1	Cover, Wire, Tube, Pin Puller	.0050
	A/R	Adhesive EC 2086, Minn. Min. and Mfg. Co.	.0001
	1	Bushing, Support	.0005
	2	Bushing, Guide	.0011
	1	Leg, Elevating	.0440
	2	Offset Bushing, Guide	.0031
	1	Bracket, Pin Puller	.0112
	1	Sleeve, Pin Puller	.0008
	4	Wire No. 22 Hook-up	.0096
	1	Squib	.0233
	1	Pin Puller	.1190
	2	No. 8-36 x 3/8 RHMS. St. St.	.0057
	1	Connector, Bendix PTSO6A-8-4-S (300)	.0178
	4	No. 8-36 x 1 RHMS St. St.	.0256
	3	Nut, Hex, 8-36 St. St.	.0026
	4	No. 5-44 x 7/16 RHMS St. St.	.0050
Total	30		.2799

2. **Reduce weight.** The above pieces account for a total of 0.2799 lb.

3. Improve reliability. The fewer number of pieces present, the higher the reliability of the over-all instrument. The reliability of such items as squibs, pin pullers, and connectors, although constantly improving in design, have not yet reached a reliability level as high as desired.

4. Improve mechanical integrity. The instrument will be less likely to fail as a result of shock or vibration.

5. Simplify spacecraft sequencing and manipulations. Eliminate need for second density reading and program for firing the pin puller.

6. Reduce envelope requirements. The height required would be reduced by approximately 1.5 in.

7. Improve positional stability. The c. g. would be located on the instrument centerline, and the device would not have to land in a tilted

position. The danger of toppling when the legs are released would be eliminated.

It would appear from the above consideration that, unless there is a very strong possibility that the lunar density is below 0.3 g/cm^3, it would be quite desirable to delete the legs and associated assemblies from the surface density instrument. Even if the lunar density is less than 0.3 g/cm^3, the data obtained related to other parameters such as hardness and acoustic travel time should help resolve any uncertainty.

G. Memorandum Recommending Addition of Shield Cone Housing

4 April 1962

TO: R. E. Canup

FROM: R. Clinard

SUBJECT: Shield Cone Housing—Surface Density Instruments, Addition of

It is recommended that the Surface Density Instrument be modified to include a housing to be attached to the cone shield section to enclose the source-holder assembly in the extended position. The reasons for including such a housing are:

1) Shield the source holder mechanism from any damage which might be encountered as the density instrument is lowered with source extended.

2) Insure that there would always be space available so that the source can be extended.

3) Completely enclose the source-positioning mechanism to protect it from foreign materials such as dust or fine chips.

An increase in the outline envelope may be required in order to include this modification. Since development work is presently being carried out to optimize the shielding and source-positioning requirements, the exact increase in length is not known. It is estimated at not over one (1) inch.

H. Memorandum Discussing the Feasibility of Using a Charge Amplifier with the Penetrometer

December 2, 1961

TO: R. E. Camp

FROM: W. L. Hall

cc: V. M. Barnes, Jr.

SUBJECT: Feasibility of Using a Charge Amplifier with the Penetrometer

The penetrometer (an instrument for measuring hardness of lunar surface) uses an Endevco accelerometer Model 2233 M-11 with a sensitivity of 37.8 mv/g peak to peak or 30.8 pcoul/g. This sensitivity varies slightly from accelerometer to accelerometer. The feasibility measurements were taken with 3 ft of cable having a capacity of 94 pf. The normal output from the accelerometer is approximately 378 mv for sand (10 g's) to 49 volts for quartzite (1300 g's) or a charge output from 308 pcoul to 40,000 pcoul (drop height, 3 inches). Feasibility measurements were made with the Endevco charge amplifier Model 2620, as it seemed to be the most practical unit to amplify the accelerometer output. It is available as a tested flight unit, is subminiature in size, has low power requirements, 28.5 v dc ±2.5 v dc at 25 ma, and has an output from 0 to 5 volts peak to peak. The only problem in using the Model 2620 is that high outputs from the accelerometer cause clipping of the signal; therefore, direct reading can not be obtained.

A series of tests were made to determine if it was possible to attenuate the output from the accelerometer enough to keep the signal from being clipped on the high outputs and still be able to get sufficient output when the penetrometer was dropped on sand. After numerous tests the circuit in Figure 59 was chosen.

All accelerometers are shipped with individual calibration charts. The accelerometer that was used for the following tests had the following factory calibration:

Sensitivity in peak mv/peak g (E_s) = 31.3

Accelerometer capacity in pf (C_p) = 890

Sensitivity in peak pcoul/peak g (q_s) = 37.3

with low-noise cable approximately 120 inches long with capacity of 300 pf where $q_s = E_s$ (C_p + external capacity) x 10^{-3}.

The output from the accelerometer circuit or input to the Model 2620 amplifier was found by the following method:

$$q_s = E_s (C_t) \times 10^{-3}$$

$$= 31.3 \text{ mv } (38.3 \text{ pf}) \times 10^{-3}$$

$$= 1.2 \text{ pcoul/g}$$

where E_s is the accelerometer sensitivity voltage and C_t is the measured capacity of the accelerometer circuit.

Since the gain of the amplifier was set at 2.4 mv/pcoul and the input to amplifier was 1.2 pcoul/g, the output was calculated to be 2.88 mv/g.

After this circuit seemed usable, comparison tests were made on various materials with both the charge Amplifier Model 2620 and the high-impedance amplifier Model 2607. The circuit for the Model 2607 was the same as used by Bellaire Lab. The circuit is shown in Figure 60.

The measured results of these comparison tests are given in the attached table. The series capacity added to attenuate the signal input to the charge amplifier must be changed when the cable length is changed if the input to the amplifier is to remain constant at 1.2 pcoul/g. However, this change is small compared to the change in cable length. For example, when 3-ft cable was used, the input to amplifier was 1.2 pcoul/g. When 13 ft of cable was used, the input to amplifier was 1.06 pcoul/g.

In the final design when it is known what the exact cable length between accelerometer and amplifier will be, the size of the attenuating capacitor can be easily calculated to give 1.2 pcoul/g input to amplifier.

From comparing the photographs and the tabulated experimental data, it appears that the charge amplifier Model 2620 can be successfully used to amplify the accelerometer output.

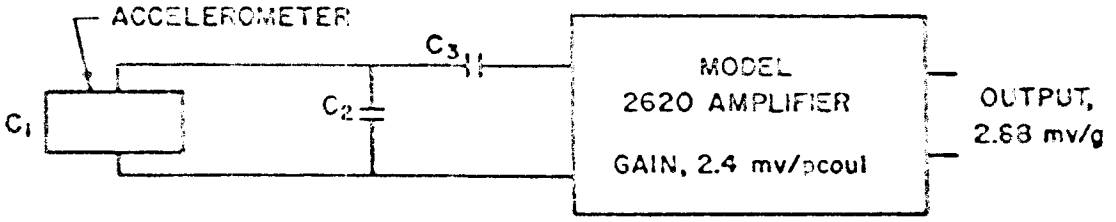

FIGURE 59. CHARGE AMPLIFIER CIRCUIT

C_1 ACCELEROMETER CAPACITY (890 pf)
C_2 LOW-NOISE CABLE CAPACITY (94 pf)
C_3 SERIES CAPACITY ADDED TO ATTENUATE SIGNAL INPUT TO AMPLIFIER (25 pf)
E_s ACCELEROMETER SENSITIVITY (31.3 mv/g)

C_t = 38.3 pf (MEASURED CAPACITY OF ACCELEROMETER CIRCUIT.)
INPUT TO AMPLIFIER, 1.20 pcoul/g (CALCULATED)
OUTPUT SENSITIVITY, 2.88 mv/g

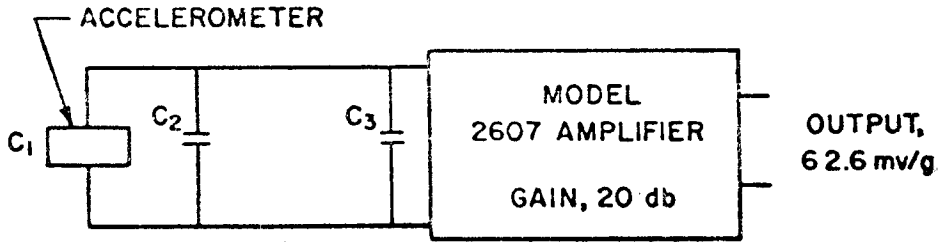

FIGURE 60. CONVENTIONAL AMPLIFIER CIRCUIT

C_1 = 890 pf ACCELEROMETER CAPACITY
C_2 = 94 pf CABLE CAPACITY
C_3 = 0.00497 μf SHUNT CAPACITY
C_4 = 1190 pf FACTORY CALIBRATION CAPACITY

THE OUTPUT FROM THE AMPLIFIER WAS CALCULATED AS FOLLOWS:

$$\text{VOLTAGE OUTPUT} = \frac{E_s \times \text{AMPLIFIER GAIN} \times C_4}{C_1 + C_2 + C_1} = 62.6 \text{ mv/g}$$

Our limited data indicated that this charge amplifier gives better results than the high-impedance amplifier originally used.

COMPARISON OF AMPLIFIER OUTPUTS

Material	Measured Peak Acceleration, g's		Pulse Width, msec		Voltate Output from Amplifiers	
	Model 2620	Model 2607	Model 2620	Model 2607	Model 2620, mv	Model 2607, v
Sand	18.7	24	14.	15.	5.4	1.5
Lead	132	200	0.94	0.94	360	12.5
Lava	163	166	3.8	4.4	470	10.4
Austin Chalk	208	240	0.7	0.7	600	15.0
Marble	434	447	0.3	0.32	1250	28.0
Tool Bit Steel (Rockwell Hardness C65)	1390	1360	0.16	0.16	4000	75.0

APPENDIX I

PENETROMETER CHECKOUT AND CALIBRATION PROCEDURE

The complete checkout procedure for the penetrometer device consists of the following specifications:

1.	387-241-89	Material Acceptance Test for Tip of Penetrometer
	387-241-88	Penetrometer Tip Material Acceptance Check Sheet
2.	387-241-97	Inspection Procedures for Penetrometer Conical Tips
	387-241-96	Inspection of Penetrometer Conical Tips Check Sheet
3.	387-241-99	Accelerometer Acceptance Tests
	387-241-98	Accelerometer Acceptance Tests Check Sheet
4.	387-241-95	Checkout Procedure for Penetrometer
	387-241-94	Penetrometer Checkout Procedure Check Sheet
5.	387-241-93	Penetrometer Calibration Procedure
	387-241-92	Penetrometer Calibration Procedure Check Sheet

Material Acceptance Test for Tip of Penetrometer

I. General

The material, AISI M-2 high-speed steel, will be purchased as 1/8-inch-diameter Rex AA tool bit, hardened and ground to diameter in 4-inch lengths. Each length will be qualified for use by checking the Rockwell hardness of one end.

II. Equipment Needed

A. Tool grinder or surface grinder

B. Rockwell hardness tester, C scale

III. Procedure

A. Each length of tool steel will have a 3/4-inch-long flat ground on one end, depth to be half the diameter so as to expose the center of the rod for checking. Care will be taken not to overheat the rod and drew its temper.

B. The hardness will be checked in two spots along the axis of the rod on the ground flat.

C. The Rockwell C scale hardness must be above 60. Record.

D. Record the batch number of the tips to be fabricated from this length of stock.

Penetrometer Tip Material Acceptance Check Sheet

Date of Test _____

Mfg. of Material _____

Observer _____

A. Material AISI M-2 tool steel _____ (check)

Test No. 1 _____ hardness (60 or above)

2 _____ hardness (60 or above)

B. The tips fabricated from this length of stock will be identified as Batch No. _____

I certify that to the best of my knowledge the test results above are valid.

_____

Signature

Inspection Procedures for Penetrometer Conical Tips

I. General

The tip should be examined before installation in its base. It is important that all tips be alike, because each tip cannot be calibrated on the harder materials since one drop blunts the tip. Reproducibility of the uncalibrated tip must be insured by careful inspection.

II. Required

A. 0-1 inch micrometer calipers

B. 6x comparator with 60° angle and 0.020-inch circle reticles

C. Drawing No. 1-00053

III. Procedure

A. With micrometer, check length, 0.20 ± 0.010 inch, and diameter, 0.125 ± 0.001 inch. Reject all units not within tolerance.

B. Check angle and tip radius with comparator; tip-radius deviation should not be distinguishable under 6x observation; angle should be within 1°.

C. Examine the tip for finish; no roughness should be apparent under 6x observation.

Inspection of Penetrometer Conical Tips Check Sheet

Date of Test _____

Batch No. _____

No. of Samples _____

Inspector _____

1. Diameter: All units not in tolerance discarded _____ (check). Tolerance limits 0.200 ±0.010 inch.

2. Length: All units not in tolerance discarded _____ (check). Tolerance limits 0.125 ±0.001 inch.

3. Tip radius conforms to TEI 1-00053_____ (check) (60° angle, 0.020-inch radius on tip).

4. Tip finish has no roughness under 6x magnification _____ (check).

I certify that all points were inspected and that all accepted units are within the tolerance limits specified.

_____
Signature

Accelerometer Acceptance Tests

I. General

A. All accelerometers must be acceptance tested according to this document before they are used in the penetrometer or sonic devices.

B. After the tests are performed, a certified copy of the completed test sheet for the particular accelerometer must accompany the instrument in which the unit is installed.

II. Equipment Required

A. Shake table, Ling Tempco Type, Model 219-CP-3/4 or equivalent

B. Amplifier, accelerometer Endevco Type 2620

C. Hot and cold test box, Delta Type 1060W

D. Shake fixture TEI 1-00319

E. Oscilloscope, Tektronix Type 535 or equivalent with Type c/a preamplifier

F. Low-noise accelerometer cable, Endevco 3090-36

G. Test jig - dropped weight type TEI 1-00320

III. Environmental Tests

A. Temperature Cycling

1. Place the accelerometer in the temperature test box; raise the temperature to 150°C for 30 to 40 min.

2. After 30 min at 150°C reduce the temperature to -50°C and hold for 30-40 min at -50°C.

3. Raise the temperature to room temperature and hold for 30 min or more.

4. Repeat steps 1, 2, and 3 three times. Record on check sheet, Item 1.

B. Shock

1. Mount the accelerometer in the test jig.

2. Raise the weight in the test jig and release. Resulting shock is approximately 2200 g's.

3. Repeat 10 times; record Item 2.

C. Vibration

1. After the temperature cycling and shock testing has been completed, mount the accelerometer on the shake table (fixture TEI 1-00319).

2. Vibrate the accelerometer at a constant acceleration of 10 g's over the frequency range of 25 to 5000 cps. The frequency shall be swept logarithmically from 25 to 5000 cps and back to 25 cps in a total time of 30 min. Record Item 3.

IV. Operation Tests - Vibration

A. Connect the accelerometer to the accelerometer amplifier through the low-noise cable. Connect the output of the accelerometer amplifier to the oscilloscope Channel A. Set the gain of the amplifier to 10.

B. Set gain of Channel A of the oscilloscope to 1000 mv/cm. Set the sweep to 20 msec/cm.

C. Mount the accelerometer on the shake table. Set vibration equipment to give 10 g's acceleration. Sweep the range of 25 to 5000 cycles in 10 min.

D. Connect the output of the vibration equipment accelerometer to Channel B of the oscilloscope. Set the gain to 1000 mv/cm.

E. Position the traces of the scope so that the output of the two accelerometers can be viewed simultaneously.

F. Operate the vibration equipment. The output of the two accelerometers should be approximately the same over the full vibration range. Record Item 4.

V. Conclusion

The tests are designed to weed out early failures. Recalibration of the device is not required as impirical calibration of the device will be accomplished in the calibration procedures for the hardness equipment.

Accelerometer Acceptance Tests Check Sheet

Date of Test _____ Observer _____

Accelerometer No. _____ _____ _____

1.	Temp. Cycle No. 1	_____ min at 150°C	(30-40 min)
		_____ min at -50°C	(30-40 min)
		_____ min at room temp.	(30 min. minimum)
	Temp. Cycle No. 2	_____ min at 150°C	(30-40 min)
		_____ min at -50°C	(30-40 min)
		_____ min at room temp.	(30 min. minimum)
	Temp. Cycle No. 3	_____ min at 150°C	(30-40 min)
		_____ min at -50°C	(30-40 min)
		_____ min at room temp.	(30 min. minimum)
2.	Shock	_____ No. of shocks	(10 or more)
		Approximately 2200 g's	
3.	Vibration	Sweep range _____	(25-5000 cps)
		Acceleration _____	(10-15 g's)
		Time of vibration _____	(30 min. minimum)
4.	Output	Output of accelerometer approximates that of std. _____ (check)	

5. I hereby certify that no evidence of malfunction, excessive noise, or other incident occurred during these tests which would indicate that there was reason to believe that this accelerometer would fail under proposed spacecraft usage.

_____
Signature

Checkout Procedure for Penetrometers

I. Required Instruments

A. 1/16-inch-diameter pin punch

B. 0.030 ±0.0005 inch brass pin 2 inches long (or Microdot plug)

C. 1/8-inch screw driver

D. 0.018-inch feeler gauge

E. Scale, 0-100 grams

II. Procedure

A. Check tightness of conical tip in base of penetrator; tip should remain in place under finger pressure on pin punch from rear (1-4 lb) (cone tip unit only).

B. Examine accelerometer electrical connection. Thread should be clean; center socket should grip 0.030-inch pin; Teflon insulation should be clean and smooth.

C. Make sure the stud is snug in the accelerometer.

D. Screw the tip onto the accelerometer stud; it should run up until the space between the accelerometer and penetrator is less than shim thickness.

E. Weight each accelerometer (with stud) with 0.020-inch-diameter stainless steel wire to 34.1 ±0.05 grams for use during calibration. Remove after final inspection.

F. Inspect each penetrometer initially after assembly and finally after calibration.

G. Measure final delivered weights, with and without tip, to the nearest 0.0005 lb. Do not include the wire weight.

Penetrometer Checkout Procedure Check Sheet

		Initial Inspection	Final Inspection
Device No. _____	Date	_____	_____
Tip, cone ____	Inspector	_____	_____
spherical ____			

1. Conical tip remains in place under 1-4 lb pressure (not applicable to spherical tip).	_____	_____
2. Threads of connector are clean.	_____	_____
3. Center connector grips pin.	_____	_____
4. Teflon insulation clean and smooth.	_____	_____
5. Stud is seated firmly in accelerometer.	_____	_____
6. Clearance between tip and body is less than 0.018 inch	_____	_____
7. Weight of weighted accelerometer with stud in grams (34.10 $\pm$0.05 grams).	_____	_____
8. Weight of accelerometer with stud to nearest 0.0005 lb.		_____
9. Final delivered weight to nearest 0.0005 lb.		_____

I certify that there is no evidence of damage to this penetrometer device or that there is any reason to believe that this device will fail under the proposed spacecraft usage.

_____

Signature
(final inspector)

Penetrometer Calibration Procedure

I. General

Accelerometers which have successfully passed the acceptance tests (TEI 387-241-99) are empirically calibrated for the penetrometer experiment. The calibration is to be accomplished in accordance with this document.

II. Equipment Required

A. Test fixture, TEI No. 1-00084

B. Urethane foam test block

C. Gum rubber test block

D. Hard rubber test block

E. Aluminum test block

F. Steel test block

G. Test box, TEI No. 1-00318 (with Endevco 2620 charge amplifier)

H. Hot and cold oven, Delta 1060W or equivalent

I. Oscilloscope, Tektronix 535 or equivalent

J. Oscilloscope Camera

K. Chromel-constantan thermocouple, 40 B and S or equivalent

L. Thermocouple meter, Keithley mμvoltmeter No. 149 or equivalent

M. Hot air blower, Alpha Heat Gun HG-1 or equivalent

N. Dry ice and acetone bath for cooling

O. Impedance bridge, ESI Model 250 or equivalent

P. Signal generator, Hathaway Model N-2

Q. AC Voltmeter, Ballantine Model 317

R. Calibration Check Sheet, TEI No. 387-241-92

III. Procedure

A. Calculation of Output Sensitivity

1. Connect the circuit as shown on TEI 1-00318 and the schematic diagram below.

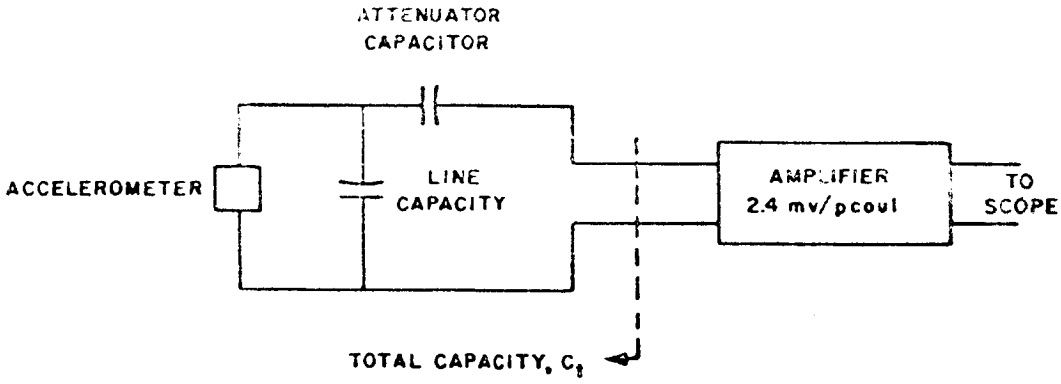

2. Disconnect the Microdot connector from the input terminal of the charge amplifier and connect it to the impedance bridge. Measure the total capacity of the accelerometer, line, and attenuating capacitor, C_t.

3. Calculate the voltage sensitivity of the system by means of:

$$\text{System } E_s = C_t \times E_s \times 2.4 \times 10^{-3} \text{ mv/g}$$

using,

a. the total capacitance, C_t, in pf, measured in (2),

b. the voltage sensitivity of the accelerometer, E_s, in peak mv/peak g, from the factory calibration chart, and

c. the charge amplifier gain, 2.4 mv/pcoul.

4. Copy the manufacturer's calibration onto the check sheet in the space provided.

B. Calibration of Materials

1. Set up and level the calibration test jig.

2. Remove the tip assembly from the accelerometer and install the accelerometer and tip assembly in the test jig. Tighten the accelerometer to the tip assembly to 18 in.-lb torque.

3. Position the arm so that the tip is 3 inches above the test sample and the pivot is 8.5 inches above the test sample. Place the first sample under the drop point of the penetrometer. Fasten it securely to the base.

4. Connect the accelerometer to the test box.

5. Connect the signal generator to the oscilloscope input and the ac voltmeter to measure the voltage input.

6. Set the required voltage input and adjust the oscilloscope gain to fill the 6-cm vertical grid exactly.

Calibration Settings and Voltage Correction for Model 317 Ballantine AC Voltmeter, Serial No.66

Test Block Material	Voltmeter Reading, mv/6 cm	Corrected rms Voltage, mv/6 cm	Oscillograph Sweep, msec/cm
Foam (cone)	15.00	15.00	5.00
Gum rubber (spherical)	54.00	53.95	1.00
Gum rubber (cone)	36.00	36.00	1.00
Hard rubber (cone)	90.00	89.58	0.50
Aluminum (cone)	280.00	277.30	0.10
Mild steel (cone)	600.00	599.50	0.05

7. Set the required sweep and replace the calibration circuit with the test circuit. Turn the test box on.

8. Adjust the oscilloscope sync-trigger mechanism on the test jig so that the output from the penetrometer falls in the center of the sweep. Adjust the base line to fall just below the top horizontal grid line of the oscilloscope.

9. Drop the penetrometer from a height of 3 inches, cone tip to top of sample, and record the oscilloscope pattern with the oscilloscope camera. Repeat the test and make a second picture.

10. Repeat this for each test. Reposition metal samples for each drop to present a smooth surface.

11. Record for each sample on the data sheet:

    a. Date

    b. Observer

    c. Device No. and Accelerometer Serial No.

    d. Identification of oscilloscope records

C. Calibration at Temperatures

1. Set up equipment as in A, using a 3-inch drop height on the gum rubber test block only.

2. Remove the entire pivoting assembly, which comprises the accelerometer, mount, and arm. Tape a thermocouple to the outside of the accelerometer.

3. Soak the assembly in the oven at test temperature for a half hour. Then assemble fixture rapidly; connect thermocouple to meter. Use external source, blower or bath, to bring TC reading to test temperature. Record the results of two drops as in A, bringing TC temperature back to test temperature between tests if necessary. Test at the following temperatures.

   a. -65°C (-85°F)

   b. +125°C (257°F)

4. Record as above. Do not allow the hot or cold penetrometer to rest on the test block any longer than is necessary, since a change in temperature of the test block may vary the results.

D. Preparation for Final Inspection

1. Remove the penetrometer from test fixture and clean it up.

2. Repeat checkout procedure on each unit.

3. Assemble them in the shipping carton.

E. Computation

1. Having established the system voltage sensitivity (system E_g), calculate the vertical sensitivity (0.4714 x corrected rms calibration voltage) and then the g sensitivity (vertical sensitivity + system E_g).

2. Measure the pulse height and width in centimeters on the oscilloscope record. Width is measured at the base line; where departure from the base line is in question, extend the tangent at a point on the curve 0.5 cm below the base line.

3. Calculate pulse height in g's (g sensitivity x measured pulse height) and pulse width in milliseconds (sweep x measured pulse width).

Penetrometer Calibration Procedure Check Sheet

Device No._____ Date _____

Accelerometer Ser. No._____ Observer _____

Mfg. Calibration:

Mfg. and Model _____

Sensitivity in peak mv/peak g (E_s) _____

Sensitivity in rms mv/peak g (E_c) _____

Accelerometer capacity in pf (C_p) _____

Sensitivity in peak pcoul/peak g
$=E_s\ (C_p + 300) \times 10^{-3}$ _____

Maximum transverse sensitivity in % _____

Note: 300 pf total external capacity added for all sensitivity calibrations.

Frequency	20	50	100	200	400	1000	2000	4000
% Deviation	___	___	___	___	___	___	___	___

Calibration date _____

Accelerometer Circuit:

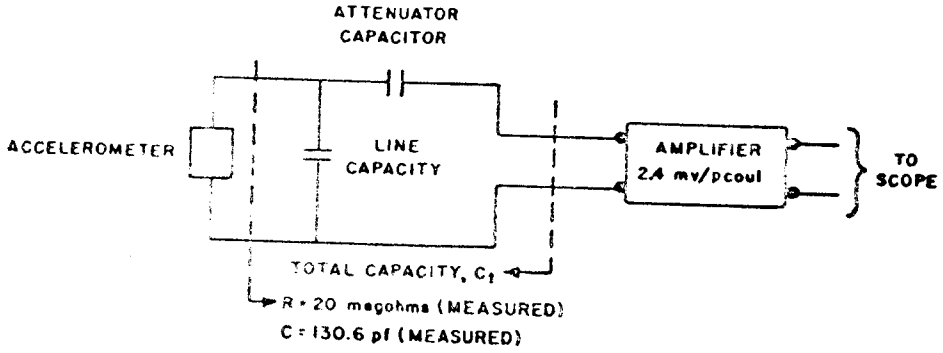

Accelerometer circuit C_t = _____pf (measured)

Accelerometer E_s = _____peak mv/peak g

System $E_s = C_t \times E_s \times 2.4 \times 10^{-3}$ = _____ mv/g

Accelerometer with stud weighted to _____$\pm$0.05 grams

Penetrometer static load on test block = 71 grams

Device No. _____ Vert. Sens. = $2\sqrt{2}/6$x rms Cal. Voltage System $E_s = C_t \times E_s \times 2.4 \times 10^{-3}$ mv/g

Accel. Ser. No. _____ = _____ mv/g

Accel. E_s _____ peak mv/peak g Date _____ Scope g Sens. = Vert. Sens. + System E_s

Circuit C_t _____ pf (measured) Observer _____ Note: g units refer to earth g's

Fig. No.	Material	Drop Ht., in.	Temp., °C	Tip		Oscilloscope				Measured		Calculated		Standard	
				Sphere	Cone	rms Cal. Voltage, mv/6 cm	Vert. Sens., mv/cm	g Sens., g's/cm	Sweep, msec/cm	Pulse Height, cm	Pulse Width, cm	Pulse Height, g's	Pulse Width, msec	Pulse Height, g's	Pulse Width, msec
	Urethane Foam	3	Room		x	15.00	7.071		5.00						
	Gum Rubber	3	Room	x		53.95	25.43		1.00						
	Gum Rubber	3	Room		x	36.00	16.97		1.00						
	Hard Rubber	3	Room		x	89.58	42.23		0.50						
	Aluminum	3	Room		x	277.3	130.7		0.10						
	Mild Steel	3	Room		x	599.5	282.6		0.05						
	Gum Rubber	3	-65°C	x		53.95	25.43		1.00						
	Gum Rubber	3	125°C	X		53.95	25.43		1.00						

APPENDIX J

GEOPHONE INCOMING ACCEPTANCE TESTS

I. General

A. All geophones must be acceptance tested according to this document before they are used in the acoustic sensor device.

B. After the tests are performed, a certified copy of the completed test sheet for the particular geophone must accompany the device in which the unit is installed.

II. Equipment Required

A. TEI test box 387-462-00-00

B. Oscilloscope: Tektronix Type 535 with Type c/a plug-in preamplifier

C. Oscillator: Hathaway Type N-2 or equivalent

D. Breakdown tester: Hathaway C-6B or equivalent

E. Impedance bridge: ESI 250 DA or equivalent

F. Oscilloscope camera

G. Shake table: Ling Tempco Type 219-CP-3/4 or equivalent

H. Hot and cold test box: Delta 1060W or equivalent

I. Shake fixture TEI 387-466-0A

J. Standard geophone

K. Test jig - dropped weight TEI 387-464-0A

III. General Tests

A. Check the plating of the geophone. It should be nickel. Record Item 1 on Geophone Check Sheet.

B. Resistance Tests

1. Connect geophone to test box.

2. Set geophone in an upright position (threaded end down).

3. Switch the test box to "Res. Test" position. With the impedance bridge, measure the dc resistance between the resistance test terminals on the test box. The resistance should be about 215 ohms. Record Item 2.

4. Remove the impedance bridge and check for electrical breakdown between case and coil with the breakdown tester. There should be no breakdown with 500 volts dc applied for 3 min. Record Item 3.

IV. Operational Tests

A. Vibration

1. Connect the output of the geophone to the geophone test box, TEI 387-462-00-00.

2. Connect the standard geophone to the "Std." input of the test box.

3. Set the test box to "total damping." Connect the "A" vertical input to the oscilloscope to the respective terminals on the test box. Set the scope sweep length to 20 msec, set the "A" vertical input sensitivity to 200 mv/cm. Connect the "B" vertical input to the B output on the test box; set the "B" vertical input to 200 mv/cm.

4. Mount the geophones on the shake table. Set the vibration equipment to give constant velocity of 1 in./sec. Set to sweep the range of 25 to 3,000 cycles in 10 min.

5. Position the traces of the scope so that the output of the two geophones can be viewed simultaneously.

6. Operate the vibration equipment. The output of the two geophones should be approximately the same over the full vibration range. Record Item 4.

B. Resonant Frequency

1. Connect geophone to test box. Switch the test box to "Resonant Freq." position. Connect the oscillator to the proper terminals. Set the oscillator output to 13.5 volts (no load) or 0.3 volts (plugged into test box) and 20 cycles.

2. Connect the vertical and horizontal inputs of the oscilloscope to the proper terminals on the test box.

3. Adjust the gain of the vertical channel to give about 4 cm deflection on the screen. Position the trace in the center of the screen.

4. Set the oscilloscope for horizontal input, remove the vertical input temporarily, and adjust the gain of the horizontal channel to give 4-cm deflection. Position the trace in the center of the screen.

5. Reconnect the vertical input. The resultant trace should be an elongated elipse at an angle of 45°.

6. Adjust the frequency of the oscillator until the resultant trace is a single-line closed elipse. This is the resonant frequency of the geophone. Record Item 5.

C. Self Damping

1. Switch the test box to "Self Damping" position.

2. Set the oscilloscope vertical input to dc and gain to 200 mv/cm. Set the sweep time to 20 msec/cm. Set the horizontal display to single sweep; set the triggering slope to "Int.+", stability to 0, and triggering level to +.

3. Install the oscilloscope camera; set the scale illumination to f-11; turn oscilloscope intensity off; pre-expose grids for 1 sec; turn scale illumination off; set oscilloscope intensity to 0.4 of full scale.

4. Close and hold shut the damp test switch on the test box. Press reset button or oscilloscope open shutter of camera.

5. Release the damp test switch. This removes the voltage from coil and allows the geophone to vibrate freely.

6. The resultant wave form should be as shown.

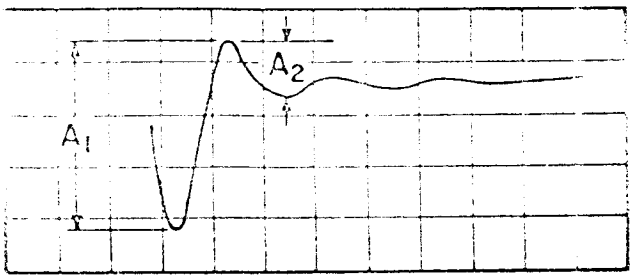

7. Measure height of A_1 and A_2 and record Item 6 on Geophone Check Sheet.

8. Divide A_1 by A_2 and record this value (6) on Geophone Check Sheet.

9. Take A_1/A_2 value; use Damping Curve Sheet, Figure 61 to find b_o. Record Item 6.

D. Total Damping

1. Switch the test box to "Total Damping."

2. Repeat Steps 1 through 5 above.

3. Measure A_1 and A_2 and record Item 7 on Geophone Check Sheet.

4. Divide A_1 by A_2 and record Item 7 on Geophone Check Sheet.

5. Take A_1/A_2 value, use Damping Curve Sheet, Figure 61, to find b_t. Record Item 7.

E. Output

1. Follow Steps 5 through 7 on Geophone Check Sheet, where

E_n = natural frequency (Step C)
r = coil resistance (Step B-3)
b_o = self damping (Step D)
b_t = total damping (Step E)
m = 4.00 grams (moving mass of geophone)
R = 500 ohms (load resistor)

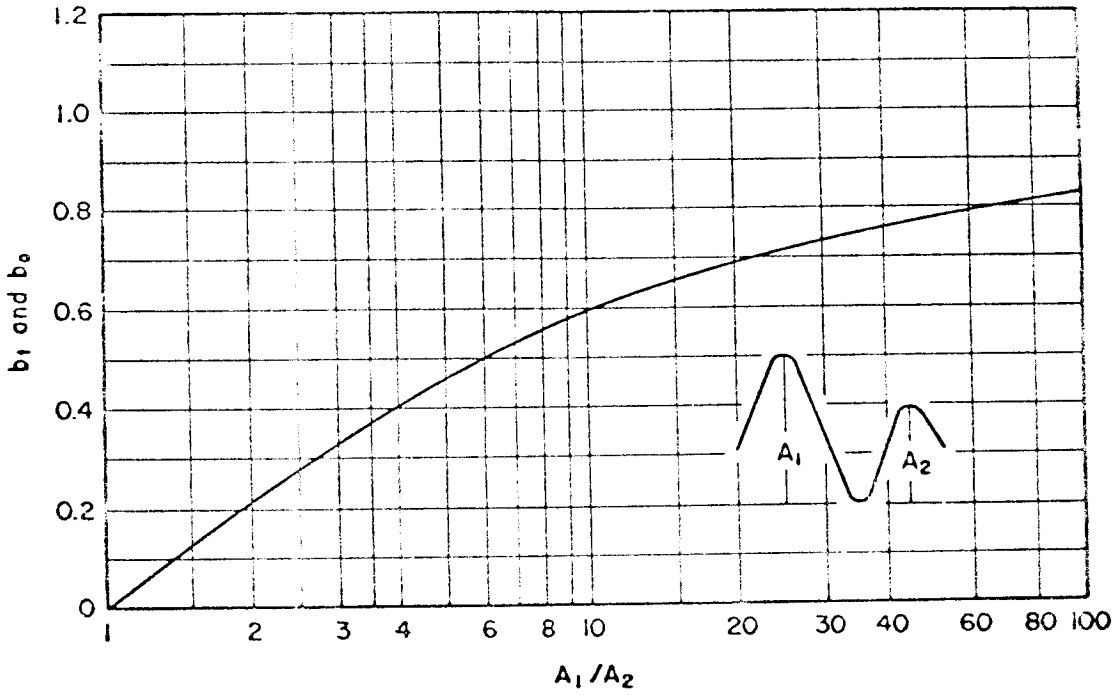

FIGURE 61. GEOPHONE DAMPING CURVE

2. The output should be about 0.110 volts/cm/sec. Record Item 8.

V. Environmental Tests

A. Temperature Cycling

1. Place the geophone in the temperature test box and raise the temperature to 150°C for 30-40 min.

2. After 30 min at 150°C reduce the temperature to -50°C and hold for 30-40 min at -50°C.

3. Raise the temperature to room temperature and hold for 30 min or more.

4. Repeat Steps 1, 2, and 3 three times. Record Item 9.

B. Shock

1. Mount the geophone in the test jig.

2. Raise the weight in the test jig and release.

3. Repeat 10 times. Record Item 10.

C. Vibration

1. After the temperature cycling and shock testing has been completed, mount the geophone on the shake table (fixture TEI 387-466-0A).

2. Vibrate the geophone at a constant acceleration of 10 g's over the frequency range of 25-5000 cps. The frequency shall be swept logarithmically from 25-5000 cps and back to 25 cps in a total time of 30 min. Record Item 11.

VI. Repeat IV, B, C, D, and E.

VII. Conclusion

These tests are designed to weed out early failures as well as verify that the voltage characteristics of the device are normal.

Geophone Incoming Acceptance Check Sheet

Date of Test _____ Geophone No. _____

Observer: _____

1. Plating of geophone is nickel _____ (check).
2. Resistance of coil_____ohms, 215 ± 25 ohms (at 70°F).
3. There is no breakdown with 500 volts dc applied _____(check).
4. Output voltage of the geophone approximates that of std._____(check).
5. The resonant frequency is _____cycles, 26 ± 3 cps.
6. Open circuit damping: A_1_____, A_2_____, A_1/A_2_____, b_o_____.
7. Total damping: load resistor, 500Ω A_1_____, A_2_____, A_1/A_2_____, b_t_____.

   $(b_t - b_o)$ _____(R+r)_____ $(R+r) \times (b_t - b_o)$ _____.

   $$\text{Output} = \sqrt{4\pi F_n M(R+r)(b_t - b_o) \times 10^{-7}}$$

   $$7.07 \times 10^{-3} \sqrt{F_n(R+r)(b_t - b_o) \times 10^{-1}}$$

8. Output: Volts/cm/sec _____ , (_____ Volt ± _____).
9. Temp. Cycle No. 1 _____min at 150°C (30-40 min)
   _____min at -50°C (30-40 min)
   _____min at room temp. (30 min. minimum)
   Temp. Cycle No. 2 _____min at 150°C (30-40 min)
   _____min at -50°C (30-40 min)
   _____min at room temp. (30 min. minimum)
   Temp. Cycle No. 3 _____min at 150°C (30-40 min)
   _____min at -50°C (30-40 min)
   _____min at room temp. (30 min. minimum)

10. Shock — No. of shocks: _____ (10 or more).

11. Vibration — Sweep range _____ (25-5000 cps).

Acceleration _____ (10-15 g's).

Time of vibration _____ (30 min. minimum).

I hereby certify that no evidence of malfunction, excessive noise, or other incidents occurred during these tests which would indicate that there was reason to believe that this geophone would fail under proposed spacecraft usage.

_____
Signature